Phase Equilibria for Mixtures with Supercritical Fluids

Doctor Thesis of Engineering
Submitted to Osaka University

Daisuke KODAMA

2002

Preface

This dissertation work was carried out under the directory of Professor Masahiro Kato in his laboratory at Department of Materials Chemistry and Engineering, College of Engineering, Nihon University from 1992 to 2002. These are collected here as a thesis to be submitted to the Graduate School of Engineering Science, Osaka University, in fulfillment of requirements for the Degree of Doctor of Engineering.

The main objective of this thesis is to clarify the phase equilibria for mixtures with supercritical fluids for separation technology.

The author hopes that this research would give some suggestions about less energy consumption and high efficiency for chemical process.

Daisuke Kodama

Department of Materials Chemistry and Engineering

College of Engineering

Nihon University

Koriyama, Fukushima, 963-8642 JAPAN

CONTENTS

General Introduction

Phase equilibria, such as vapor-liquid equilibria (VLE), liquid-liquid equilibria (LLE), and vapor-liquid-liquid equilibria (VLLE) are essential in the design and operation of distillation and supercritical fluid extraction. Chemical engineering processes of primary importance are those of mixing, conversion, and separation involving gases, liquids, and solids. Many experimental and theoretical investigations have been performed in chemical engineering problems concerning with phase equilibria. Supercritical fluid extraction is now attractive as a separation technology. The physical properties of supercritical fluids and their mixtures continue to be of importance in these developments and there is increased activity regarding reactions in supercritical fluids. Supercritical carbon dioxide, water, and alcohol are excellent candidates for industrial use because of their unique and suitable solvent properties, safety, small impact on the Earth's environment, and their economic advantages.

The high-pressure phase behavior of fluid mixtures has received great attention in recent years. The growing motivation for studying equilibria of several coexisting phases at elevated pressures arose from the need to describe such phase behavior for fluid mixtures of interest in supercritical fluid extraction. A large number of applications of this technology have been recently proposed covering the food, pharmaceutical, chemical reaction, coal and oil processing, material processing, waste treatment, plastic recycling, and producing industries. High-pressure multiphase behavior is also important in the development, often at cryoscopic temperatures, of new and highly efficient separation techniques in the natural gas, oil and petrochemical industries.

The experimental methods of vapor-liquid equilibria can be classified into two groups, direct methods and indirect methods. In the direct methods, the compositions both of the vapor and liquid phases are analytically determined after attainment of equilibrium state. The direct method can be classified into static, circulation, static-circulation, and flow methods. The indirect methods do not require any analysis of phase compositions. The

synthetic or indirect methods involve an indirect determination of composition without sampling. The synthetic or indirect methods of VLE are classified into the dew-bubble point method and saturated volume method. In the dew-bubble point method, combining in the experimental dew-point curve and the bubble-point curve; the VLE relations can be determined for binary system. In the saturated volume method, the equilibrium state for binary two phase equilibria and ternary three phase equilibria is fixed at given temperatura and pressure, based on the phase rule. At the given temperature and pressure, saturated volumes of each phases are measured. Equilibrium compositions can be indirectly evaluated from the experimental data of saturated volumes. Another experimental technique is further available to determine binary VLE from the total volume of both phases and their densities.

This thesis is concerned with the measurement and correlated of phase equilibrium properties for fluid mixtures, and is subdivided into seven chapters.

Chapter 1 is concerned with the high-pressure vapor-liquid equilibrium relations for carbon dioxide + methanol system by use of indirect method (Kato *et al.*, 1991), based on mass balance and the phase rule. The equilibrium compositions and saturated densities of vapor and liquid phases were measured for the carbon dioxide + methanol system at 313.15 K. Unsaturated density behaviors were further measured for the carbon dioxide + methanol system at 313.15 K up to the vicinity of the critical point. The saturated points near the critical point of mixture are measured by the conventional dew-bubble point pressure method. A technique is presented to determine the saturated vapor points, assuming the linear relation between molar volume and mole fraction. The experimental data obtained are correlated with PPHS (Kato *et al.*, 1989; Ozawa and Kato, 1991) and SRK (Soave, 1972) equations of state.

Chapter 2 is concerned with partial molar volumes of methanol and ethanol at infinite dilution in supercritical carbon dioxide. Partial molar volumes of solutes at infinite dilution in supercritical fluids are very important thermodynamic properties of supercritical fluid mixtures. Few studies have been dedicated to the measurements of these properties.

Partial molar volumes of alcohol at infinite dilution were evaluated from the molar volumes of pure carbon dioxide and homogeneous fluid mixtures at the same temperature and pressure. The experimental data obtained were correlated with the SRK equation of state (Soave, 1972).

Chapter 3 is concerned with saturated densities of carbon dioxide + water mixture at 304.1 K and pressures up to 10 MPa, using the apparatus equipped with vibrating tube density meters. The densities of pure water were additionally measured. The supercritical fluid extraction is attractive for saving energy in separation processes. Carbon dioxide is the most popular gas in the supercritical fluid extraction. The saturated density data containing carbon dioxide and water are further required for carbon dioxide ocean sequestration process.

Chapter 4 is concerned with high-pressure multi phase separations, such as vapor-liquid-liquid equilibria in the vicinity of critical regions by use of direct method. Suzuki *et al.* (1990) previously reported VLE for ethane + 1-propanol system at high pressures with a conventional circulation apparatus. They, however, reported no density data. Lam *et al.* (1990) previously reported only vapor-liquid-liquid locus and their saturated density for ethane + 1-propanol system at high pressures, based on mass balance and phase rule. The coexisting phase compositions and their saturated densities for ethane + 1-propanol mixture at high pressures were measured at 314.15 K including in the vicinity of the critical region. The experimental data obtained are correlated with pseudocubic (Kato and Tanaka, 1986; Yoshikawa *et al.*, 1994) and SRK (Soave, 1972) equations of state.

Chapter 5 is concerned with phase equilibria including the vicinity of critical regions by use of direct method. Kuenen *et al.* (1899) previously reported only the upper critical end point (UCEP) as 317.15 K and the approximate lower critical end point (LCEP) range from 311.15 K to 315.15 K. They further observed the three layers at temperatures below 311.15 K down to about 298.15 K. Kuenen *et al.* (1899) estimated the phase separation behaviors probably owing to its impurity in 2-propanol. The VLE data are not available in literature for ethane + 2-propanol system. The coexisting phase compositions and their saturated densities for ethane + 2-propanol mixture at high pressures were measured at 308.15 K and

313.15 K. The experimental data obtained are correlated with pseudocubic (Kato and Tanaka, 1986) and SRK (Soave, 1972) equations of state.

Chapter 6 is concerned with the vapor-liquid equilibra in the dilute composition range of solutes at atmospheric pressures. The equilibrium compositions were determined with an ultraviolet spectrometer. The vapor-liquid equilibrium behavior of ferrocene in methanol or ethanol was measured at atmospheric pressure in the dilute composition range of ferrocene. The vapor-phase composition of ferrocene is extremely larger than the estimated value, that is, the complex of ferrocene easily volatilizes from the diluted alcohol solution. The ferrocene is shortly investigated as a candidate, which would put out an azeotrope.

The vapor-liquid equilibrium behavior of 1,4-dihydroxybenzene in methanol or ethanol was further measured at atmospheric pressure in the dilute composition range of 1,4-dihydroxybenzene with a recirculation. 1,4-Dihydroxybenzene is practically used such as polymerization inhibitor and assistant developer.

Chapter 7 is concerned with homogenizing effect of ethers added to immiscible binary mixtures of alcohol and oil for alternative automobile fuels. Immiscibility of the mixtures was eliminated by adding a small amount of ether. The homogenizing ability of ethers is important for developing alternative automobile fuels, for which mixtures of ethanol or methanol with diesel fuel or with seed oils are promising. The homogenizing effect of six ethers: methyl *tert*-butyl ether (MTBE), ethyl *tert*-butyl ether (ETBE), *tert*-amyl methyl ether (TAME), tetrahydrofuran (THF), tetrahydropyran (THP), or 1,4-dioxane were investigated for immiscible binary fuels, in which ethanol was mixed with diesel fuel, with soybean oil, and with rapeseed oil, at 298.15 K. The ignition behaviors were further observed for ether + alcohol + diesel fuel mixtures.

Chapter 1 High-Pressure Vapor-Liquid Equilibrium Relations for Carbon Dioxide + Methanol System at 313.15 K

Introduction

Vapor-liquid equilibrium (VLE) properties at high pressures are required in the practical use, such as in the design and operation of distillation and supercritical fluid extraction. Kato *et al.* (1991) previously proposed an apparatus for determination of binary VLE at high pressures, introducing the density meters effectively. The VLE compositions can be evaluated by combining a couple of data at the same temperature and pressure, without any analysis of phase compositions, based on mass balance and the phase rule. Applying the experimental apparatus presented in the previous work (Kato *et al.*, 1991), an experimental method for determination of gas solubilities in nonvolatile liquid mixtures was proposed by Kato *et al.* (1991). The solubility of gas in liquid can be evaluated, based on mass balance. The solubilities of carbon dioxide in heavy hydrocarbons and their mixtures have been determined without any analysis of phase compositions (Kato *et al.*, 1992; Tanaka *et al.*, 1993; Tanaka and Kato, 1994).

Ohgaki and Katayama (1976) and Yoon *et al.* (1993) previously measured the VLE relations of carbon dioxide + methanol system at 313.15 K with a vapor-recirculation apparatus. The compositions of vapor and liquid phases were analyzed using a gas chromatography. The equilibrium data reported by Ohgaki and Katayama (1976) and Yoon *et al.* (1993), however, have no density data.

In this chapter, the VLE compositions and their saturated densities were measured for the carbon dioxide + methanol system at 313.15 K, including unsaturated density behaviors. The saturated points near the critical region were measured by the conventional dew-bubble point pressure method; a simple technique was further introduced to determine the saturated vapor points. The present experimental data include the VLE relations and further density

behaviors. The present experimental data obtained were correlated with the SRK equation of state (Soave, 1972) and pseudocubic perturbed hard-sphere equation of state (Kato *et al.*, 1989; Ozawa and Kato, 1991).

1.1 Experimental

1.1.1 Materials

In the present experiments, carbon dioxide was supplied by Nihon Sanso Co. Ltd. with the guarantee of 99.999% purity. Methanol was the special-grade reagent of Wako Pure Chemical Industries, Ltd.

1.1.2 Experimental Apparatus

The experimental apparatus equipped with two density meters is the same as that in the previous study (Kato *et al.*, 1991). The schematic diagram of experimental apparatus is shown in **Fig. 1-1**. The apparatus is suitable for operations with a maximum temperature of 400 K and pressure up to 20 MPa. The main parts of the apparatus are a cell A, piston P, Ruska 2465-752 air dead weight gauge N, Ruska 2480-700 oil dead weight gauge O, hand pump syringe S, Anton Paar DMA 512S density meters D, circulation pumps C, Ruska 2413-705 and 2439-702 pressure transducers T, and gas reservoir F. The VLE behavior in the cell is observed through the visual glass window W. The apparatus is placed in the constant temperature liquid bath E controlled within ±0.01 K. The temperatures were measured with a Hewlett Packard 2804A quartz thermometer. The volume of the cell is determined by means of a digital counter connected to the piston P. The volume of the cell A can be varied from 78 cm^3 to 134 cm^3 by the motion of the piston P with a sensitivity of 0.01 cm^3. The accuracy of the volume is about ±1 cm^3. The meters used in the present apparatus and their accuracies are shown in **Table 1-1**.

1.1.3 Experimental Principle and Procedures

The experimental principle is based on mass balance and the phase rule, previously proposed by Kato *et al.* (1991). The equilibrium compositions for binary vapor-liquid equilibria are fixed by giving the temperature and pressure, as the degree of freedom is two. For the first experiment,

$$W = \rho_V V_V + \rho_L V_L \tag{1-1}$$

$$WX_F = \rho_V V_V Y + \rho_L V_L X \tag{1-2}$$

$$V_T = V_V + V_L \tag{1-3}$$

For the second experiment,

$$W' = \rho_V V_V' + \rho_L V_L' \tag{1-4}$$

$$W'X_F' = \rho_V V_V' Y + \rho_L V_L' X \tag{1-5}$$

$$V_T' = V_V' + V_L' \tag{1-6}$$

where, W, V, X, Y, and ρ, respectively, denote the feed mass, volume, liquid mass fraction, vapor mass fraction, and density. The subscripts V, L, T, and F denote the vapor phase, liquid phase, their total, and feed respectively. The superscript ' denotes the second-run data at the same temperature and pressure.

The equilibrium compositions of liquid and vapor phases, X and Y, can be derived from Eqs. (1-1) to (1-6) as follows:

$$X = \frac{WX_F - \rho_V V_V Y}{\rho_L V_L}, \qquad Y = \frac{W'X_F' - \left(V_L'/V_L\right)WX_F}{\rho_V\left[V_V' - \left(V_L'/V_L\right)V_V\right]} \tag{1-7}$$

where,

$$V_V = \frac{W - \rho_L V_T}{\rho_V - \rho_L}, \quad V_V' = \frac{W' - \rho_L V_T'}{\rho_V - \rho_L}, \quad V_L = \frac{\rho_V V_T - W}{\rho_V - \rho_L}, \quad V_L' = \frac{\rho_V V_T' - W'}{\rho_V - \rho_L} \tag{1-8}$$

At the start of the experiment, carbon dioxide was charged into the cell after the evacuation of cell A. The pressure difference between the upper and lower spaces was kept null. The temperature, pressure, and density were measured. The amount of carbon dioxide was evaluated from the volume and density. Methanol was charged with the hand

pump syringe S to the cell. The amount of methanol was evaluated from the movement of the hand pump syringe S with a sensitivity of 0.01 cm^3. The accuracy of feed composition was about ±0.0003 mass fraction.

The vapor and liquid phases were both circulated with the circulation pump C. The pressure difference between the upper and lower spaces in the variable volume cell A was maintained null with the piston P. After attainment of equilibrium, the densities of vapor and liquid, pressure, and temperature were measured, observing the coexistence of vapor and liquid phases through the visual glass window W. The total volume was further evaluated by the movement of the piston P.

The second experiment was done at the same temperature and pressure, at different feed composition. Combining the couple of data at the same temperature and pressure, the equilibrium vapor and liquid compositions were calculated by Eqs. (1-7) and (1-8).

Dew-Bubble Point Pressure Method

At the critical point, the equations to evaluate equilibrium compositions become zero divided by zero. The experimental method (Kato *et al.*, 1991) is therefore troublesome in the vicinity of critical region.

The conventional dew-bubble point pressure method was therefore applied to determine the saturated liquid points near the critical region. Unsaturated fluid of known composition was prepared with the experimental procedures almost similar to those in the VLE measurements. Compressing the fluid by the piston P in the variable volume cell, the cell volume and pressure were measured. The saturated point was evaluated from the broken point on a cell volume *vs.* pressure curve.

A technique was presented to determine the saturated vapor points in the present study. In the binary system made of supercritical carbon dioxide and alcohol, the equilibrium vapor compositions near the critical region are close to unity in mole fraction of carbon dioxide. The saturated vapor composition can be evaluated from the homogeneous density of known composition, saturated density of mixture, and density of carbon dioxide at the same

temperature and pressure. **Figs. 1-2** and **1-3** show the experimental principle. Assuming the linear relation on the molar volume *vs.* mole fraction curve as shown in **Fig. 1-3**, the saturated vapor composition can be evaluated as follows.

$$y_1 = \frac{\bar{v}_2^{\infty} - (M_2/\rho)}{\bar{v}_2^{\infty} - (M_2/\rho) - v_1^0 + (M_1/\rho)} \tag{1-9}$$

where,

$$v_1^0 = \frac{M_1}{\rho_1^0}, \qquad \bar{v}_2^{\infty} = \frac{v^G - y_1^G v_1^0}{y_2^G} \tag{1-10}$$

$$v^G = \frac{y_1^G M_1 + y_2^G M_2}{\rho^G} \tag{1-11}$$

in which, M, v, $\bar{v}$, y, and ρ denote molar mass, molar volume, partial molar volume, vapor mole fraction, and density, respectively. The superscripts, 0, ∞, and G, mean pure component, infinite value, and given composition, respectively. The subscripts 1 and 2 denote carbon dioxide and methanol, respectively.

1.2 Results and Discussion

Figs. 1-4 to **1-7** shows the experimental results by the dew-bubble point pressure method. The saturated point very close to the critical point was evaluated from the crossing point between the homogeneous line of fixed composition and saturated curve as shown in **Fig. 1-8**. The experimental data obtained in the present study are listed in **Table 1-2**. **Figs. 1-9** and **1-10** show the density behaviors and VLE relations, respectively. The accuracies of the evaluated vapor and liquid compositions were about 0.005 and 0.001 mole fraction, respectively. The accuracy of density was about 0.1 $kg \cdot m^{-3}$. Unsaturated densities of carbon dioxide, methanol, and their mixtures were measured with the present apparatus, as shown in **Table 1-3** and **Fig. 1-9**.

Comparing the present VLE data obtained with the previous data of Ohgaki and

Katayama (1976), the average differences in liquid and vapor compositions are seem to be 0.017 and 0.007 mole fractions, respectively. Comparisons on density behaviors are unfortunately impossible, as the data of Ohgaki and Katayama (1976) and Yoon *et al.* (1993) have no volumetric values.

1.3 Correlations

The experimental VLE data obtained were correlated with the following pseudo cubic perturbed hard-sphere (PPHS) equation of state previously proposed by the authors (Kato *et al.*, 1989) and the conventional SRK equation of state (Soave, 1972).

$$P = \frac{RT}{v^* - b} - \frac{a}{\left(v^* + m\right)\left(v^* - n\right)} \tag{1-12}$$

where,

$$\frac{v^*}{v} = 4\psi + \frac{\left(1-\psi\right)^3}{1+\psi+\psi^2-\psi^3}, \qquad \psi = \frac{b}{4v} \tag{1-13}$$

in which,

$$a = K_a \cdot a_c, \qquad a_c = \Omega_a \frac{\left(RT_c\right)^2}{P_c}, \qquad \Omega_a = \left(1-\alpha\right)^3 \tag{1-14}$$

$$b = \Omega_b \frac{RT_c}{P_c}, \qquad \Omega_b = Z_c \tag{1-15}$$

$$m = \Omega_m \frac{RT_c}{P_c}, \qquad \Omega_m = \frac{\left(1-\alpha\right)}{2}\left(\sqrt{1-4\alpha}+1\right) - \left(\alpha + Z_c\right) \tag{1-16}$$

$$n = \Omega_n \frac{RT_c}{P_c}, \qquad \Omega_n = \frac{\left(1-\alpha\right)}{2}\left(\sqrt{1-4\alpha}-1\right) + \left(\alpha + Z_c\right) \tag{1-17}$$

$$\alpha = \left(27/83\right)Z_c \tag{1-18}$$

where,

$$K_a = 1 - S\left(1 - T_r^{2/3}\right), \qquad S = \frac{1 - K_a^{nb}}{1 - \left(T_r^{nb}\right)^{2/3}} - 0.0017 \cdot \mu_r^2 \cdot \Delta T_r \qquad (1\text{-}19)$$

$$\mu_r^2 = \mu^2 \Big/ \left[9.8694 \cdot 10^{-5} \left(RT_c\right)^2 / P_c\right], \qquad \Delta T_r = T_r - T_r^{nb} \qquad (1\text{-}20)$$

Given temperature and pressure, the PPHS equation of state has at most three real roots for volume. The equation of state strictly satisfies the critical point requirements.

In the present study, the following mixing rules, similar to Ozawa and Kato (1991), were introduced for the application of the equation of state to mixtures.

$$a = \sum_i \sum_j x_i x_j a_{ij}, \qquad a_{ij} = \left(1 - k_{ij}\right)\sqrt{a_i a_j} \qquad (1\text{-}19)$$

$$b^{1/3} = \sum_i \sum_j x_i x_j b_{ij}^{1/3}, \qquad b_{ij}^{1/3} = \left(1 - l_{ij}\right)\left(b_i^{1/3} + b_j^{1/3}\right)/2 \qquad (1\text{-}20)$$

$$m^{1/3} = \sum_i \sum_j x_i x_j m_{ij}^{1/3}, \qquad m_{ij}^{1/3} = \left(1 - l_{ij}\right)\left(m_i^{1/3} + m_j^{1/3}\right)/2 \qquad (1\text{-}21)$$

$$n^{1/3} = \sum_i \sum_j x_i x_j n_{ij}^{1/3} \qquad n_{ij}^{1/3} = \left(1 - l_{ij}\right)\left(n_i^{1/3} + n_j^{1/3}\right)/2 \qquad (1\text{-}22)$$

where, "k_{ij}" and "l_{ij}" are the binary interaction parameters.

The PPHS and SRK equations were applied to the correlation of the experimental VLE relations. The binary interaction parameters were determined to minimize the sum of deviations on liquid compositions. Correlation results are given in **Table 1-4**. In the present calculations, the critical values and dipole moments of pure components were obtained from Reid *et al.* (1977).

In **Fig. 1-9**, calculation results of saturated and unsaturated densities by the equations of state are included. The solid and broken lines show the calculation results by the PPHS equation and the SRK equation, respectively. As shown in **Table 1-4** and **Fig. 1-9**, the PPHS equation gave better results for saturated and unsaturated liquid densities rather than the SRK equation; the SRK equation, however, gave more suitable results on saturated vapor densities than the PPHS equation.

Summary

In the present chapter, high-pressure vapor-liquid equilibria, saturated densities, and unsaturated densities were measured for the carbon dioxide + methanol system at 313.15 K. The equilibrium vapor and liquid compositions were evaluated from a couple of data at the same temperature and pressure, based on mass balance and the phase rule. At the critical region, the saturated points were measured by the conventional dew-bubble point pressure method. A technique was presented to determine the saturated vapor point. The experimental VLE data obtained were correlated with the PPHS and SRK equations.

Ohgaki and Katayama (1976) previously reported the vapor-liquid equilibria of carbon dioxide + methanol at 313.15 K. The vapor pressures of carbon dioxide and methanol are very much different. The system is the typical asymmetric mixtures. The vapor-liquid equilibrium relations obtained show the complex behavior. The complex phase equilibrium relation reported Ohgaki and Katayama (1976) became as the target to check the reliability of the equations of state and their mixing rules for the applicability on vapor-liquid equilibria. The VLE data for the carbon dioxide + methanol system reported by Ohgaki and Katayama (1976) are the reference standard data in the development of EOS. Recently, several remarkable mixing rules of equations of state have been developed with the VLE data of Ohgaki and Katayama (1976) as the reference standard. In general, the vapor-liquid equilibrium data have no volumetric one. Many researchers on VLE know the impossibility to evaluate the volumetric properties with satisfactory accuracy. All researchers had calculated only the pressure-liquid composition -vapor composition with equation of state.

The author believes the volumetric properties are also important with the equilibrium properties. In the near future, not only the VLE relations but also the volumetric properties are the target to check the prediction or correlation with equations of state. In the experimental field of VLE, the volumetric properties are not popular. Ohgaki and Katayama (1976) reported reliable worthy VLE data, but no volumetric one. The author however

believe the volumetric properties are further important similar to the VLE data. By the reason described the above, the VLE and volumetric data has been reported for carbon dioxide + methanol at 313.15 K. The author believes the present data obtained will be a new target for the prediction and correlation of phase equilibrium properties with equations of state.

Table 1-1 Meters used in the present apparatus

Meters	Type	Pressure range	Accuracy
Density meter	Anton Paar DMA 512S	0 – 40 MPa	0.1 $kg \cdot m^{-3}$
Thermometer	Hewlett Packard 2804A	Resolution 0.0001 K	
Pressure gauge	Ruska 2465-752 (Air DWG)	0.014 – 7 MPa	0.01%
	2480-700 (Oil DWG)	0.22 – 103 MPa	0.01%
Pressure transducer	Ruska 2439-702 (Usual Type)	– 7 MPa	50 ppm
	2413-705 (Special Type)	– 103 MPa	5 ppm

Table 1-2 Experimental VLE data for carbon dioxide + methanol system at 313.15 K

P, MPa	ρ_L, kg·m^{-3}	ρ_V, kg·m^{-3}	x_1	y_1
1.006	782.0	18.3	——	——
2.011	794.0	37.6	0.106	0.975
2.915	803.2	57.0	0.159	0.977
4.101	815.2	87.6	0.233	0.977
5.035	823.2	116.3	0.298	0.978
5.969	829.4	151.6	0.375	0.977
6.507	831.2	177.5	0.426	0.980
7.022	829.0	207.2	0.492	0.989
7.506	819.6	247.9	0.585	0.981
7.655	812.2	267.2	——	——
7.748**	——	——	——	0.978**
7.779	797.4	284.5	——	——
7.830*	——	——	0.698*	——
7.857	781.8	298.0	——	——
7.905	762.6	307.3	——	——
7.990*	——	——	0.800*	——
8.034	666.3	341.1	——	——
8.081	639.4	364.1	——	——
8.123	607.9	395.0	——	——
8.125*	——	——	0.900*	——
8.146	586.9	420.2	——	——
8.178	556.2	448.4	——	——
8.187*	——	——	0.950*	——
8.188*	506.0*		——	——

*, Dew-bubble point pressure method

**, Molar volume linear approximation method

Table 1-3 Unsaturated densities of carbon dioxide + methanol system at 313.15 K

	Mole fraction of carbon dioxide					
	0.00	0.25	0.50	0.75	0.90	1.00
P, MPa	ρ, kg·m^{-3}					
0.1013	772.6	——	——	——	——	——
1.065	773.3	——	——	——	——	18.9
1.999	774.5	——	——	——	——	37.1
2.991	775.4	——	——	——	——	58.7
3.996	776.3	——	——	——	——	83.6
5.035	777.5	——	——	——	——	114.0
6.086	778.7	820.1	——	——	——	152.5
7.064	779.7	822.0	830.8	——	——	201.2
8.028	780.8	823.8	834.2	773.1	——	279.9
8.450	——	——	——	——	668.5	——
9.061	781.6	825.7	838.2	788.4	701.5	498.8
9.887	782.4	827.2	841.3	798.6	729.2	619.0

Table 1-4 Correlation results of VLE with equations of state for carbon dioxide + methanol system at 313.15 K

EOS	k_{ij}	l_{ij}	$\lvert\Delta\rho_L\rvert_{av}$	$\lvert\Delta\rho_V\rvert_{av}$	$\lvert\Delta x_1\rvert_{av}$	$\lvert\Delta y_1\rvert_{av}$
PPHS	0.0144	0.0014	38.4	22.1	0.001	0.006
SRK	0.0753	——	134.7	1.2	0.032	0.006

PPHS, Pseudocubic perturbed hard sphere equation of state

SRK, Soave-Redlich-Kwong equation of state

$\lvert\Delta\rho_L\rvert_{av}$, Average absolute difference of saturated liquid density

$\lvert\Delta\rho_V\rvert_{av}$, Average absolute difference of saturated vapor density

$\lvert\Delta x_1\rvert_{av}$, Average absolute difference of liquid mole fraction

$\lvert\Delta y_1\rvert_{av}$, Average absolute difference of vapor mole fraction

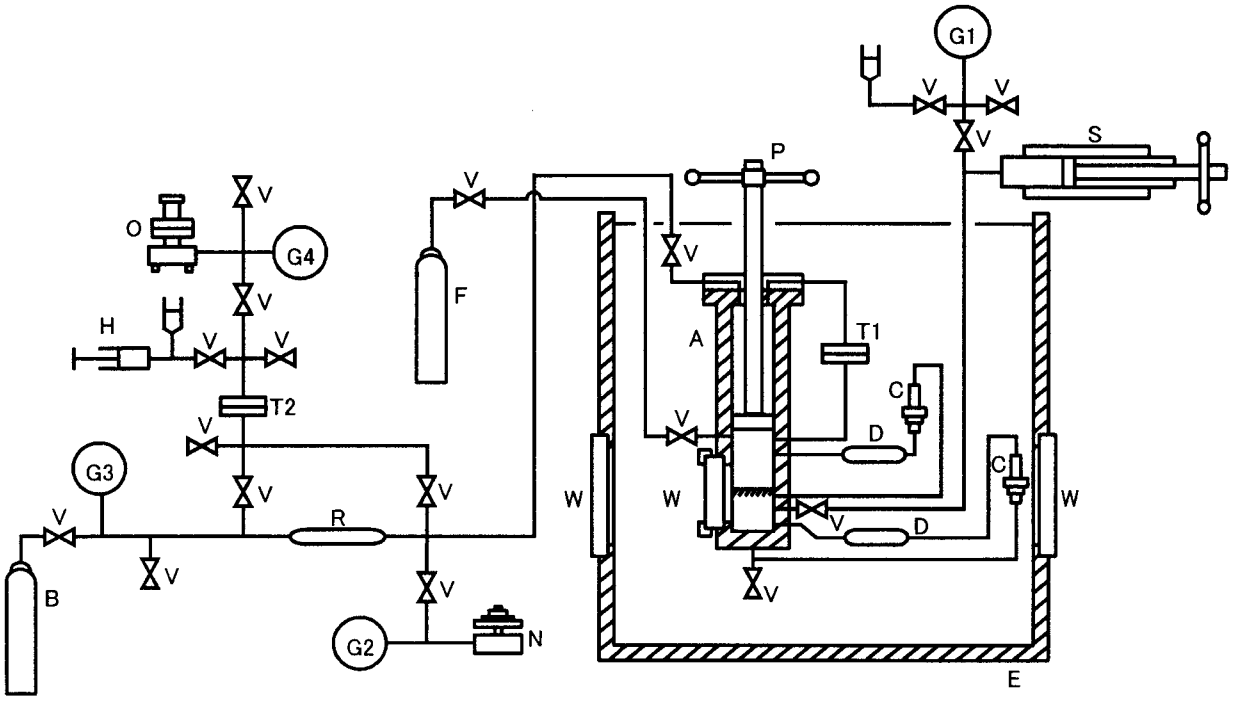

Fig. 1-1 Schematic diagram of experimental apparatus

A, variable volume cell; B, nitrogen reservoir; C, circulation pump; D, density meter; E, constant temperature liquid bath; F, gas reservoir; G, pressure gauge; H, hand pump; N, air dead weight gauge; O, oil dead weight gauge; P, piston; R, reservoir; S, hand pump syringe; T, pressure transducer; V, valve; W, visual glass window

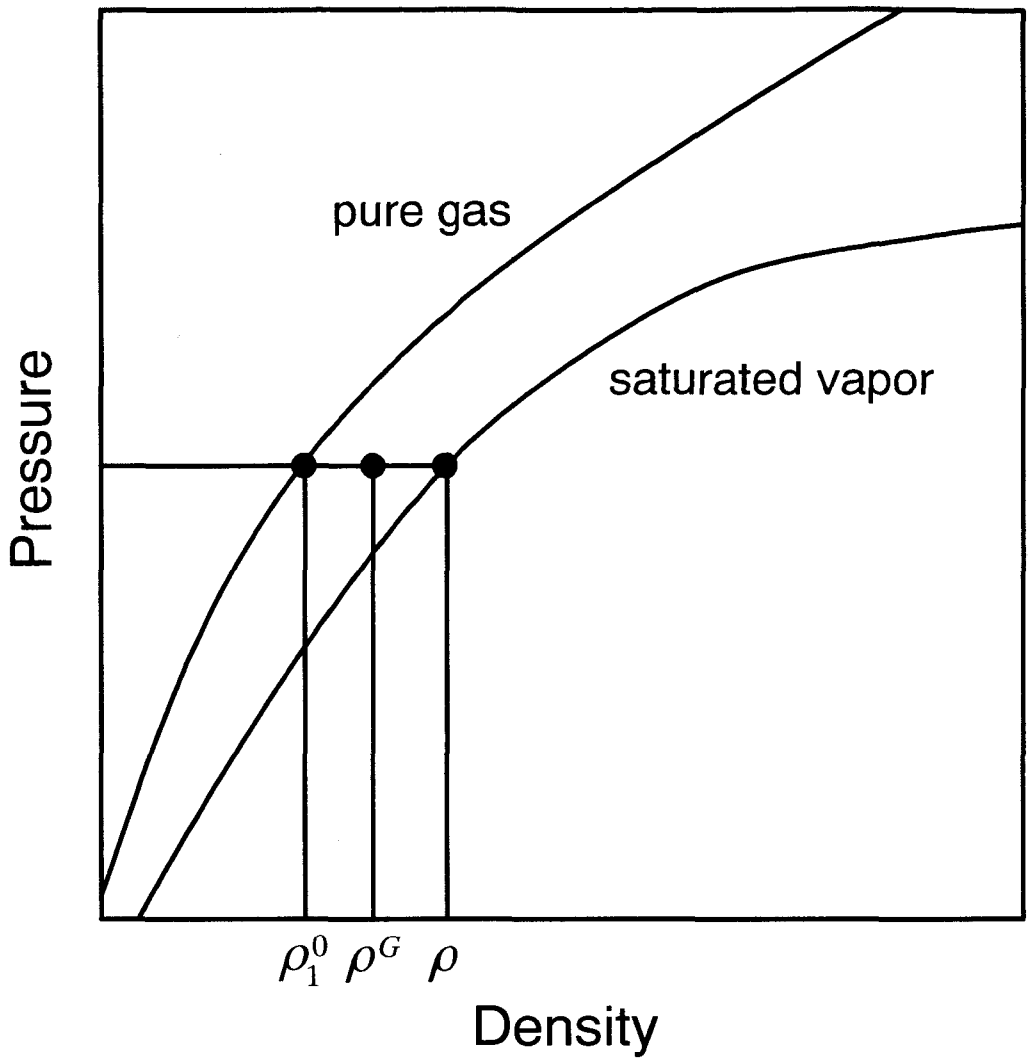

Fig. 1-2 Density measurements at constant temperature and pressure

ρ_1^0, density of pure gas; ρ^G, density of given composition; ρ, saturated vapor density

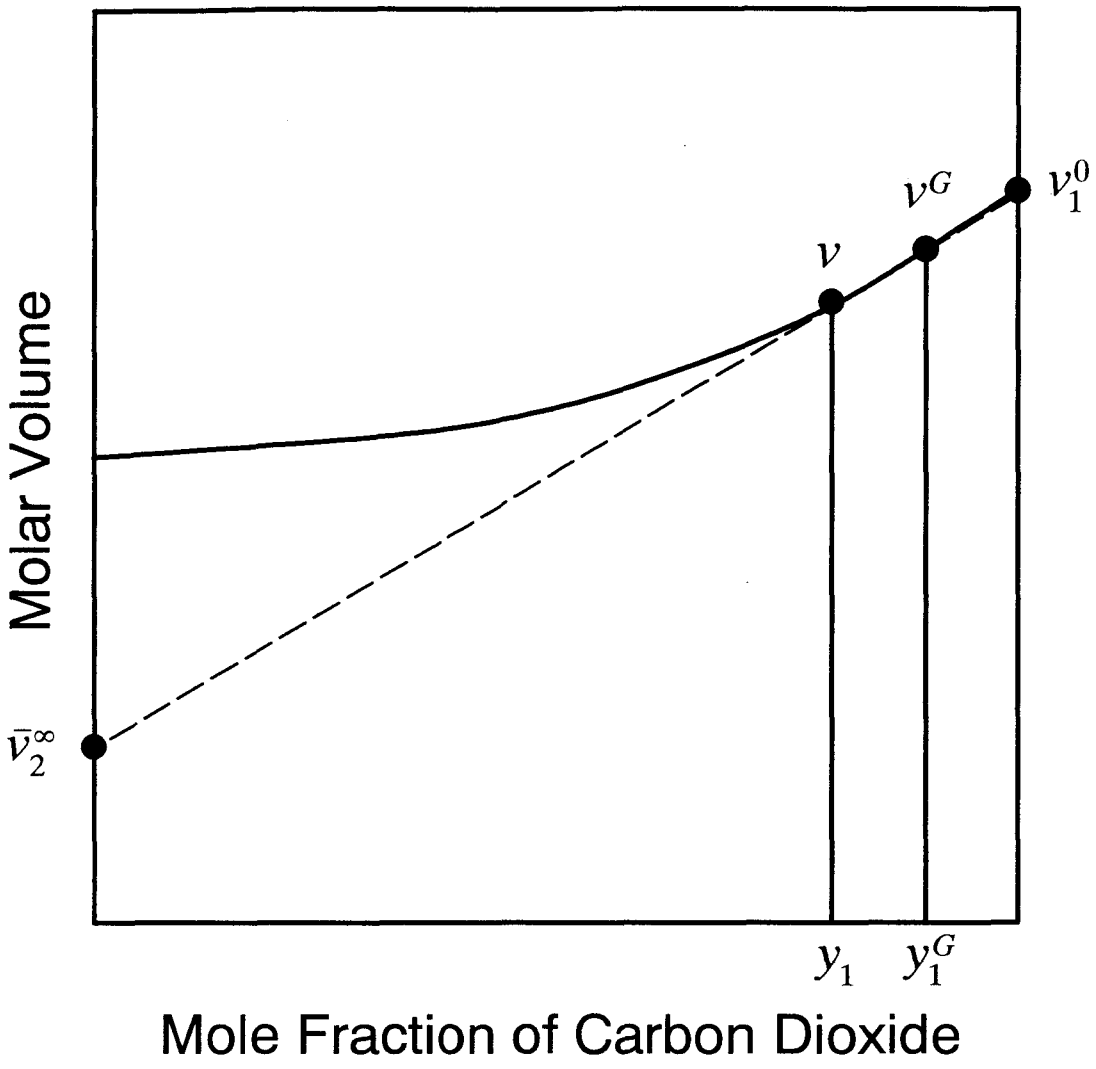

Fig. 1-3 Molar volume linear approximation method

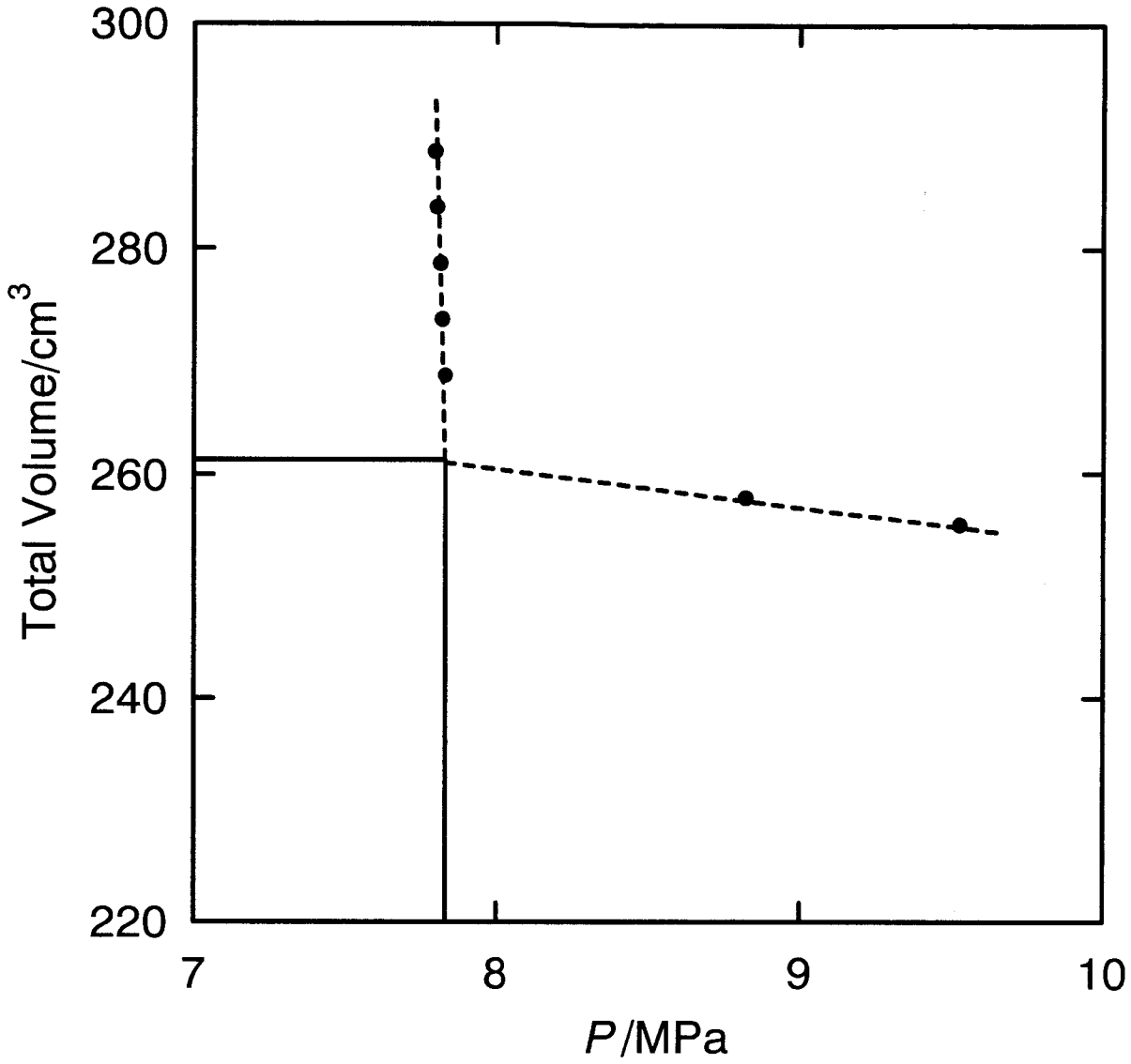

Fig. 1-4 Experimental results by dew-bubble point pressure method

0.698 CO_2 mole fraction; ●, experimental

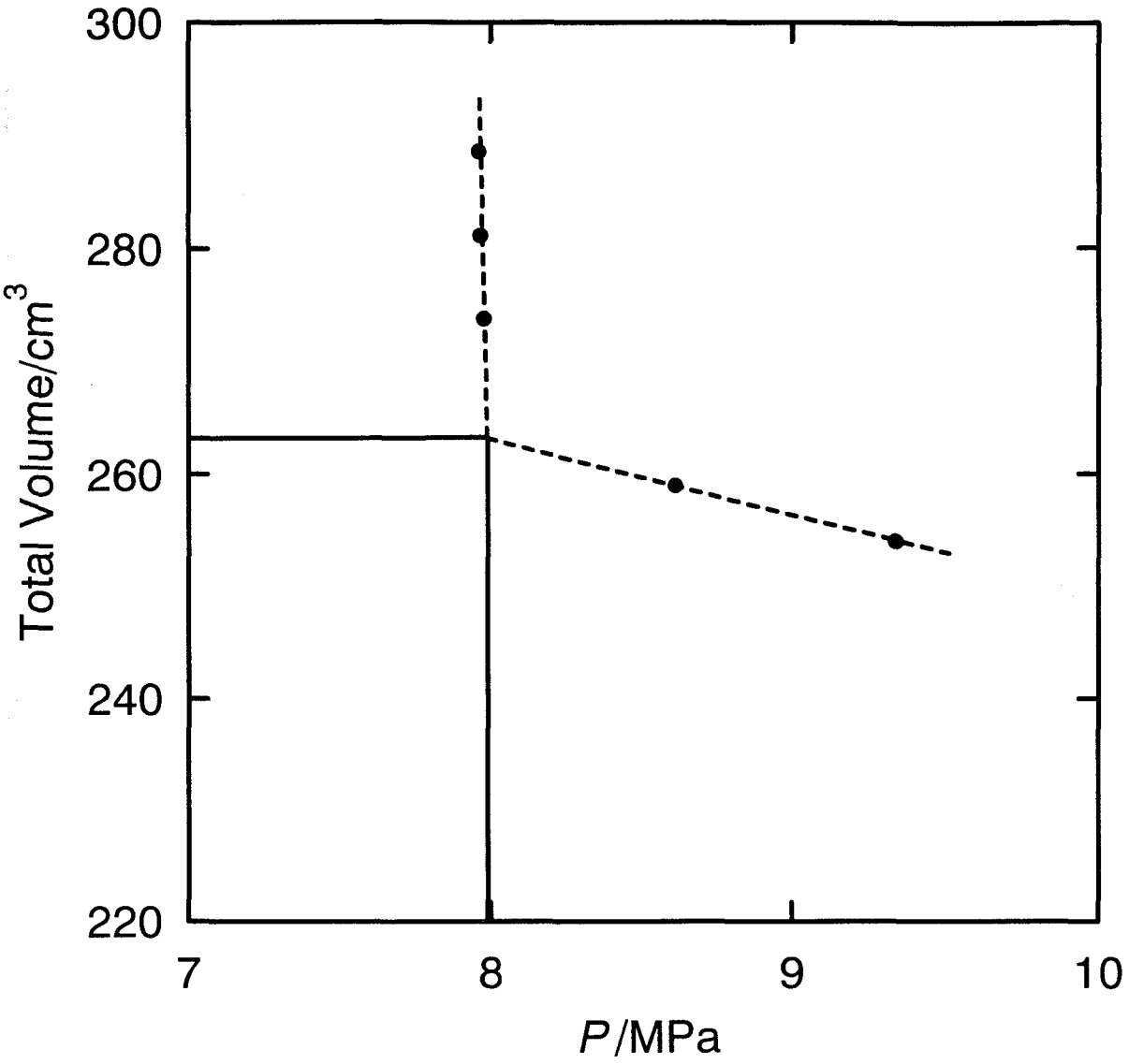

Fig. 1-5 Experimental results by dew-bubble point pressure method

0.800 CO_2 mole fraction; ●, experimental

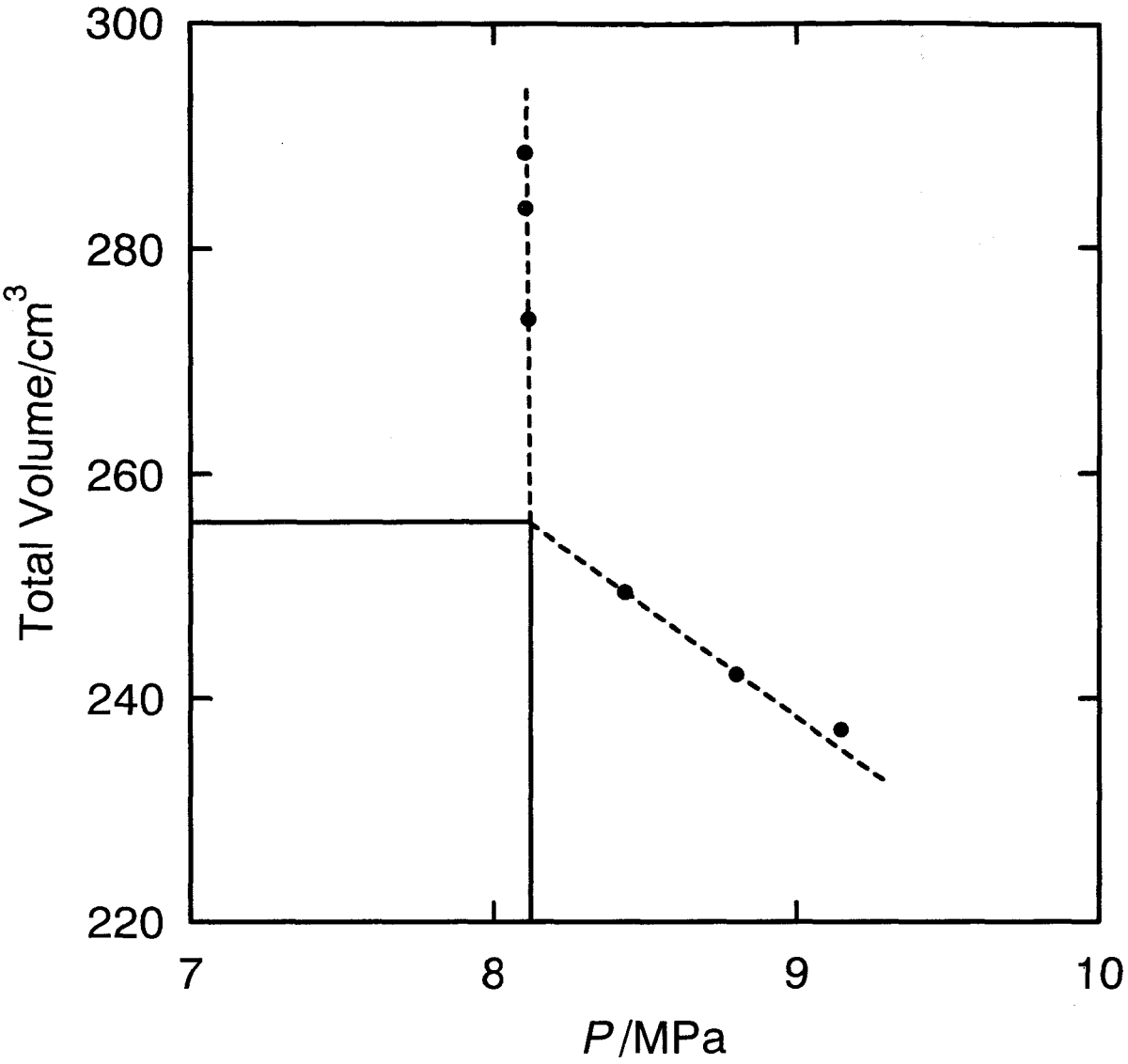

Fig. 1-6 Experimental results by dew-bubble point pressure method

0.900 CO_2 mole fraction; ●, experimental

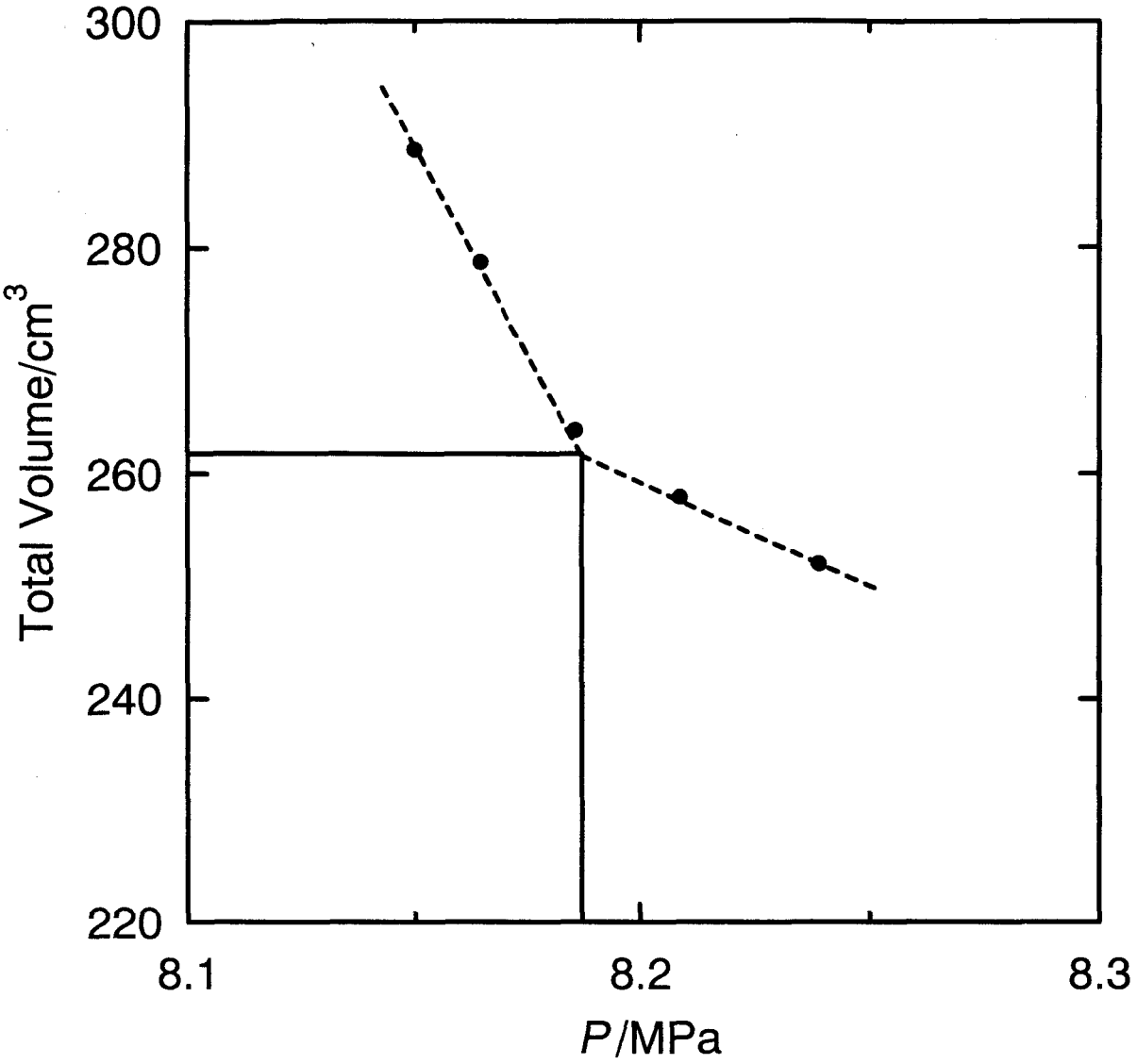

Fig. 1-7 Experimental results by dew-bubble point pressure method

0.950 CO_2 mole fraction; ●, experimental

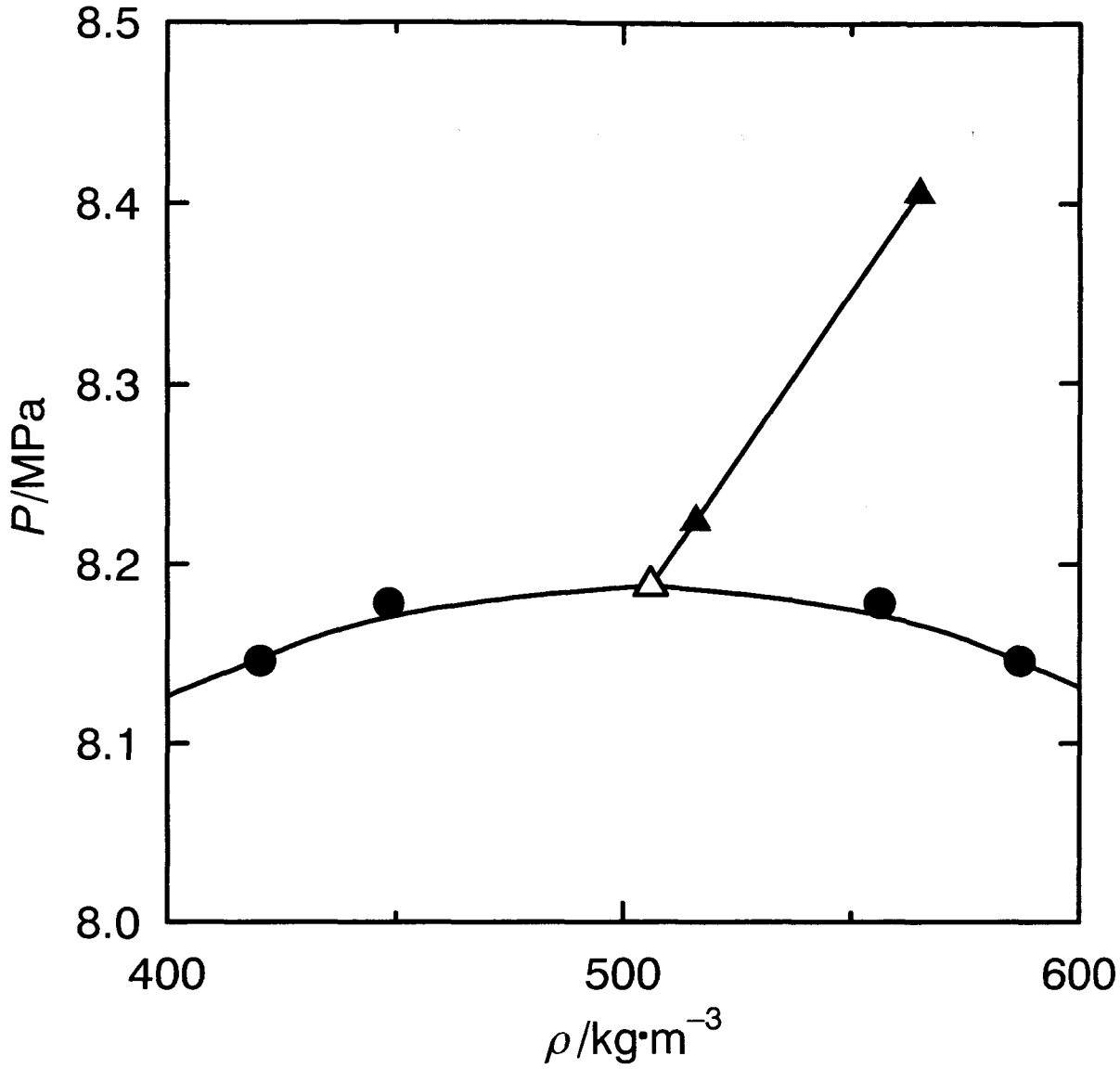

Fig. 1-8 Saturated point determination near critical point of carbon dioxide (1) + methanol (2) system at 313.15 K

—●— , saturated curve; —▲—, unsaturated line of fixed composition;

△ , evaluated saturated point

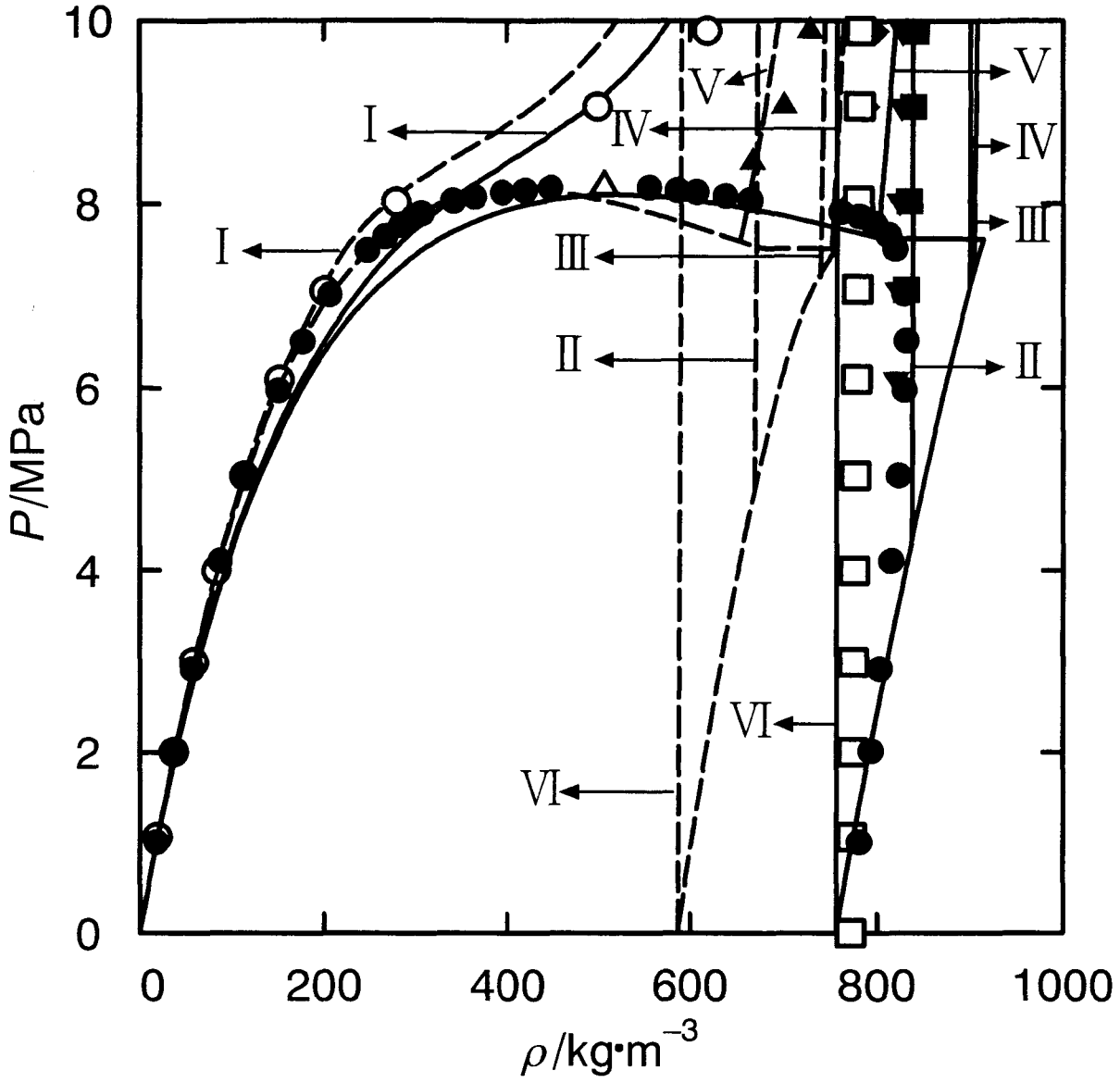

Fig. 1-9 Density behaviors of carbon dioxide (1) + methanol (2) system at 313.15 K

<Experimental> ●, saturated; ○, carbon dioxide; ▼, 0.25 CO_2 mole fraction; ■, 0.50 CO_2 mole fraction; ◆, 0.75 CO_2 mole fraction; ▲, 0.90 CO_2 mole fraction; □, methanol; △, dew-bubble point method

<Calculated> ———, PPHS EOS; – – – – –, SRK EOS

I, carbon dioxide; II, 0.25 CO_2 mole fraction; III, 0.50 CO_2 mole fraction; IV, 0.75 CO_2 mole fraction; V, 0.90 CO_2 mole fraction; VI, methanol

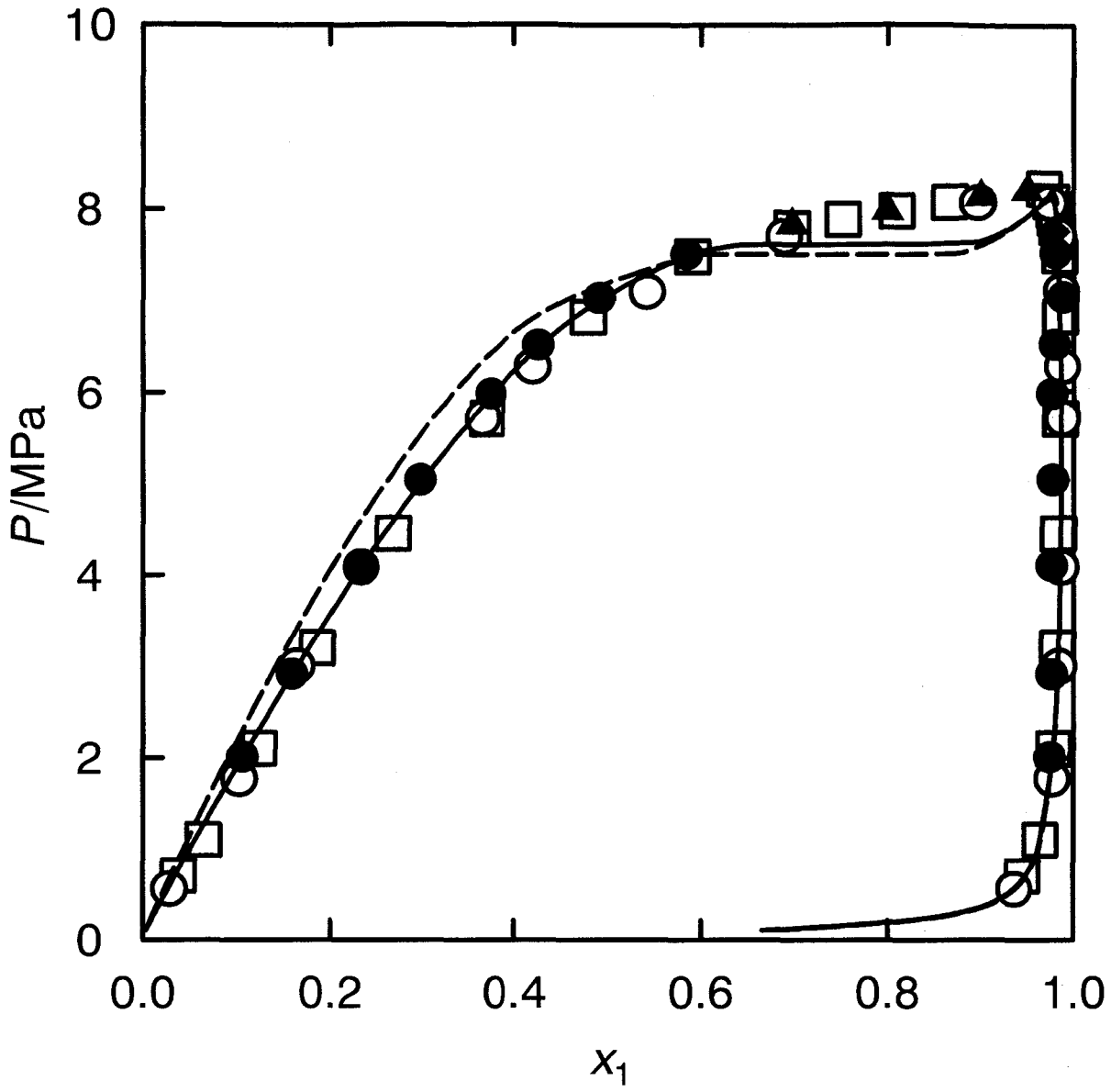

Fig. 1-10 Vapor-liquid equilibria for the carbon dioxide (1) + methanol (2) system at 313.15 K

<Experimental> ●, VLE measurement; ▲, dew-bubble point pressure method; ◆, molar volume linear approximation method; ○, Ohgaki and Katayama (1976); □, Yoon *et al.* (1993)

<Calculated> ———, PPHS EOS; – – – –, SRK EOS

Chapter 2 Partial Molar Volumes of Methanol and Ethanol at Infinite Dilution in Supercritical Carbon Dioxide

Introduction

Partial molar volumes of solutes at infinite dilution in supercritical fluids are very important thermodynamic properties of supercritical fluid mixtures. Few studies have been dedicated to the measurements of these properties.

Eckert *et al.* (1986) developed a novel technique for the measurement of the partial molar volume of solutes at infinite dilution in supercritical fluids. The experimental results for five systems were interpreted in terms of solvent structure and intermolecular forces. Yun *et al.* (1991) reported solubility and partial molar volume of cholesterol at infinite dilution in supercritical carbon dioxide, including the considerations on cluster size. Liong *et al.* (1991) measured the partial molar volume of DHA and EPA esters in supercritical carbon dioxide. The experimental results were correlated by the PR and SRK equations of state. Spicka *et al.* (1994) and Cortesi *et al.* (1996) measured the partial molar volumes of hydrocarbons, benzaldehyde, alcohols and terpenes at infinite dilution in supercritical carbon dioxide, applying the supercritical fluid chromatography. Srinivasan and McCoy (1991) evaluated partial molar volumes of ethyl acetate at infinite dilution from supercritical carbon dioxide desorption data. Liu and Macedo (1995) presented a systematic study on various models for the representation of partial molar volumes.

In the previous chapter, high-pressure vapor-liquid equilibria and saturated densities were measured for carbon dioxide + methanol system at 313.15 K without any analysis of phase compositions, based on mass balance and the phase rule. Unsaturated densities were additionally measured. Vapor-liquid equilibria and saturated densities were further reported for carbon dioxide + ethanol system at 308.15 K, developing a static-recirculation apparatus equipped with three density meters (Tanaka and Kato, 1995).

In this chapter, partial molar volumes of methanol at 313.15 K and ethanol at 308.15 K at infinite dilution in supercritical carbon dioxide were measured between 7 MPa and 10 MPa. Partial molar volumes of alcohol at infinite dilution were evaluated with the molar volume of pure carbon dioxide and the one of the homogeneous fluid made of carbon dioxide and a small amount of alcohol at the same temperature and pressure. The experimental data obtained were correlated with the SRK equation of state (Soave, 1972).

2.1 Experimental

2.1.1 Materials

In the present experiments, carbon dioxide was supplied by Nihon Sanso Co. Ltd. with the guarantee of 99.999% purity. Methanol and ethanol was the special grade reagent of Wako Pure Chemical Industries, Ltd.

2.1.2 Experimental Apparatus

The experimental apparatus is almost the same as the previous one (Kato *et al.*, 1991) used for vapor-liquid equilibrium measurements. The hand syringe pump used in the previous studies was replaced to the HPLC pump. The schematic diagram of the apparatus is shown in **Fig. 2-1**.

2.1.3 Experimental Procedures

At the start of the experiment, carbon dioxide was charged into cell A. The pressure difference between the upper and lower rooms in the cell was kept null. The temperature, pressure, volume, and density of feed gas were measured. The volume was determined by the motion of the piston P. The amount of carbon dioxide was evaluated from the volume and density. A small amount of alcohol was further charged with the HPLC pump S to the cell. The fluid in the cell was circulated with the circulation pump C until achieving the

homogeneous phase. Controlling the volume of cell A, the pressure was kept constant in the experiment. As unsaturated homogeneous vapor, the density of the fluid should be between the one of pure carbon dioxide and the saturated vapor density at the same temperature and pressure. The saturated vapor densities and compositions are available in the previous studies (Kodama *et al.*, 1996; Tanaka and Kato, 1995). The unsaturated homogeneous vapor regions are narrow, as the saturated vapor is close to pure carbon dioxide for the present systems as shown in the previous studies (Kodama *et al.*, 1996; Tanaka and Kato, 1995). Certifying the difference between the experimental density and the saturated vapor density, the fluid was confirmed to be in the homogeneous unsaturated region. After attainment of the homogeneous fluid, the density, total volume, pressure, and temperature were measured. The amount of mixture was evaluated from the total volume and density. From the difference between the amounts of carbon dioxide and mixture, the amount of alcohol was evaluated. The composition was evaluated from the amounts of each component.

The partial molar volume of alcohol at infinite dilution $\bar{v}_2^{\infty}$ is given by

$$\bar{v}_2^{\infty} = v_1^0 - \left(\frac{dv}{dy_1}\right)_{y_1=1} \tag{2-1}$$

As schematically shown in **Fig. 2-2**, the derivative of the molar volume with respect to the composition was approximated by the ratio of the small differences of molar volumes and compositions at the end of composition.

$$\bar{v}_2^{\infty} = v_1^0 - \left(\frac{\Delta v}{\Delta y}\right)_{y_2 \to 0} \tag{2-2}$$

where

$$\Delta v = v_1^0 - v, \qquad \Delta y = y_2 = 1 - y_1 \tag{2-3}$$

$$v_1^0 = \frac{M_1}{\rho_1^0}, \qquad v = \frac{y_1 M_1 + y_2 M_2}{\rho} \tag{2-4}$$

in which, $\bar{v}$, v, y, M, ρ, and Δ, respectively, denote the partial molar volume, the molar volume, the mole fraction, the molar mass, the density, and the difference. The subscripts 1

and 2 denote carbon dioxide and alcohol, respectively. The superscripts 0 and ∞, respectively, denote pure substance and infinite dilution value.

2.2 Results and Discussion

The experimental data obtained are listed in **Table 2-1**. The linear approximation of molar volume in the narrow region seems reasonable as the values of y_2 are smaller than 0.01 as shown in **Table 2-1**. For the molar volume behaviors, the linear relation was preliminary confirmed in the experiment between the molar volume and mole fraction at the end of composition close to pure carbon dioxide at the same temperature and pressure. The difference of density is significantly large relative to the difference of composition, especially near the critical pressure of carbon dioxide. The accuracies of mole fraction of alcohol and molar volume are about 1% for and 1×10^{-7} $m^3 \cdot mol^{-1}$, respectively. The estimated uncertainty of partial molar volume of alcohol at infinite dilution is given in **Table 1**. The partial molar volumes of alcohol at infinite dilution are negative and large in the vicinity of critical regions.

Figs. 2-3 and **2-4** give the experimental partial molar volumes of alcohol at infinite dilution for carbon dioxide + methanol system at 313.15 K and for carbon dioxide + ethanol system at 308.15 K, respectively, showing experimental uncertainties.

2.3 Correlations

The experimental partial molar volume data at infinite dilution at the end of composition were correlated with the following SRK equation of state (Soave, 1972).

$$P = \frac{RT}{v-b} - \frac{a}{v(v+b)} \tag{2-5}$$

where,

$$a = a_c\left\{1+S\left(1-T_r^{0.5}\right)\right\}^2 \tag{2-6}$$

$$a_c = 0.42748\frac{\left(RT_c\right)^2}{P_c} \tag{2-7}$$

$$b = 0.08664\frac{RT_c}{P_c} \tag{2-8}$$

$$S = 0.480+1.54\omega-0.176\omega^2 \tag{2-9}$$

In the present study, the following conventional mixing rules were used.

$$a = \sum_i\sum_j y_i y_j a_{ij}\,, \qquad a_{ij} = (1-k_{ij})\sqrt{a_i a_j} \tag{2-10}$$

$$b = \sum_i\sum_j y_i y_j b_{ij}\,, \qquad b_{ij} = \frac{b_i+b_j}{2} \tag{2-11}$$

where k_{ij} is the binary interaction parameter.

Correlating the experimental partial molar volumes of alcohol at infinite dilution with the SRK equation, the binary interaction parameter k_{ij} was evaluated to be 0.1136 and 0.1605 for carbon dioxide + methanol system at 313.15 K and for carbon dioxide + ethanol system at 308.15 K, respectively. The values of binary interaction parameter k_{ij} were previously evaluated as 0.0753 and 0.0795 for carbon dioxide + methanol system and carbon dioxide + ethanol system, respectively, from vapor-liquid equilibrium relations (Kodama *et al.*, 1996; Tanaka and Kato, 1995). The different values of k_{ij} for the same systems show the imperfection of the equation of state.

The solid curves in **Figs. 2-3** and **2-4**, respectively, show the correlation results for carbon dioxide + methanol system at 313.15 K and for carbon dioxide + ethanol system at 308.15 K. The broken curves in **Figs. 2-3** and **2-4** give the prediction results with the k_{ij} values evaluated from vapor-liquid equilibria.

When using the binary interaction parameters k_{ij} evaluated from the partial molar volume at infinite dilution, significantly poor results were predicted for phase equilibrium relations. For the carbon dioxide + methanol system, vapor-liquid-liquid phase separation was

calculated. For the carbon dioxide + methanol system, only the vapor-liquid phase separation was observed in the experiment (Kodama *et al.*, 1996).

In the present correlations, the critical values and acentric factor of pure components were obtained from Reid *et al.* (1987).

Summary

Partial molar volumes of methanol at 313.15 K and ethanol at 308.15 K at infinite dilution in supercritical carbon dioxide were measured between 7 MPa and 10 MPa. Partial molar volumes of alcohol at infinite dilution were evaluated with the molar volume of pure carbon dioxide and that of the homogeneous fluid made of carbon dioxide and a small amount of alcohol at the same temperature and pressure. The experimental data obtained were correlated with the SRK equation of state.

In the research field of vapor-liquid equilibria, the temperature-pressure-liquid composition-vapor composition relations were the main problem. The author however believes the volumetric properties will be required in the prediction and correlation of equilibrium properties in the near future. The author cannot satisfy the poor calculation results on volumetric properties, even if the EOS gives satisfactory results on VLE prediction. The volumetric property data of mixtures are significant as well as the VLE data.

Appendix

According to Yun *et al.* (1991), the cluster size is evaluated from the experimental partial molar volumes of alcohol at infinite dilution and molar volume of pure carbon dioxide at the same temperature and pressure,

$$N = -\frac{\overline{v}_2^{\infty}}{v_1^0} \tag{A-1}$$

where, N, $\overline{v}_2^{\infty}$, and v_1^0, respectively, denote the cluster size, partial molar volume of alcohol at infinite dilution, and molar volume of pure carbon dioxide. The evaluation results of cluster size are listed in **Table A-1**.

Table A-1 Evaluation of cluster size from the experimental results

P, MPa	N
Carbon Dioxide (1) + Methanol (2) System at 313.15 K	
7.078	2
7.607	3
8.088	7
8.500	13
8.989	11
9.447	6
9.921	5
Carbon Dioxide (1) + Ethanol (2) System at 308.15 K	
7.099	6
7.556	10
7.898	26
7.999	40
8.087	24
8.481	8
9.006	4
9.913	2

Table 2-1 Experimental partial molar volumes of alcohol at infinite dilution in supercritical carbon dioxide

P, MPa	ρ_1^0, kg·m^{-3}	v_1^0, m^3·mol^{-1}	y_2	ρ, kg·m^{-3}	v, m^3·mol^{-1}	$\bar{v}_2^\infty$, m^3·mol^{-1}
Carbon Dioxide (1) + Methanol (2) System at 313.15 K						
7.078	202.6	0.0002172	0.0068	206.7	0.0002125	-0.00047±0.00005
7.607	240.1	0.0001833	0.0060	246.1	0.0001785	-0.00061±0.00006
8.088	288.2	0.0001527	0.0033	295.3	0.0001489	-0.00100±0.00017
8.500	353.8	0.0001244	0.0039	372.9	0.0001179	-0.00154±0.00016
8.989	482.1	0.0000913	0.0055	516.8	0.0000850	-0.00105±0.00005
9.447	572.4	0.0000769	0.0051	593.9	0.0000740	-0.00049±0.00002
9.921	622.3	0.0000707	0.0038	636.0	0.0000691	-0.00035±0.00002
Carbon Dioxide (1) + Ethanol (2) System at 308.15 K						
7.099	228.6	0.0001925	0.0045	235.7	0.0001867	-0.00109±0.00011
7.556	281.2	0.0001565	0.0051	297.3	0.0001481	-0.00150±0.00010
7.898	364.8	0.0001206	0.0037	404.7	0.0001088	-0.00309±0.00021
7.999	415.6	0.0001059	0.0028	469.7	0.0000937	-0.00425±0.00033
8.087	478.6	0.0000920	0.0051	549.4	0.0000801	-0.00223±0.00008
8.481	609.5	0.0000722	0.0033	627.3	0.0000702	-0.00055±0.00003
9.006	663.2	0.0000664	0.0027	672.1	0.0000655	-0.00026±0.00001
9.913	710.0	0.0000620	0.0027	716.3	0.0000615	-0.00014±0.00001

ρ_1^0, density of pure carbon dioxide; v_1^0, molar volume of pure carbon dioxide; y_2, mole fraction of alcohol in experimental dilution mixture; ρ, density of experimental mixture; v, molar volume of experimental mixture; $\bar{v}_2^\infty$, partial molar volume of alcohol at infinite dilution

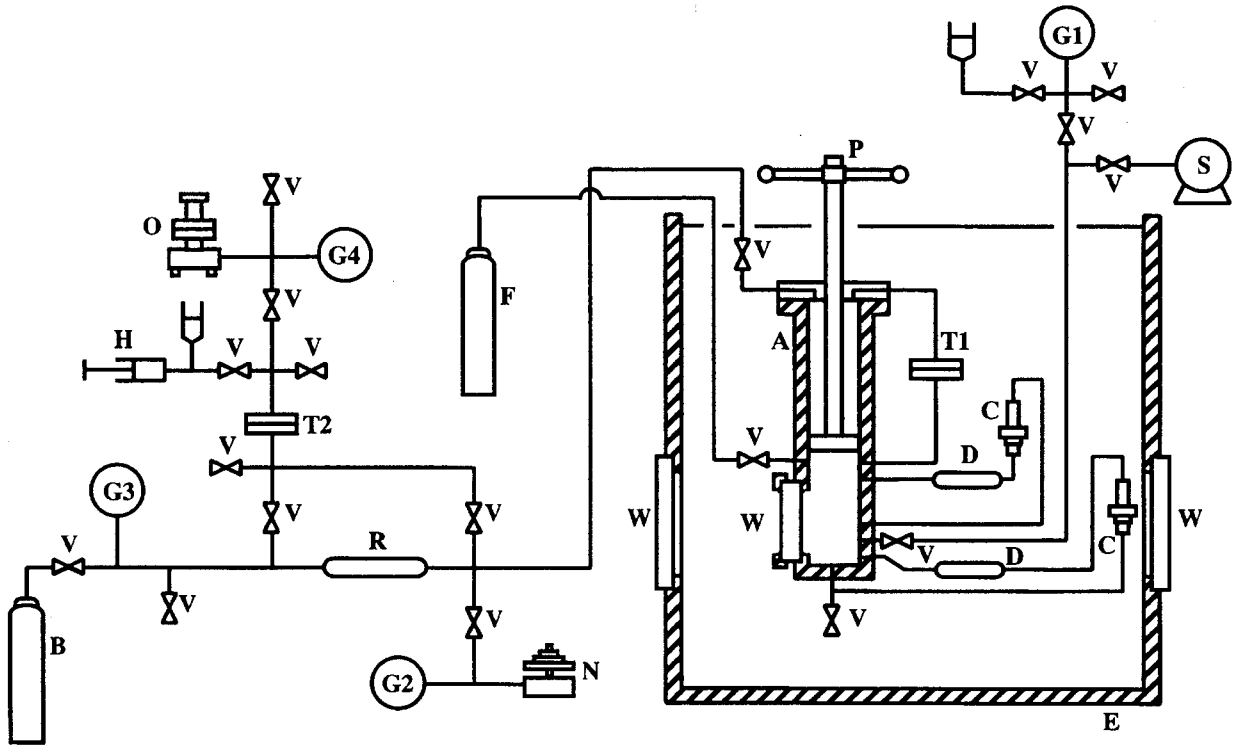

Fig. 2-1 Schematic diagram of experimental apparatus

A, variable volume cell; B, nitrogen reservoir; C, circulation pump; D, density meter; E, constant temperature liquid bath; F, gas reservoir; G, pressure gauge; H, hand pump; N, air dead weight gauge; O, oil dead weight gauge; P, piston; R, reservoir; S, HPLC pump; T, pressure transducer; V, valve; W, visual glass window

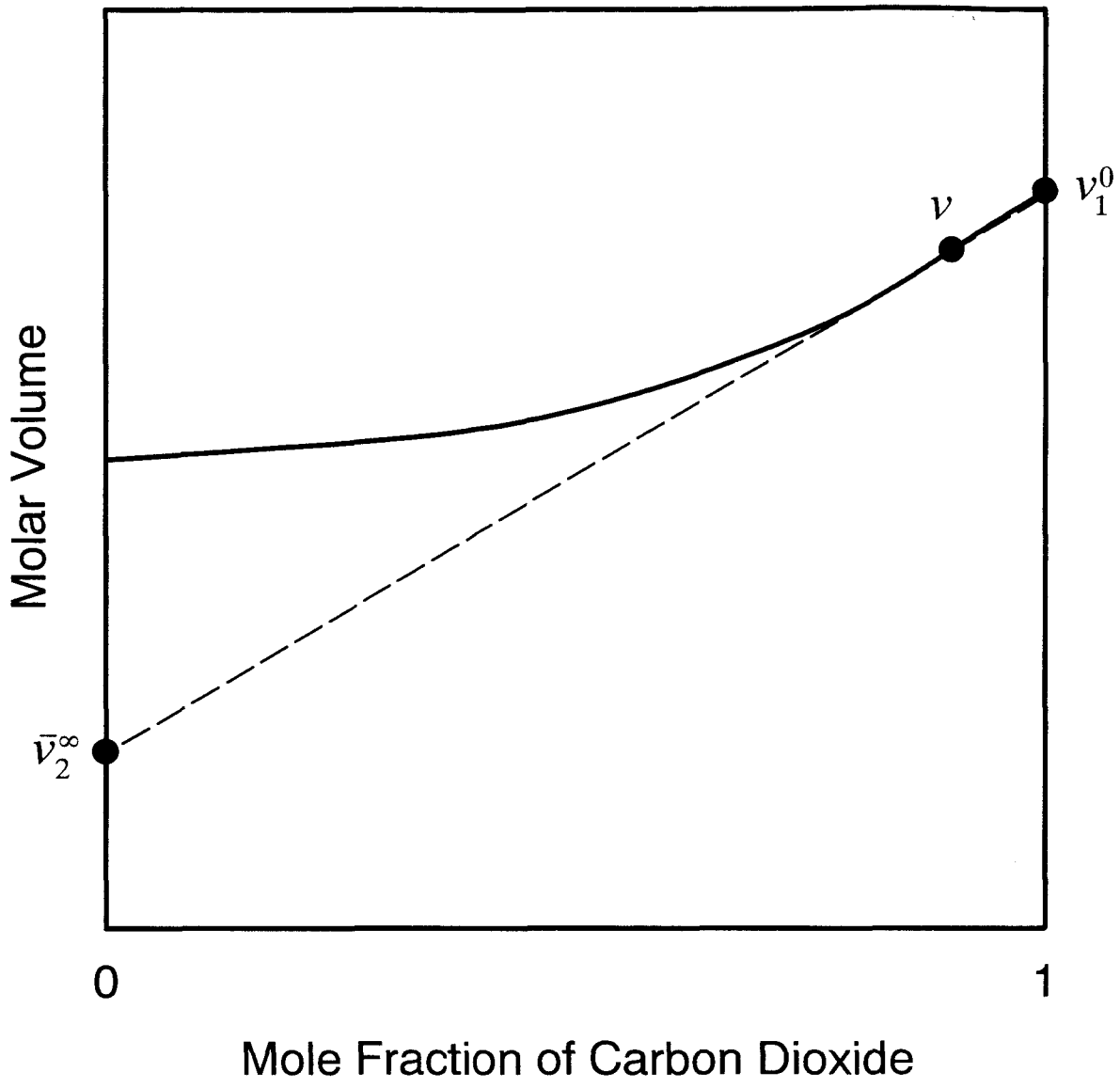

Fig. 2-2 Schematic diagram of molar volume

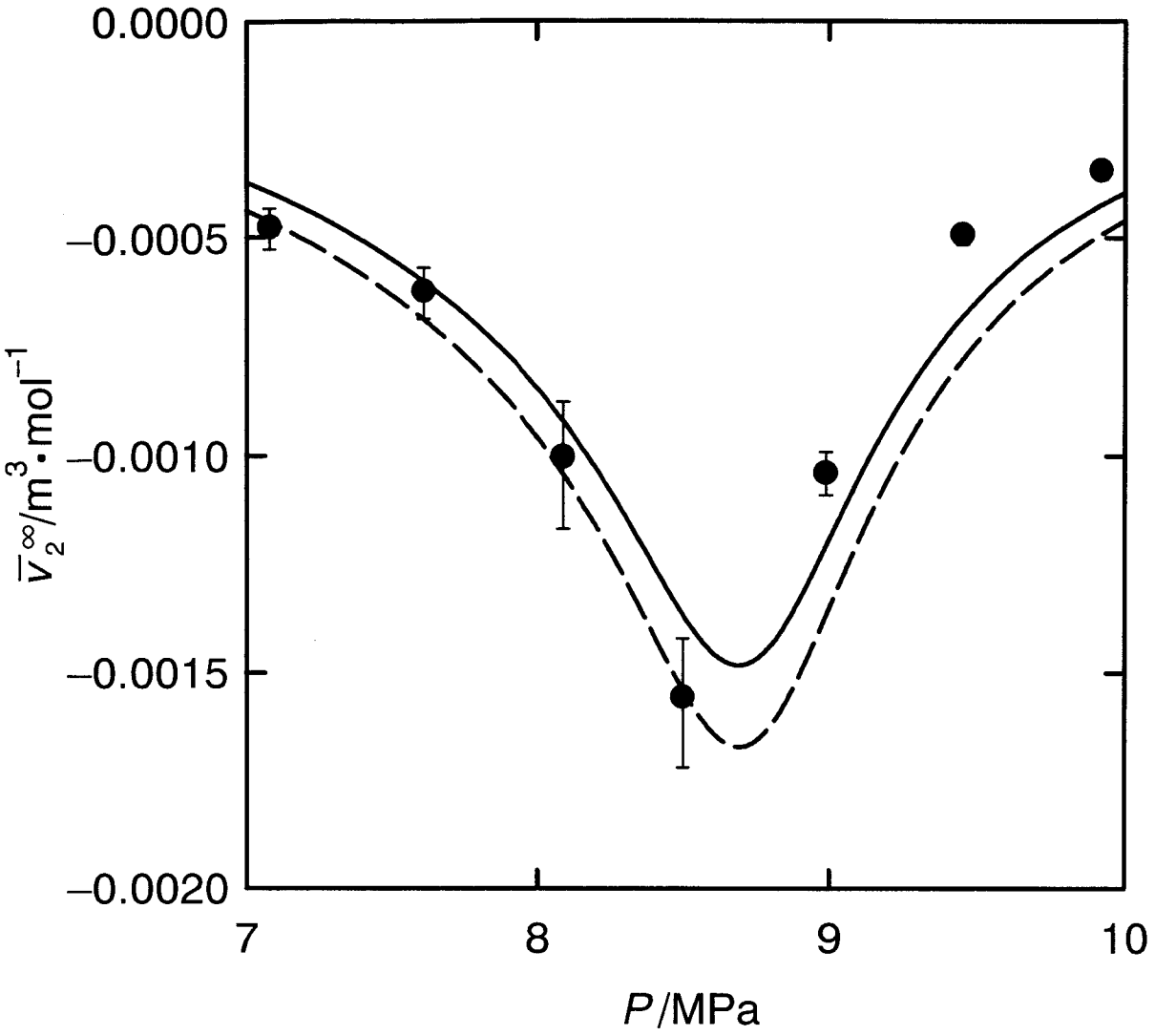

Fig. 2-3 Partial molar volume of methanol at infinite dilution in supercritical carbon dioxide at 313.15 K

●, experimental

———— , correlated by SRK EOS (k_{ij}=0.1136)

– – – – , predicted by SRK EOS (k_{ij}=0.0753; Kodama *et al.*, 1996)

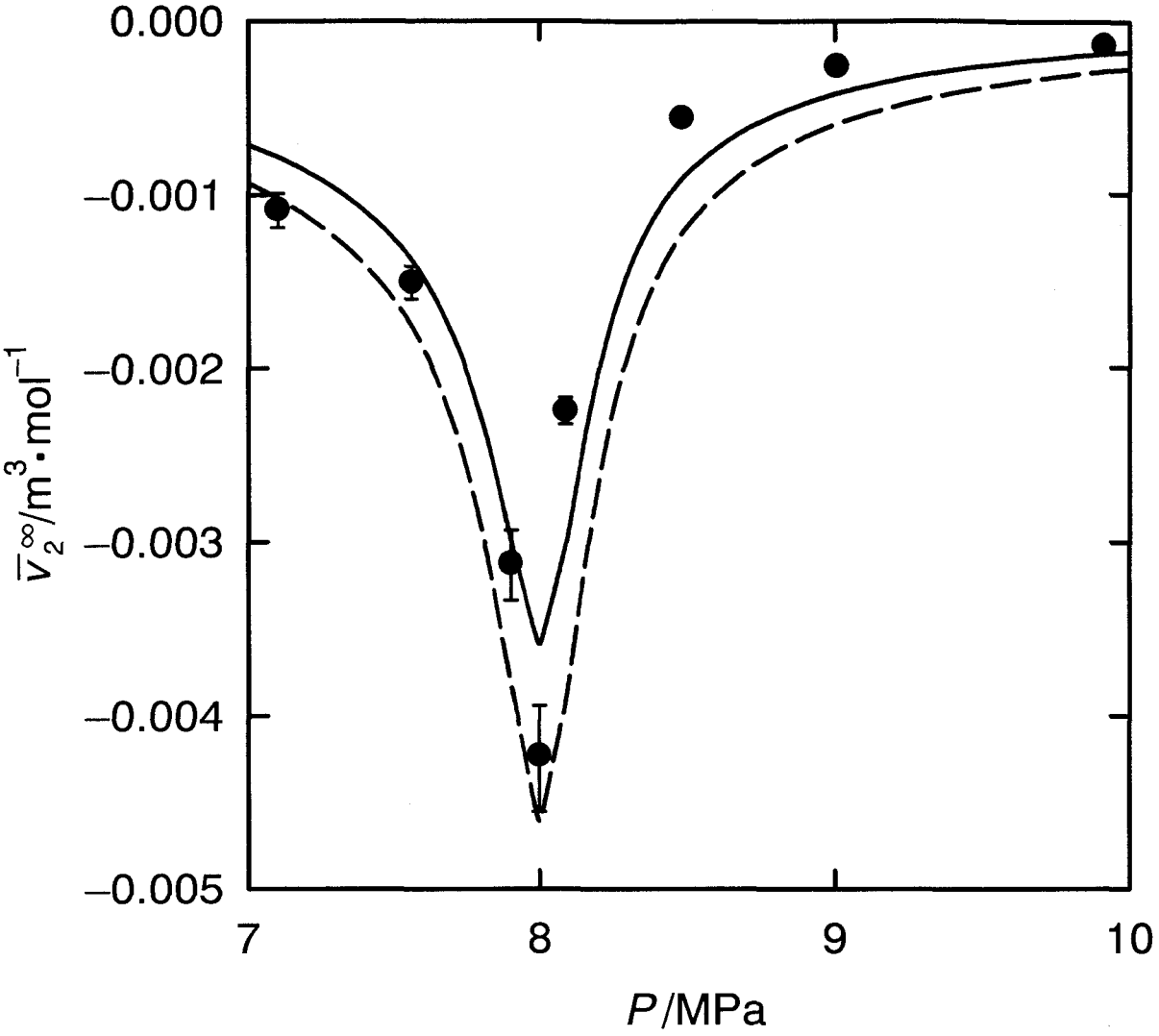

Fig. 2-4 Partial molar volume of ethanol at infinite dilution in supercritical carbon dioxide at 308.15 K

●, experimental

———, correlated by SRK EOS (k_{ij} =0.1605)

– – – –, predicted by SRK EOS (k_{ij} =0.0795; Tanaka and Kato, 1995)

Chapter 3 Saturated Densities of Carbon Dioxide + Water Mixture at 304.1 K and Pressures to 10 MPa

Introduction

Recently, the global warming has become a serious problem because of the rapid increase of carbon dioxide concentration in the atmosphere (Kojima, 1997; Akai, 1997). A method of carbon dioxide storage on the ocean floor using gas hydrates was proposed by Ohgaki and Inoue (1991). The sequestration of carbon dioxide in the deep ocean by shallow injection was further investigated by Haugan and Drange (1992). In the design and operation of storage process, the volumetric properties for the carbon dioxide + water system are required. King *et al.* (1992) reported few saturation densities for the carbon dioxide + water system at various temperatures.

In a high temperature region, the carbon dioxide and water system is also attractive as a candidate for supercritical-fluid solvent, because of its low energy cost in separation process. It is well known that carbon dioxide is the most popular gas in the supercritical fluid extraction.

In this chapter, the saturated densities of carbon dioxide + water system were measured at 304.1 K, critical temperature of carbon dioxide, and pressures up to 10 MPa, using the apparatus equipped with vibrating tube density meters. The densities of pure water were additionally measured.

3.1 Experimental

3.1.1 Materials

Carbon dioxide was supplied by Nihon Sanso Co. Ltd. with the guarantee of 99.9 mol% purity. Water was distillated and used in the experiment.

3.1.2 Experimental Apparatus

The experimental apparatus is completely the same as that described in the previous study (Kato *et al.*, 1991).

3.1.3 Experimental Procedures

At the start of the experiment, carbon dioxide was charged into the cell, after it was evacuated. Next, water was charged with the hand syringe pump to the cell. The phase separation was confirmed from visual glass window. The vapor in the cell was circulated into the liquid phase through the vibrating tube density meter by the circulation pump. The liquid was further circulated into the liquid phase through the density meter by the circulation pump. The pressure difference between the upper and lower spaces was kept null. After attainment of equilibrium state, the pressure, temperature and saturated densities of each phases were measured. Changing the cell volume with the piston, the saturation densities were measured at different pressure.

The experimental accuracies of density, temperature, and pressure were ±0.1 $kg \cdot m^{-3}$, ±0.01 K, and ±1 kPa, respectively.

3.2 Results and Discussion

Table 3-1 gives the experimental saturated densities of carbon dioxide + water system at 304.1 K, including the densities of pure water. The phase equilibria of vapor-liquid (VLE), liquid-liquid (LLE), and vapor-liquid-liquid (VLLE) were observed, as shown in **Table 3-1**. **Fig. 3-1** shows the experimental saturated densities, including the critical point of carbon dioxide given by Reid *et al* (1987). The critical point of carbon dioxide cannot be measured in the present study, by the reason of the limitation of the experimental apparatus. **Fig. 3-2** shows the expanded diagram in the vicinity of the vapor-liquid-liquid separation between 7.0 MPa and 7.5 MPa, in which the critical point of carbon dioxide is the reported value by Reid

et al. (1987) not the experimental one. The pressure-composition diagram at the critical temperature of carbon dioxide was reported by King *et al.* (1992), Takishima *et al.* (1986), Kuenen *et al.* (1899), and Wiebe *et al.* (1939, 1941). Only King *et al.* (1992) among the literature (King *et al.*, 1992; Takishima *et al.*, 1986; Kuenen *et al.*, 1899; Wiebe *et al.*, 1939, 1941) reported the density data.

Fig. 3-3 gives the densities of saturated liquid and pure water, comparing with the reported values by King *et al.* (1992) and Meyer *et al.* (1967). The dotted line in **Fig. 3-3** denotes the interpolated values at 304.1 K with Meyer *et al.* (1967). The average difference of the experimental density and the interpolated one of Meyer *et al.* (1967) for pure water was 0.5%. The present experimental densities of saturated liquid seem reasonable, considering the experimental temperatures are different as shown in **Fig. 3-3**. The density of saturated liquid was greater than the one of pure water at fixed pressure, as shown in **Table 3-1** and **Fig. 3-3**. This density behavior suggests the possibility of the storage of carbon dioxide into water. Converting the pressure to the water depth, **Fig. 3-4** was observed. As shown in **Fig. 3-4**, by the injection of carbon dioxide into the water at the depth of 200 m, the liquid saturated with carbon dioxide gives the density of 1002 $kg \cdot m^{-3}$ greater than the one of pure water. The saturated liquid is heavier than the pure water at the water depth. The saturated liquid obtained will drop to the depth of 1320 m, as schematically shown in **Fig. 3-5**. The present technique seems attractive to storage carbon dioxide into the ocean.

Summary

Saturated densities of carbon dioxide + water mixture were measured at 304.1 K and pressures up to 10 MPa, using the apparatus equipped with vibrating tube density meters. The phase separations of vapor-liquid, liquid-liquid, and vapor-liquid-liquid were observed. The densities of pure water were also measured. The density of saturated liquid was greater than that of pure water at fixed pressure.

As the first step of the researches on storage of carbon dioxide in the sea to prevent the global warming, the experimental temperature was 304.1 K to keep the satisfactory accuracy on the temperature control. The average temperature of the seawater is about 280.15 K lower than the present temperature 304.1 K. At present, the author however cannot control the temperature at 280.15 K with the satisfactory accuracy. Some improvements are required for the experiments at 280.15 K. In the near future, the author will challenge for the experiments at the temperature of the seawater 280.15 K, after the improvement of the apparatus. The author believes the volumetric properties are essential in the design and development of the process to prevent the global warming.

Table 3-1 Experimental densities for the carbon dioxide + water system at 304.1 K

	Density, $kg \cdot m^{-3}$			
P, MPa	Saturated Vapor	Saturated Liquid		Pure Water
1.000	18.8 [a]	999.4 [a]		996.0
2.000	41.8 [a]	1001.3 [a]		996.5
3.000	66.9 [a]	1004.4 [a]		996.9
4.000	95.7 [a]	1006.9 [a]		997.4
5.000	127.0 [a]	1009.0 [a]		997.9
6.000	169.0 [a]	1010.1 [a]		998.3
6.500	201.9 [a]	1010.7 [a]		——
7.000	254.2 [a]	1011.8 [a]		998.8
7.331	370.6 [b]	616.3 [b]	1012.4 [b]	——
7.337	386.2 [a]	575.4 [a]		——
7.500	——	633.9 [c]	1012.4 [c]	——
8.000	——	688.2 [c]	1012.7 [c]	999.2
8.500	——	716.2 [c]	1013.3 [c]	——
9.000	——	736.0 [c]	1013.9 [c]	999.6
9.500	——	751.8 [c]	1014.3 [c]	999.9
10.000	——	765.1 [c]	1014.7 [c]	1000.1

[a]Vapor-liquid equilibria, [b]Vapor-liquid-liquid equilibria, [c]Liquid-liquid equilibria

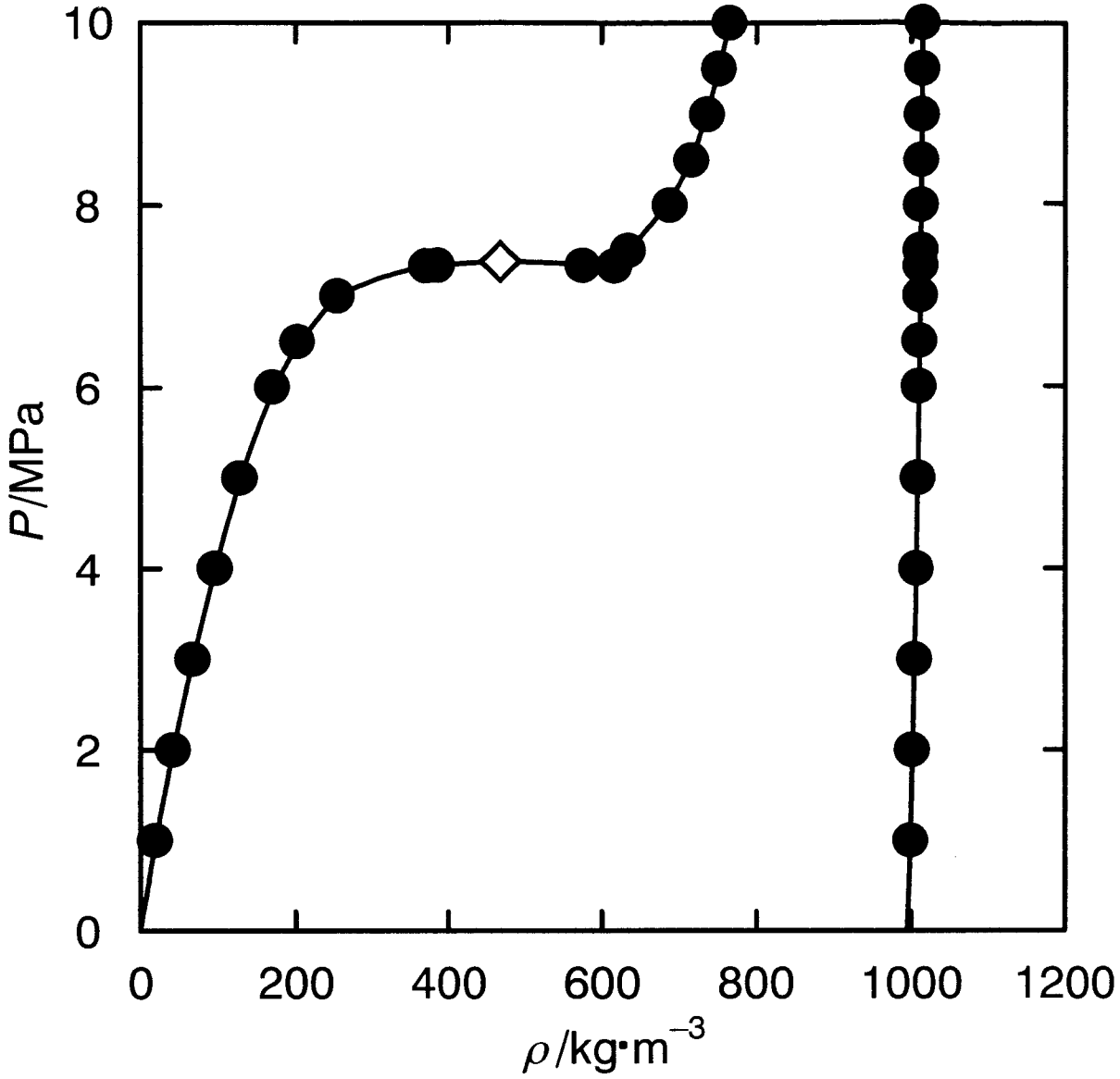

Fig. 3-1 Experimental saturated densities of carbon dioxide + water system at 304.1 K
—●— , experimental; ◇, critical point of carbon dioxide (Reid *et al.*, 1987)

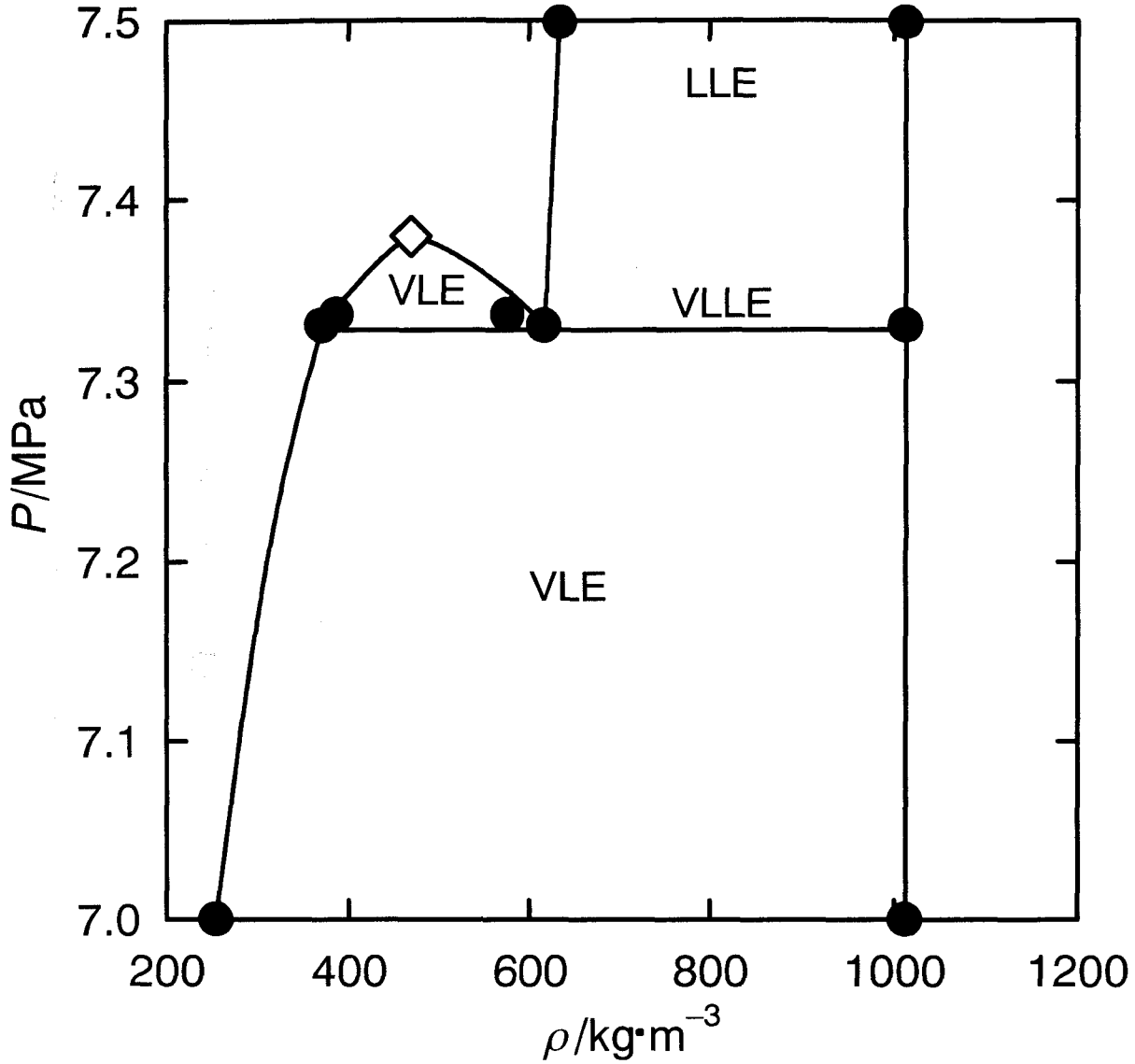

Fig. 3-2 Expanded diagram in the vicinity of vapor-liquid-liquid separation for the carbon dioxide + water system at 304.1 K

—●— , experimental; ◇, critical point of carbon dioxide (Reid *et al.*, 1987)

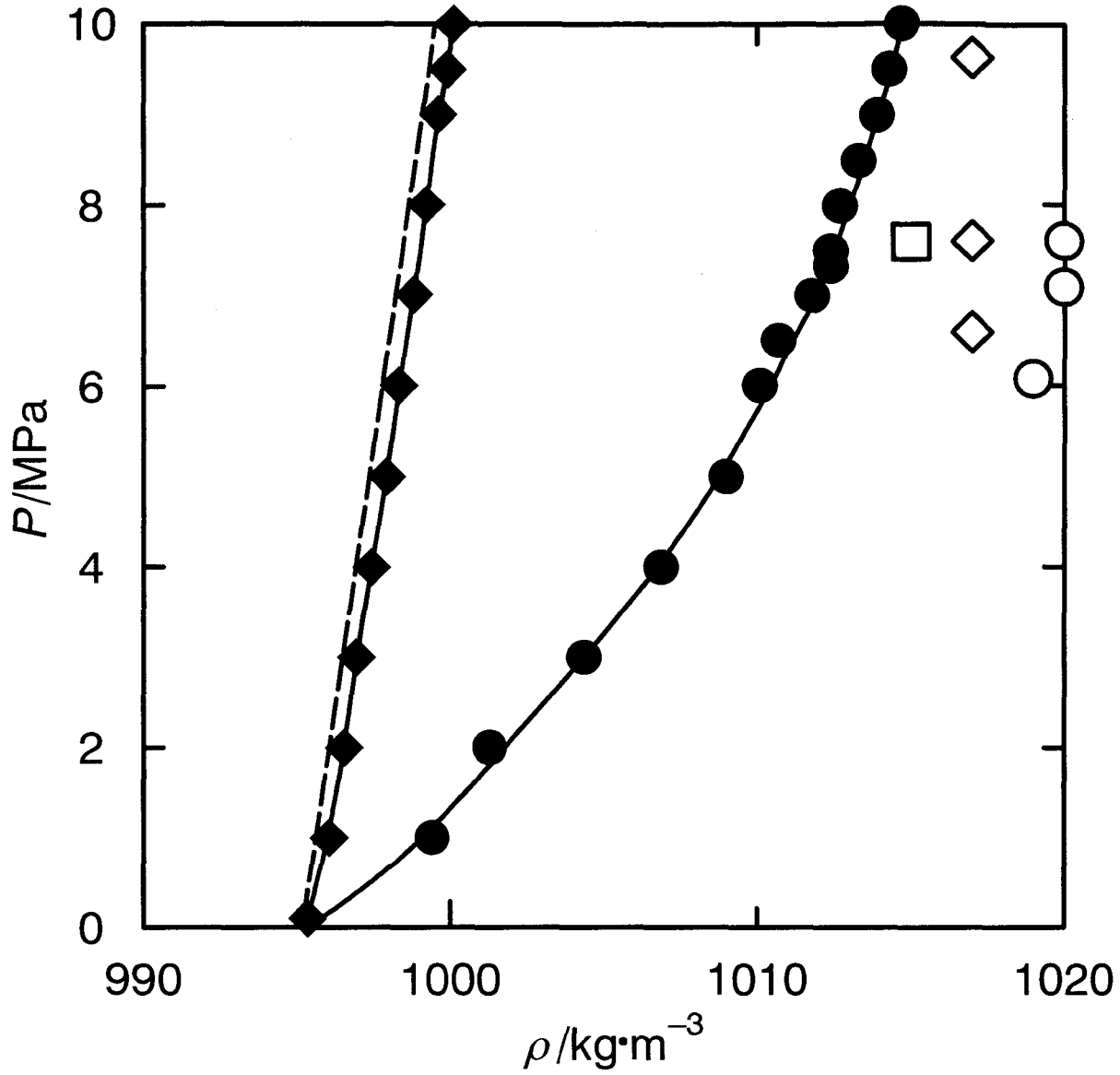

Fig. 3-3 Densities of saturated liquid and pure water at 304.1 K

<Saturated Liquid>

—●— , experimental;

reported (King *et al.*, 1992), ○, 288.2 K; ◇, 293.2 K; □, 298.2 K

<Pure Water>

—◆— , experimental; -------- , interpolated (Meyer *et al.*, 1967)

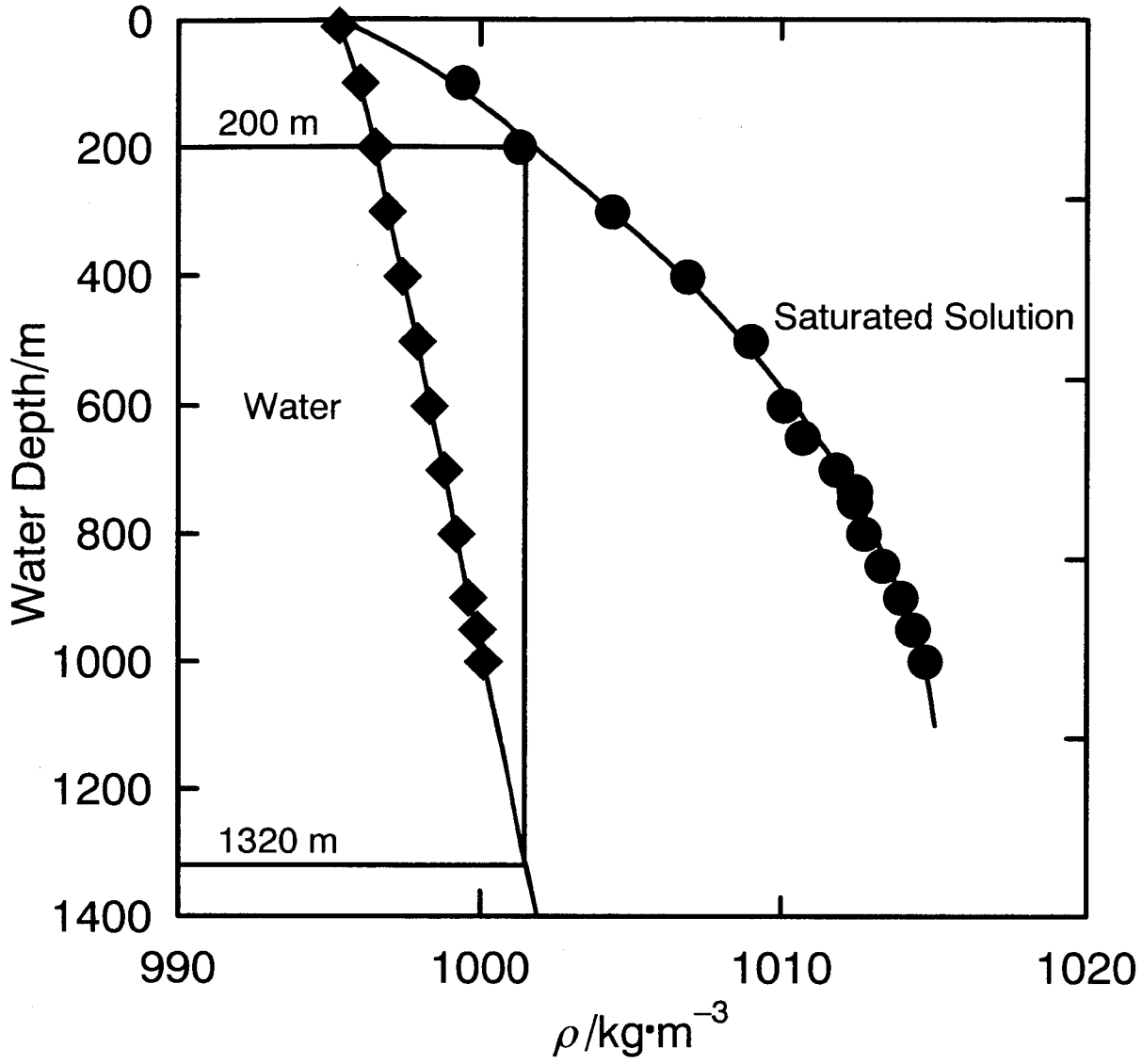

Fig. 3-4 Water depth *vs.* density diagram

—●— , saturated solution; —◆— , pure water

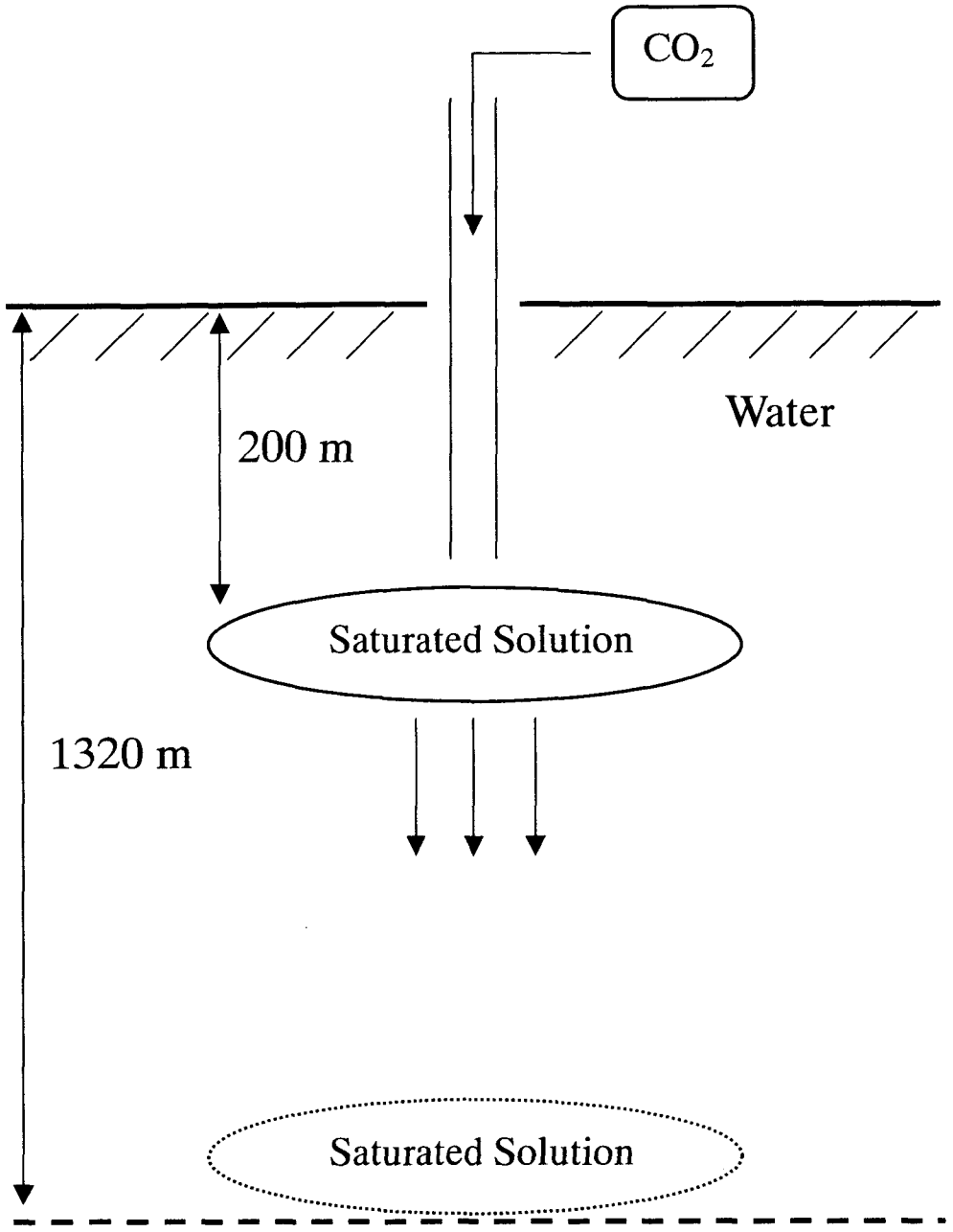

Fig. 3-5 Schematic diagram of carbon dioxide injection in ocean

Chapter 4 High Pressure Phase Equilibrium for Ethane + 1-Propanol at 314.15 K

Introduction

Phase equilibrium properties of mixtures at high pressures are required for practical use such as in the design and operation of separation equipment in the petroleum, natural gas, and related industries. Supercritical fluid extraction is now attractive as a separation technology.

Suzuki *et al.* (1990) previously reported vapor-liquid equilibria (VLE) for ethane + 1-propanol system at high pressures with a conventional circulation apparatus. They, however, reported no density data. Lam *et al.* (1990) previously reported only the vapor-liquid-liquid locus and their saturated density for ethane + 1-propanol system at high pressures, based on mass balance and phase rule.

A static-circulation apparatus equipped with three density meters for measuring vapor-liquid-liquid equilibria (VLLE) at high pressures was previously developed (Tanaka and Kato, 1995). With this apparatus, VLE and their saturated densities were measured for carbon dioxide + ethanol (Tanaka and Kato, 1995) and carbon dioxide + 1-butanol (Ishihara *et al.*, 1995) at high pressures. The phase equilibrium properties of ethane + methanol (Ishihara *et al.*, 1998) and ethane + ethanol (Kato *et al.*, 1999) have been recently measured, including VLLE.

In this chapter, the coexisting phase compositions and their saturated densities for the ethane + 1-propanol mixture at high pressures were measured at 314.15 K including in the vicinity of the critical region.

The phase equilibrium relations obtained in the present study are correlated with the SRK (Soave, 1972) and pseudocubic (Kato and Tanaka, 1986) equations of state.

4.1 Experimental

4.1.1 Materials

Ethane was supplied by Takachiho Chemical Industrial Co. Ltd. with the gas guarantee of 99.9% in purity. 1-Propanol was the special-grade reagent of Wako Pure Chemical Industries, Ltd. and was used without further purification. The purity of 1-propanol was determined to be 99.5% from gas chromatograph peak areas.

4.1.2 Experimental Apparatus

The experimental apparatus equipped with three density meters is completely the same as described previously (Tanaka and Kato, 1995). The schematic diagram of experimental apparatus is shown in **Fig. 4-1**. The apparatus is a static-circulation type, which can operate to a maximum temperature and pressure of 400 K and 20 MPa respectively, and has three Anton Paar DMA 512S vibrating tube density meters. The apparatus is in a constant-temperature liquid bath controlled within ±0.01 K. The cell volume is approximately 320 cm^3. The coexisting phases are continuously recirculated through the sampling valves and density meters with the three magnetic circulation pumps. Temperatures were measured with the Hewlett Packard 2804A quartz thermometer. Pressures were measured with the Ruska 2480-700 oil dead weight gauge and the Ruska 2439-702 pressure transducer. The equilibrium phase compositions were determined by using a Shimadzu GC-14A gas chromatograph equipped with a 3-m Porapak Q column. Helium was used as a carrier gas at a flow rate of 30 $cm^3 \cdot min^{-1}$. The injection temperature and column temperature were about 373 K and 369 K, respectively. The current value of a thermal conductivity detector (TCD) was 100 mA. The meters used in the present apparatus and their accuracies are shown in **Table 4-1**.

4.1.3 Experimental Procedures

The samples, ethane and 1-propanol, were charged into the cell after the evacuation of the cell. The fluid in the cell was mixed with the magnetic-driven agitator. Each phase was circulated through the circulation pump. After the steady state was established for 2 or 3 h, the agitator and circulation pumps were stopped. After 1 h, the densities and the pressure were measured with the density meters and the dead weight gauge, respectively. The sample of each phase was taken by the sampling valve and analyzed by gas chromatography after a circulation of 2 h in the sampling room.

4.2 Results and Discussion

Table 4-2 gives the experimental results of coexisting phase compositions and their saturated densities for the ethane + 1-propanol system at 314.15 K. The VLLE phase separation was observed at 5.489 MPa, as shown in **Table 4-2**. The uncertainties of the experimental equilibrium composition, density, temperature, and pressure are ±0.001 mole fraction, ±0.1 $kg \cdot m^{-3}$, ±0.1 K, and ±1 kPa, respectively. The uncertainty represents the difference between the experimental value and the absolute real one.

Fig. 4-2 gives the experimental pressure-composition diagram, including the values reported by Suzuki *et al.* (1990) and Lam *et al.* (1990). As shown in **Fig. 4-2**, the liquid data reported by Suzuki *et al.* (1990) certainly deviated from the present data with increasing pressures. The data reported by Suzuki *et al.* (1990) have no information near the VLLE region at high pressures. Lam *et al.* (1990) reported only VLLE, as shown in **Fig. 4-2**. **Fig. 4-3** gives the experimental saturated density, including the saturated VLLE density data of Lam *et al.* (1990).

Fig. 4-4 shows the expanded phase equilibrium diagram in the vicinity of critical region. When the present experimental VLLE data and the ones given by Lam *et al.* (1990) are compared, the differences of vapor, light liquid, and heavy liquid are 0.0192, 0.0034, and

0.0200 mole fraction, respectively. The VLLE pressure difference between the present study and that of Lam *et al.* (1990) is only 0.012 MPa, as shown in **Fig. 4-4**. The saturated vapor and liquid density data in the present study deviated from the ones reported by Lam *et al.* (1990), as shown in **Fig. 4-5**. When the present experimental VLLE data and the ones reported by Lam *et al.* (1990) are compared, the density differences of vapor, light liquid, and heavy liquid are 36.59, 25.13, and 43.5 $kg \cdot m^{-3}$, respectively. In **Figs. 4-2** to **4-5**, the solid lines were smoothly drawn for the present experimental data obtained, considering the present experimental uncertainties.

When the reliabilities of the experimental apparatus and the meters for measuring the density, temperature, pressure, and compositions are considered, the present experimental data seem the most reliable.

4.3 Correlations

The experimental data obtained were correlated with the conventional SRK (Soave, 1972) equation of state and the pseudocubic (Kato and Tanaka, 1986) equation of state.

The pseudocubic (Kato and Tanaka, 1986) equation of state is expressed as follows:

$$P = \frac{RT}{V^* - b} - \frac{a}{V^{*2}}, \qquad V^* = \frac{(V - \varepsilon b)(V + \sigma b)}{V} \tag{4-1}$$

$$\varepsilon = (1-\theta)(\xi - 2), \qquad \sigma = (1-\theta)(\xi + 2) \tag{4-2}$$

$$\xi = \sqrt{\frac{4-\theta}{1-\theta}}, \qquad \theta = \frac{8Z_c}{3}, \qquad Z_c = \frac{P_c V_c}{RT_c} \tag{4-3}$$

$$a = K_a a_c, \qquad b = \frac{RT_c}{8P_c}, \qquad a_c = \frac{27(RT_c)^2}{64P_c} \tag{4-4}$$

$$\ln K_a = S\left(1 - \sqrt{T_r}\right), \qquad S = 1.1746 + 3.4539\omega \tag{4-5}$$

where P, R, T, V, Z, and ω, respectively, denote the pressure, gas constant, temperature, molar volume, compressibility factor, and acentric factor. K_a, S, a, b, ε,

θ, σ, and ξ represent the parameters. The subscripts c and r denote the critical properties and reduced properties, respectively. The asterisk indicates the apparent value.

The following mixing rules were first used, introducing binary interaction parameter k_{ij}:

$$a = \sum_i \sum_j x_i x_j a_{ij}, \qquad b = \sum_i \sum_j x_i x_j b_{ij}, \qquad \theta = \sum_i x_i \theta_i \tag{4-6}$$

$$a_{ij} = (1 - k_{ij})\sqrt{a_i a_j}, \qquad b_{ij} = \frac{b_i + b_j}{2} \tag{4-7}$$

where x represents the mole fraction. The subscripts i and j denote the components.

The binary interaction parameter k_{12} was evaluated as 0.0907 from the present experimental bubble point-pressure data in the lower pressure regions.

The following mixing rules (Yoshikawa *et al.*, 1994) were further used in the present calculations, introducing two binary interaction parameters, k_{112} and k_{122}, almost similar to that of Hattori *et al.* (1986).

$$a = \sum_i \sum_j \sum_k x_i x_j x_k a_{ijk}, \qquad b = \sum_i \sum_j x_i x_j b_{ij}, \qquad b_{ij} = \frac{b_i + b_j}{2} \tag{4-8}$$

$$a_{112} = (1 - k_{112}) a_1^{2/3} a_2^{1/3}, \qquad a_{122} = (1 - k_{122}) a_1^{1/3} a_2^{2/3} \tag{4-9}$$

where the subscripts 1, 2, and k denote the components.

The binary interaction parameters, k_{112} and k_{122}, were evaluated as -0.0146 and -0.0475 from the present experimental bubble point-pressure data in the lower pressure regions, respectively.

In the correlations, the critical values and acentric factors of ethane and 1-propanol were obtained from the work of Reid *et al.* (1987).

Calculation results with the equations of state are shown in **Figs. 4-2** to **4-5**. Some difficulties were in the correlations with the equations of state, by the reason of complex phase equilibrium diagrams shown in **Figs. 4-2** to **4-5**. The equation of state is generally applied for the VLE correlation, mainly for the pressure-composition behavior not for the saturated vapor and liquid density behavior. The equation of state is an surely excellent tool

for correlation of the VLE composition behavior but poor for VLE density behavior. The present experimental data contain the VLE, VLLE, and LLE compositions and further their saturated densities. The perfect correlation of the present complex data with the equation of state is terribly troublesome. The authors are awaiting a new excellent equation of state and its mixing rules for the correlation of the present data with the satisfactory accuracies.

Summary

Phase equilibria and saturated densities for the ethane + 1-propanol system at high pressures were measured at 314.15 K with the static-circulation apparatus, including the VLLE. The experimental data obtained were correlated by the equations of state with little accuracy, due to the complex phase separation behaviors.

For the purification of ethanol from biomass alcohols, the supercritical carbon dioxide has a limitation, considering the similar shapes of the pressure-composition diagrams for different alcohols. Ethane seems to have the possibility as the effective supercritical fluids for the purification of ethanol from the biomass solution.

Table 4-1 Meters used in the present apparatus

Meters	Type	Pressure range	Accuracy
Density meter	Anton Paar DMA 512S	0 – 40 MPa	0.1 $kg \cdot m^{-3}$
Thermometer	Hewlett Packard 2804A	Resolution 0.0001 K	
Pressure gauge	Ruska 2480-700 (Oil DWG)	0.22 – 103 MPa	0.01%
Pressure transducer	Ruska 2439-702	– 103 MPa	5 ppm

Table 4-2 Saturation pressure P, liquid mole fraction x, vapor mole fraction y, liquid density ρ_L, and vapor density ρ_V for the ethane (1) + 1-propanol (2) at 314.15 K

P/MPa	x_1	y_1	ρ_L/(kg·m^{-3})	ρ_V/(kg·m^{-3})
1.609[a]	0.134[a]	0.991[a]	750.8[a]	21.4[a]
3.317[a]	0.300[a]	0.993[a]	697.5[a]	54.1[a]
4.550[a]	0.457[a]	0.993[a]	639.1[a]	90.3[a]
5.487[a]	0.782[a]	0.975[a]	475.4[a]	184.2[a]
5.489[b]	0.799[b], 0.903[b]	0.965[b]	450.2[b], 367.1[b]	187.7[b]
5.507[a]	0.964[a]	0.985[a]	296.6[a]	203.6[a]
5.512[a]	0.982[a]	0.996[a]	275.7[a]	222.7[a]
5.519[c]	0.810[c], 0.900[c]	——	451.3[c], 374.3[c]	——
5.537[c]	0.815[c], 0.898[c]	——	448.1[c], 383.5[c]	——

[a]Vapor-liquid equilibria. [b]Vapor-liquid-liquid equilibria. [c]Liquid-liquid equilibria.

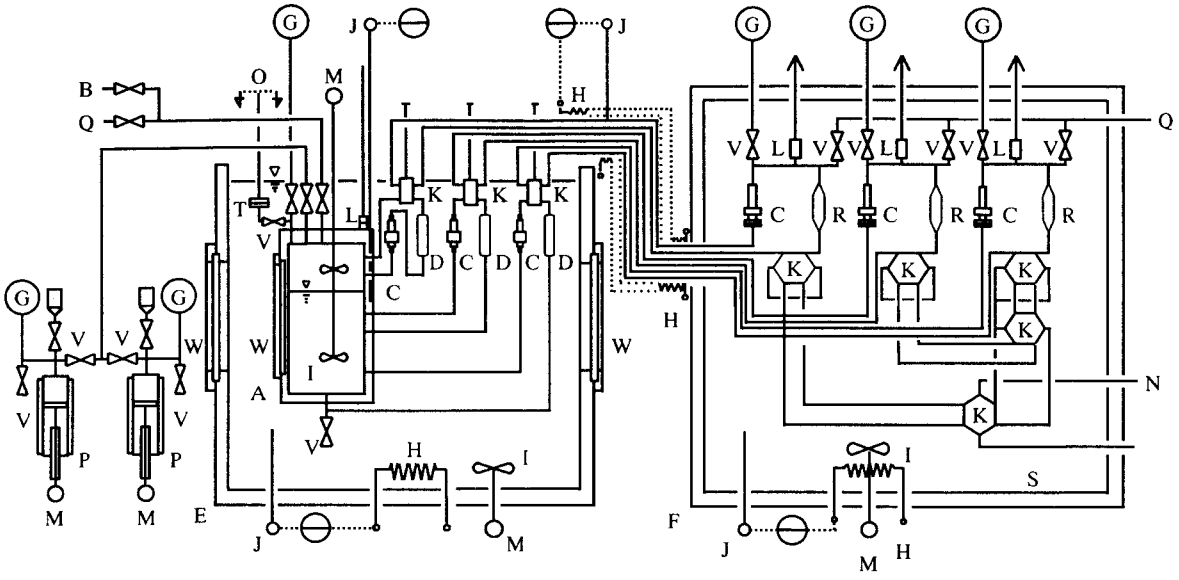

Fig. 4-1 Schematic diagram of experimental apparatus

A, equilibrium cell; B, to sample reservoir; C, circulation pump; D, density meter; E, constant temperature liquid bath; F, constant temperature air bath; G, pressure gauge, H, heater, I, agitator, J, thermometer; K, sampling valve; L, safety valve; M, motor; N, to gas chromatograph; O, to oil dead weight gauge; P, sample charging pump; Q, to vacuum pump; R, surge tank; S, sampling system; T, pressure transducer; V, valve; W, visual glass window

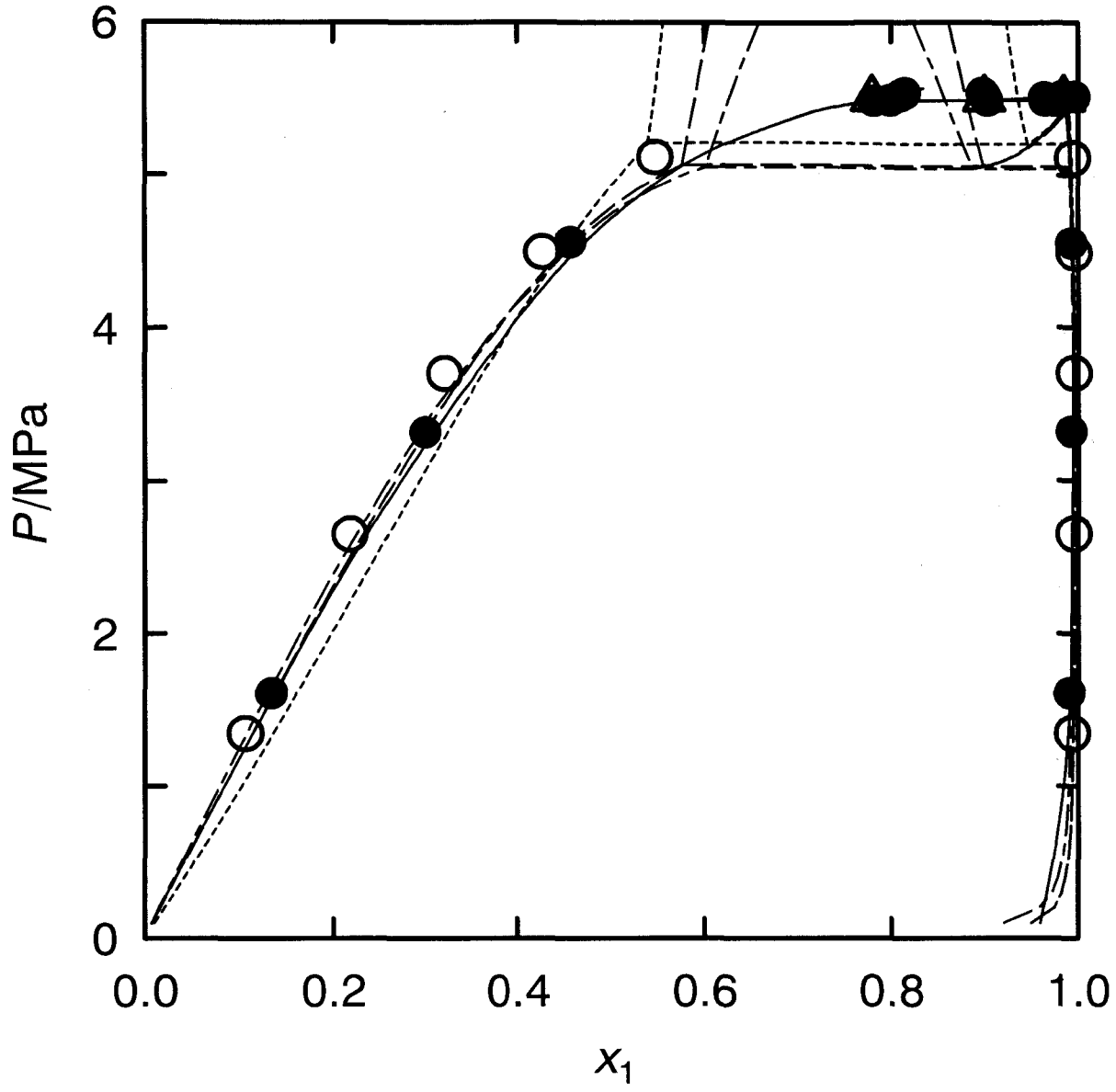

Fig. 4-2 Phase equilibria for the ethane (1) + 1-propanol (2) system at 314.15 K

—●—, this work; ○, literature data (Suzuki *et al.*, 1990); △, literature data (Lam *et al.*, 1990); – – – – –, pseudocubic EOS with two parameters (k_{112}=-0.0146, k_{122}=-0.0475); --------, pseudocubic EOS with one parameter (k_{12}=0.0907); –·–·–·–, SRK EOS (k_{12}=0.0425)

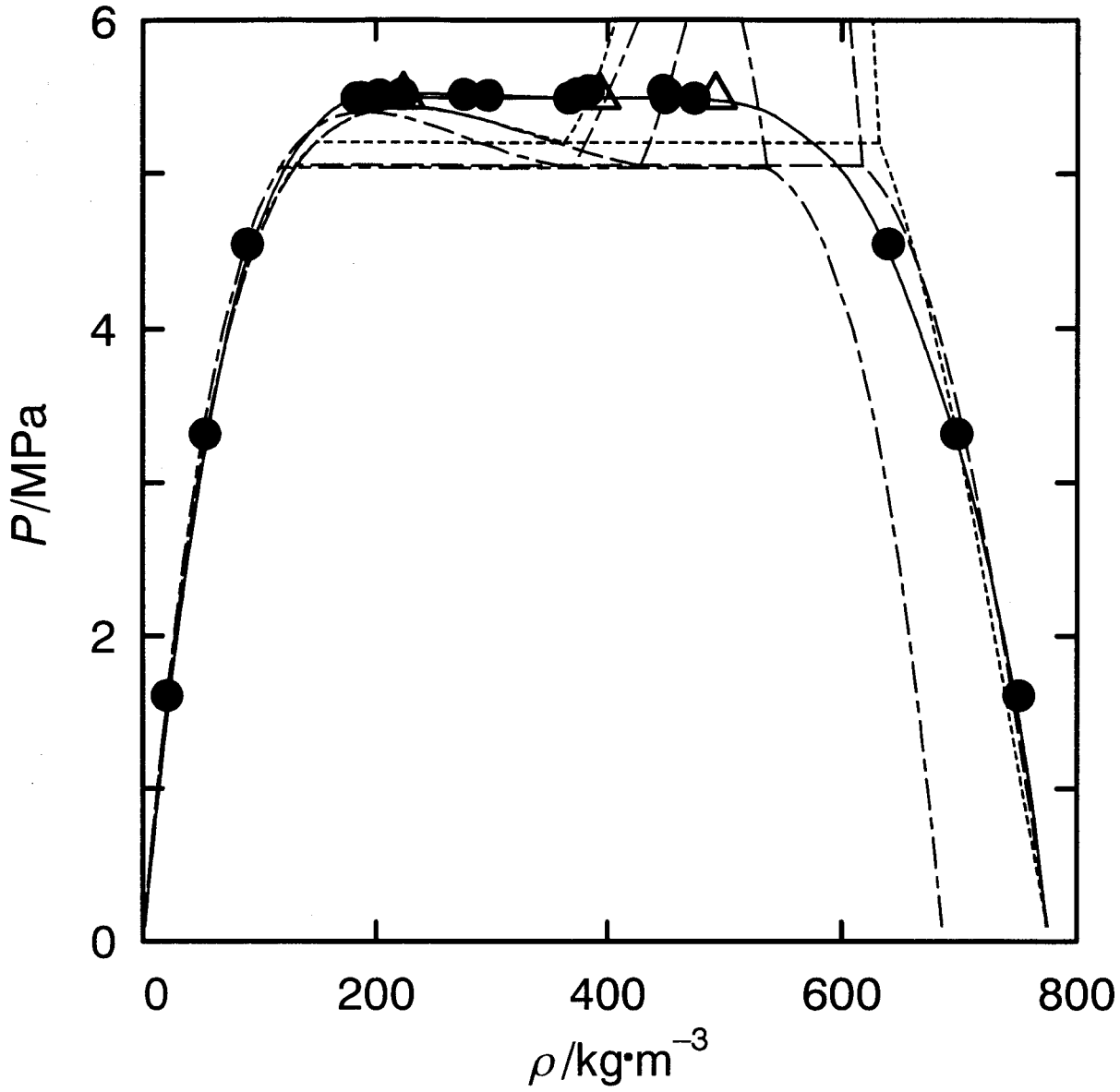

Fig. 4-3 Saturated densities for the ethane (1) + 1-propanol (2) system at 314.15 K —●—, this work; △, literature data (Lam *et al.*, 1990); – – – – –, pseudocubic EOS with two parameters (k_{112}=-0.0146, k_{122}=-0.0475); --------, pseudocubic EOS with one parameter (k_{12}=0.0907); –·–·–·–, SRK EOS (k_{12}=0.0425)

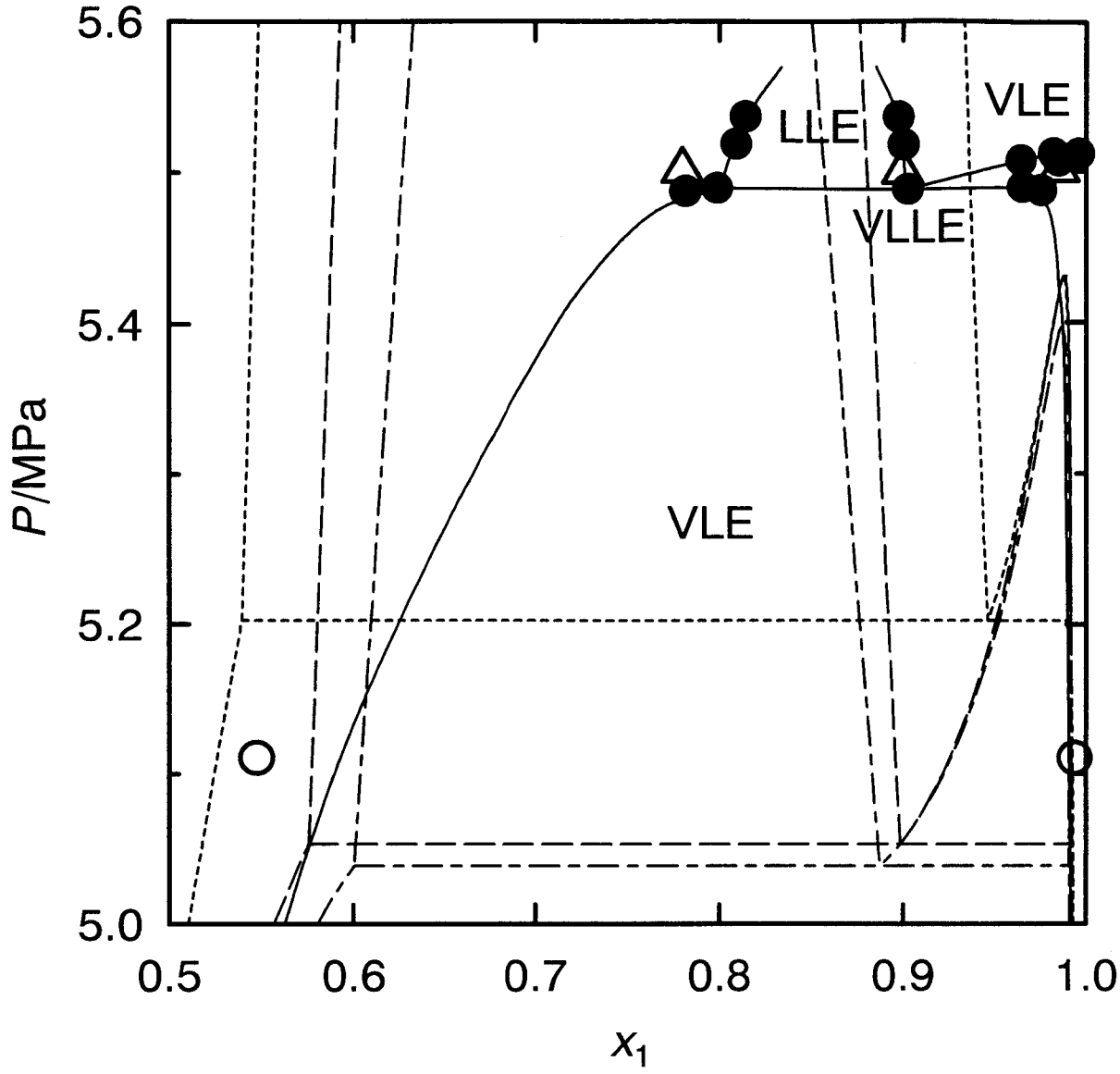

Fig. 4-4 Expanded phase equilibrium diagram in the vicinity of the critical point —●—, this work; ○, literature data (Suzuki *et al.*, 1990); △, literature data (Lam *et al.*, 1990); – – – – –, pseudocubic EOS with two parameters (k_{112}=-0.0146, k_{122}=-0.0475); - - - - - - - -, pseudocubic EOS with one parameter (k_{12}=0.0907); —·—·—·—, SRK EOS (k_{12}=0.0425)

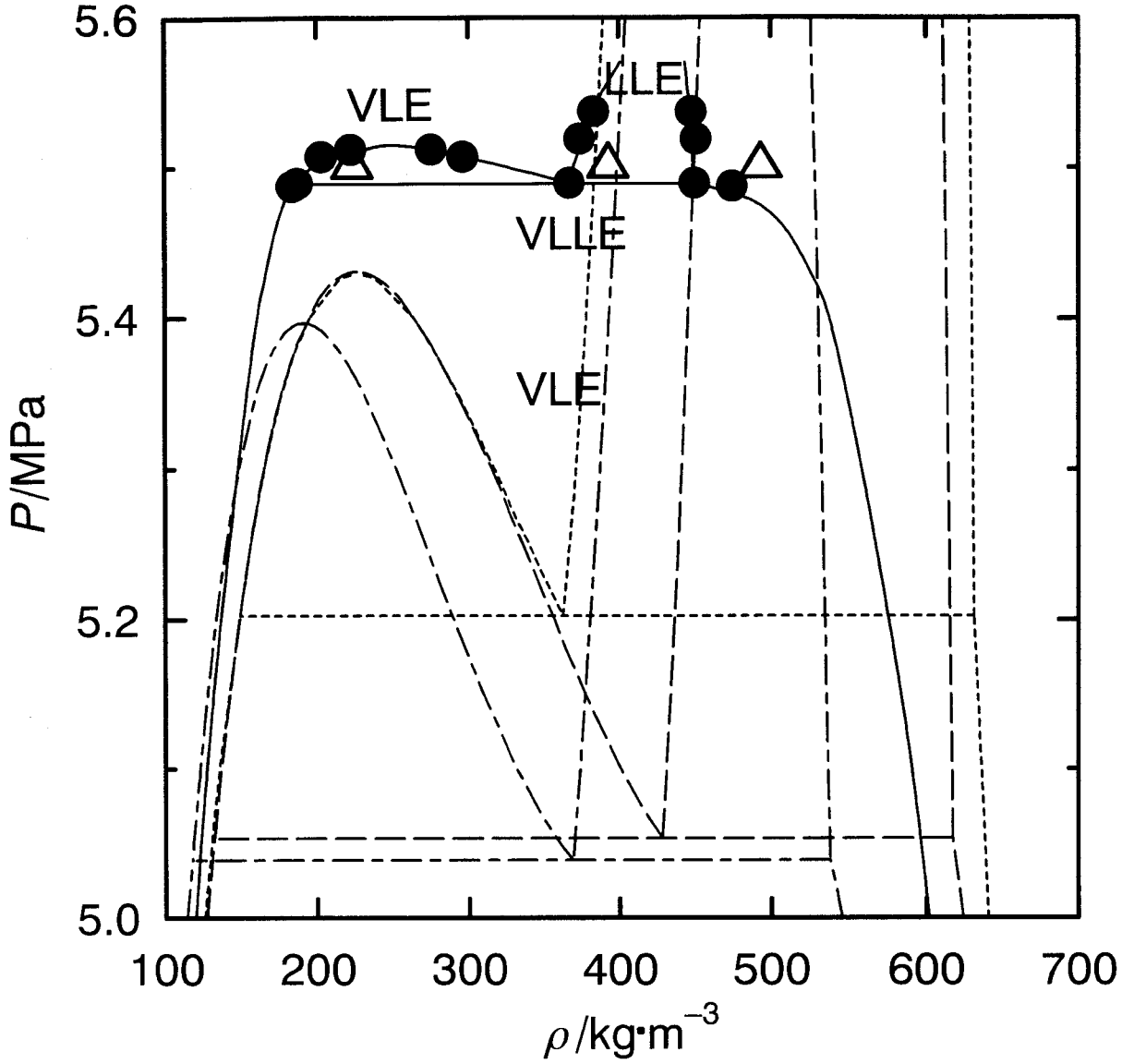

Fig. 4-5 Expanded saturated densities in the vicinity of the critical point

—●—, this work; △, literature data (Lam *et al.*, 1990); – – – – –, pseudocubic EOS with two parameters (k_{112}=-0.0146, k_{122}=-0.0475); --------, pseudocubic EOS with one parameter (k_{12}=0.0907); —·—·—, SRK EOS (k_{12}=0.0425)

Chapter 5 High-Pressure Phase Equilibrium for Ethane + 2-Propanol at 308.15 K and 313.15 K

Introduction

Phase equilibrium properties of mixtures at high pressures are required for practical use such as in the design and operation of separation equipment in the petroleum, natural gas, and related industries. Supercritical fluid extraction is now attractive as a separation technology.

Kuenen *et al.* (1899) previously reported only the upper critical end point (UCEP) as 317.15 K and the approximate lower critical end point (LCEP) range from 311.15 K to 315.15 K. Kuenen *et al.* (1899) further observed the three layers at temperatures below 311.15 K down to about 298.15 K. Kuenen *et al.* (1899) suggested that the phase separation behaviors are probably due impurities in 2-propanol. There are no published data on the vapor-liquid equilibria (VLE) for the ethane + 2-propanol system.

A static-circulation apparatus equipped with three density meters for measuring vapor-liquid-liquid equilibria (VLLE) at high pressures was described previously (Tanaka and Kato, 1995). With this apparatus, VLE and their saturated densities were measured for carbon dioxide + ethanol (Tanaka and Kato, 1995) and carbon dioxide + 1-butanol (Ishihara *et al.*, 1996) at high pressures. The phase equilibrium properties of ethane + methanol (Ishihara *et al.*, 1998), ethane + ethanol (Kato *et al.*, 1999), and ethane + 1-propanol (Kodama *et al.*, 2001) have been recently measured, including VLLE.

In this chapter, the coexisting phase compositions and their saturated densities for the ethane + 2-propanol mixture at high pressures were measured at 308.15 K and 313.15 K including in the vicinity of the critical region.

The phase equilibrium relations obtained in the present study are correlated with the SRK (Soave, 1972) and pseudocubic (Kato and Tanaka, 1986) equations of state.

5.1 Experimental

5.1.1 Materials

Ethane was supplied by Takachiho Chemical Industrial Co. Ltd. with the gas guarantee of 99.9% in purity. 2-Propanol was the special-grade reagent of Wako Pure Chemical Industries, Ltd. and was used without further purification. The purity of 2-propanol was determined to be 99.9% from gas chromatograph peak areas.

5.1.2 Experimental Apparatus

The apparatus and experimental procedures (Tanaka and Kato, 1995) are the same as described in the previous chapter. The apparatus is a static-circulation type, which can operate to a maximum temperature and pressure of 400 K and 20 MPa respectively, and has three Anton Paar DMA 512S vibrating tube density meters. The apparatus is in a constant-temperature liquid bath controlled within ±0.01 K. The cell volume is approximately 320 cm^3. The coexisting phases are continuously recirculated through the sampling valves and density meters with the three magnetic circulation pumps. Temperatures were measured with the Hewlett Packard 2804A quartz thermometer. Pressures were measured with the Ruska 2480-700 oil dead weight gauge and the Ruska 2439-702 pressure transducer. The equilibrium phase compositions were determined by using a Shimadzu GC-14A gas chromatograph equipped with a 3-m Porapak Q column. Helium was used as a carrier gas at a flow rate of 30 $cm^3 \cdot min^{-1}$. The injection temperature and column temperature were about 423 K and 403 K, respectively. The current value of a thermal conductivity detector (TCD) was 100 mA.

5.1.3 Experimental Procedures

The samples, ethane and 2-propanol, were charged into the cell after the evacuation of the cell. The fluid in the cell was mixed with the magnetic-driven agitator. Each phase was

circulated through the circulation pump. After the steady state was established for 2 or 3 h, the agitator and circulation pumps were stopped. After 1 h, the densities and the pressure were measured with the density meters and the dead weight gauge, respectively. The sample of each phase was taken by the sampling valve and analyzed by gas chromatography after the circulation of 2 h in the sampling room.

5.2 Results and Discussion

Tables 5-1 and **5-2** give the experimental results of coexisting phase compositions and their saturated densities for the ethane + 2-propanol system at 308.15 K and 313.15 K, respectively. For ethane + 1-propanol in the previous results (Kodama *et al.*, 2001), VLLE phase separation was observed similar to Kuenen *et al.* (1899). VLLE phase separation was however not observed in the present experiments for ethane + 2-propanol system. The uncertainties of the experimental equilibrium composition, density, temperature, and pressure are ±0.001 mole fraction, ±0.1 kg·m^{-3}, ±0.1 K, and ±1 kPa, respectively.

Figs. 5-1 and **5-2**, respectively, give the pressure-composition and the saturated density diagrams at 308.15 K. **Figs. 5-3** and **5-4** show the results at 313.15 K. In **Figs. 5-1** to **5-4**, the solid lines denote the experimental smoothed curves drawn by considering the uncertainties of the experimental data.

5.3 Correlations

The experimental data obtained were correlated with the conventional SRK (Soave, 1972) equation of state and the pseudocubic (Kato and Tanaka, 1986) equation of state.

The pseudocubic (Kato and Tanaka, 1986) equation of state is expressed as follows:

$$P = \frac{RT}{V^* - b} - \frac{a}{V^{*2}}, \qquad V^* = \frac{(V - \varepsilon b)(V + \sigma b)}{V} \tag{5-1}$$

$$\varepsilon = (1-\theta)(\xi - 2), \qquad \sigma = (1-\theta)(\xi + 2) \tag{5-2}$$

$$\xi = \sqrt{\frac{4-\theta}{1-\theta}}, \qquad \theta = \frac{8Z_c}{3}, \qquad Z_c = \frac{P_c V_c}{RT_c} \tag{5-3}$$

$$a = K_a a_c, \qquad b = \frac{RT_c}{8P_c}, \qquad a_c = \frac{27(RT_c)^2}{64P_c} \tag{5-4}$$

$$\ln K_a = S\left(1 - \sqrt{T_r}\right), \qquad S = 1.1746 + 3.4539\omega \tag{5-5}$$

where P, R, T, V, Z, and ω, respectively, denote the pressure, gas constant, temperature, molar volume, compressibility factor, and acentric factor. K_a, S, a, b, ε, θ, σ, and ξ represent the parameters. The subscripts c and r denote the critical properties and reduced properties, respectively. The asterisk indicates the apparent value.

The following mixing rules were used, introducing binary interaction parameter k_{ij}:

$$a = \sum_i \sum_j x_i x_j a_{ij}, \qquad b = \sum_i \sum_j x_i x_j b_{ij}, \qquad \theta = \sum_i x_i \theta_i \tag{5-6}$$

$$a_{ij} = (1 - k_{ij})\sqrt{a_i a_j}, \qquad b_{ij} = \frac{b_i + b_j}{2} \tag{5-7}$$

where x represents the mole fraction. The subscripts i and j denote the components.

The binary interaction parameter k_{12} was evaluated as 0.1055 at 308.15 K and 0.1097 at 313.15 K, respectively, from the present experimental bubble point-pressure data in the lower pressure regions for the SRK and the pseudocubic equations.

In the correlations, the critical values and acentric factors of ethane and 2-propanol were obtained from the work of Reid *et al.* (1987).

Calculation results with the equations of state are shown in **Figs. 5-1** to **5-4**. In **Figs. 5-1** to **5-4**, the solid, dotted, and broken lines, respectively, denote the experimental smoothed data, the calculation results by the SRK equation, and the ones by the pseudocubic equation. In **Figs. 5-1** to **5-4**, the horizontal lines denote the VLLE separation ranges calculated with equations of state. As shown in **Figs 5-1** to **5-4**, the VLLE separations in the narrow composition ranges were calculated by the equations of state. The equation of state is

generally applied for the VLE correlation, mainly for the pressure-composition behavior, not for the saturated vapor and liquid density behavior.

Summary

Phase equilibria and saturated densities for the ethane + 2-propanol at high pressures were measured at 308.15 K and 313.15 K with the static-circulation apparatus. The experimental data obtained were correlated by the equations of state.

The old literature of Kuenen *et al.* (1899) is however useful now because of their excellent equilibrium data. The author believes the reliable equilibrium data have no death for worth in the present and future. The author sincerely hopes the unlimited life of the present equilibrium data reported here will be permanently alive.

The author has to say that the experimental temperature should be about 316.15 K, considering UCEP and LCEP given by Kuenen *et al.* (1899). It was not possible, however, the author thought about constraint of an experimental apparatus. The present experimental temperatures are not suitable to check the possibility of the three phase separations. The author would like to do it with future assignment.

Table 5-1 Saturation pressure P, liquid mole fraction x, vapor mole fraction y, liquid density ρ_L, and vapor density ρ_V for the ethane (1) + 2-propanol (2) at 308.15 K

P/MPa	x_1	y_1	ρ_L/(kg·m^{-3})	ρ_V/(kg·m^{-3})
2.191	0.260	0.990	711.2	31.9
4.336	0.644	0.996	550.6	91.1
4.609	0.806	0.995	452.3	106.9
4.858	0.957	0.994	331.0	133.0
4.912	0.971	0.993	303.3	142.5
4.936	0.978	0.993	292.1	148.5
4.958	0.983	0.992	280.2	155.1
4.972	0.986	0.992	273.3	160.0
4.990	0.990	0.994	257.4	169.8

Table 5-2 Saturation pressure P, liquid mole fraction x, vapor mole fraction y, liquid density ρ_L, and vapor density ρ_V for the ethane (1) + 2-propanol (2) at 313.15 K

P/MPa	x_1	y_1	ρ_L/(kg·m^{-3})	ρ_V/(kg·m^{-3})
3.169	0.336	0.984	673.9	49.5
4.251	0.509	0.995	606.7	79.5
4.744	0.670	0.995	537.3	101.3
4.985	0.779	0.995	465.1	117.6
5.162	0.890	0.996	383.9	135.7
5.335	0.966	0.996	283.3	179.0
5.353	0.974	0.995	259.9	196.9
5.357	0.978	0.994	249.3	202.0

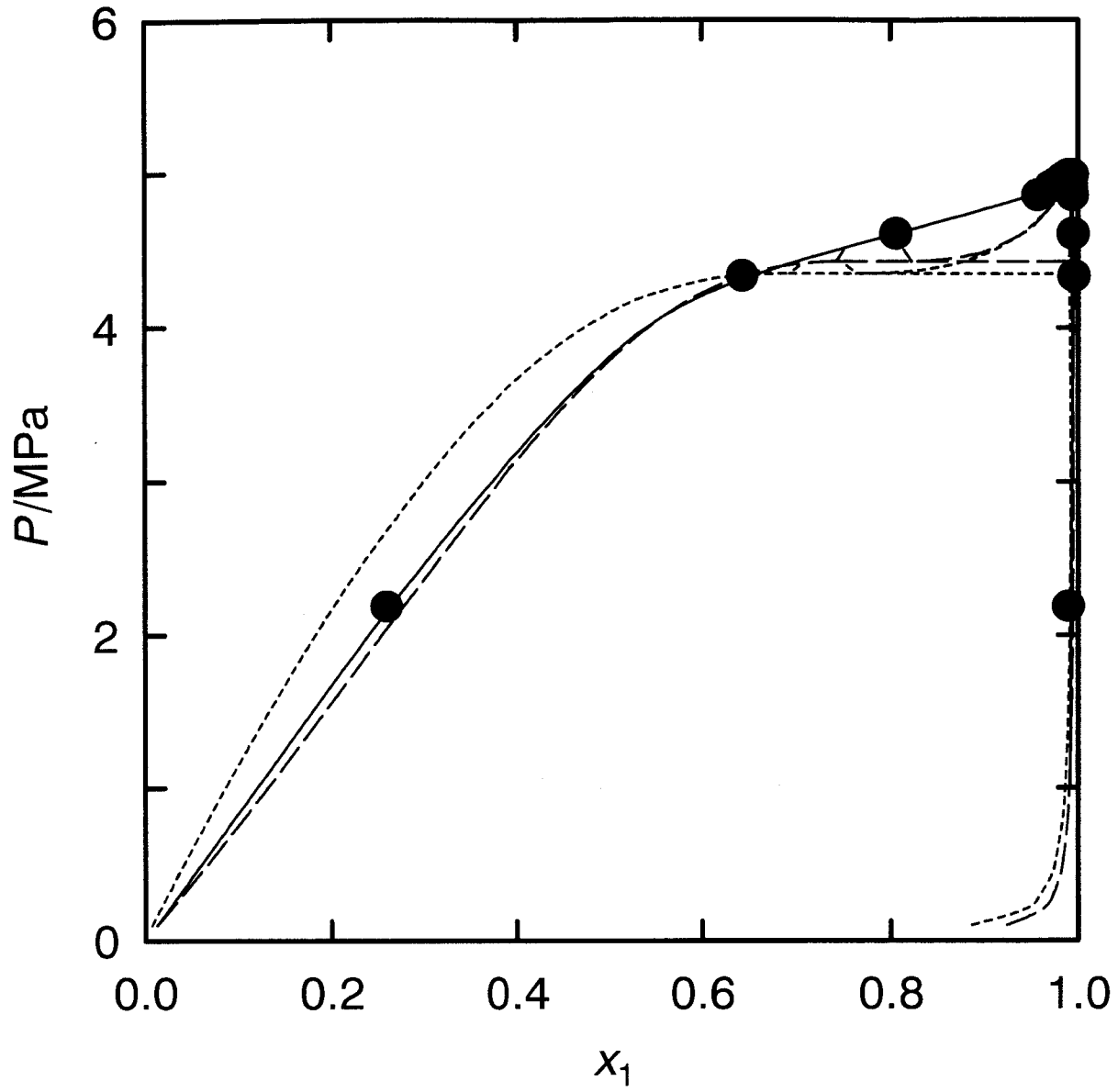

Fig. 5-1 Phase equilibria for the ethane (1) + 2-propanol (2) system at 308.15 K

—●—, this work; – – – – –, pseudocubic EOS (k_{12} =0.1055); ·····, SRK EOS (k_{12} =0.0707)

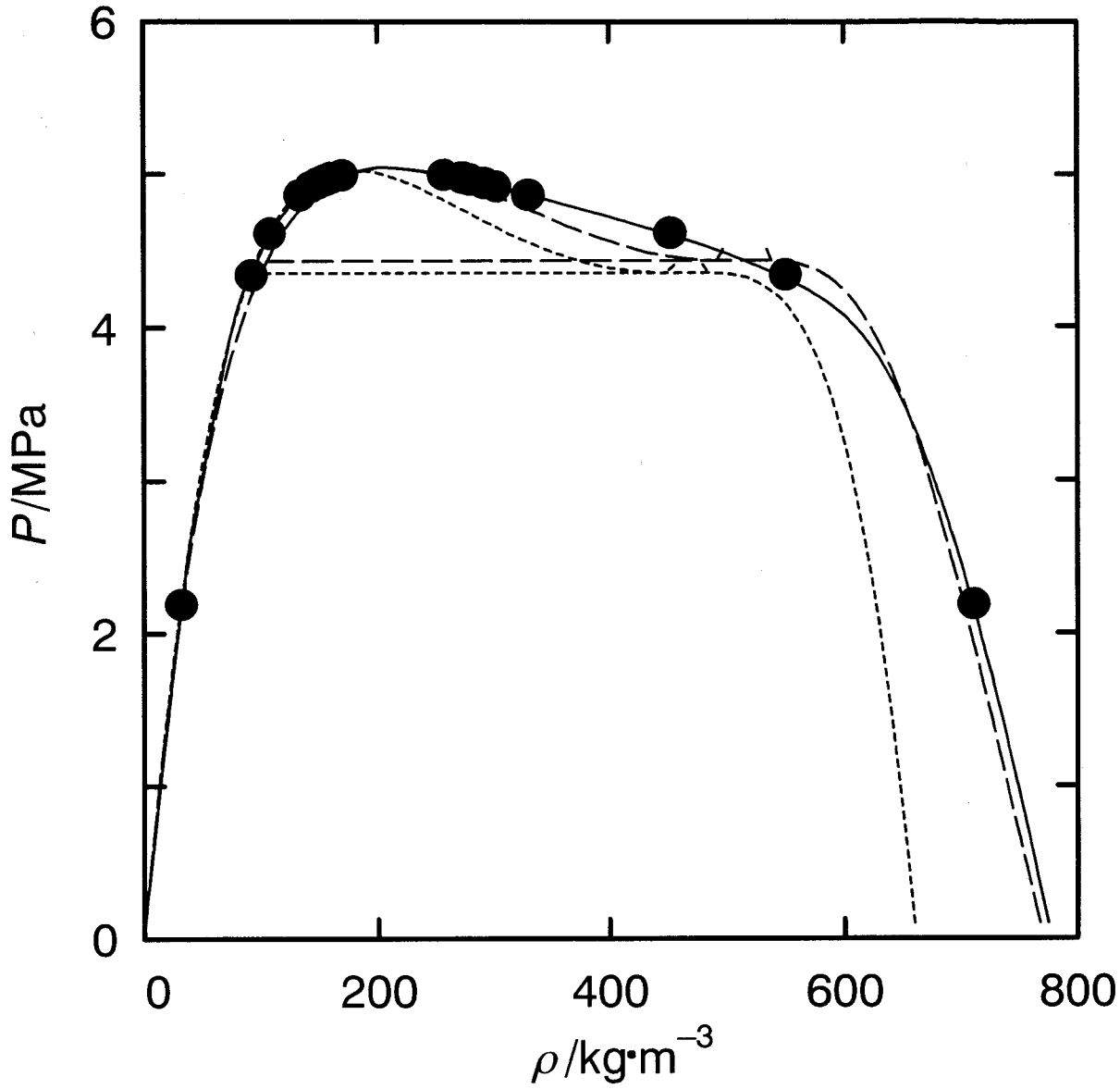

Fig. 5-2 Saturated densities for the ethane (1) + 2-propanol (2) system at 308.15 K —●—, this work; – – – – –, pseudocubic EOS (k_{12} =0.1055); ·····, SRK EOS (k_{12} =0.0707)

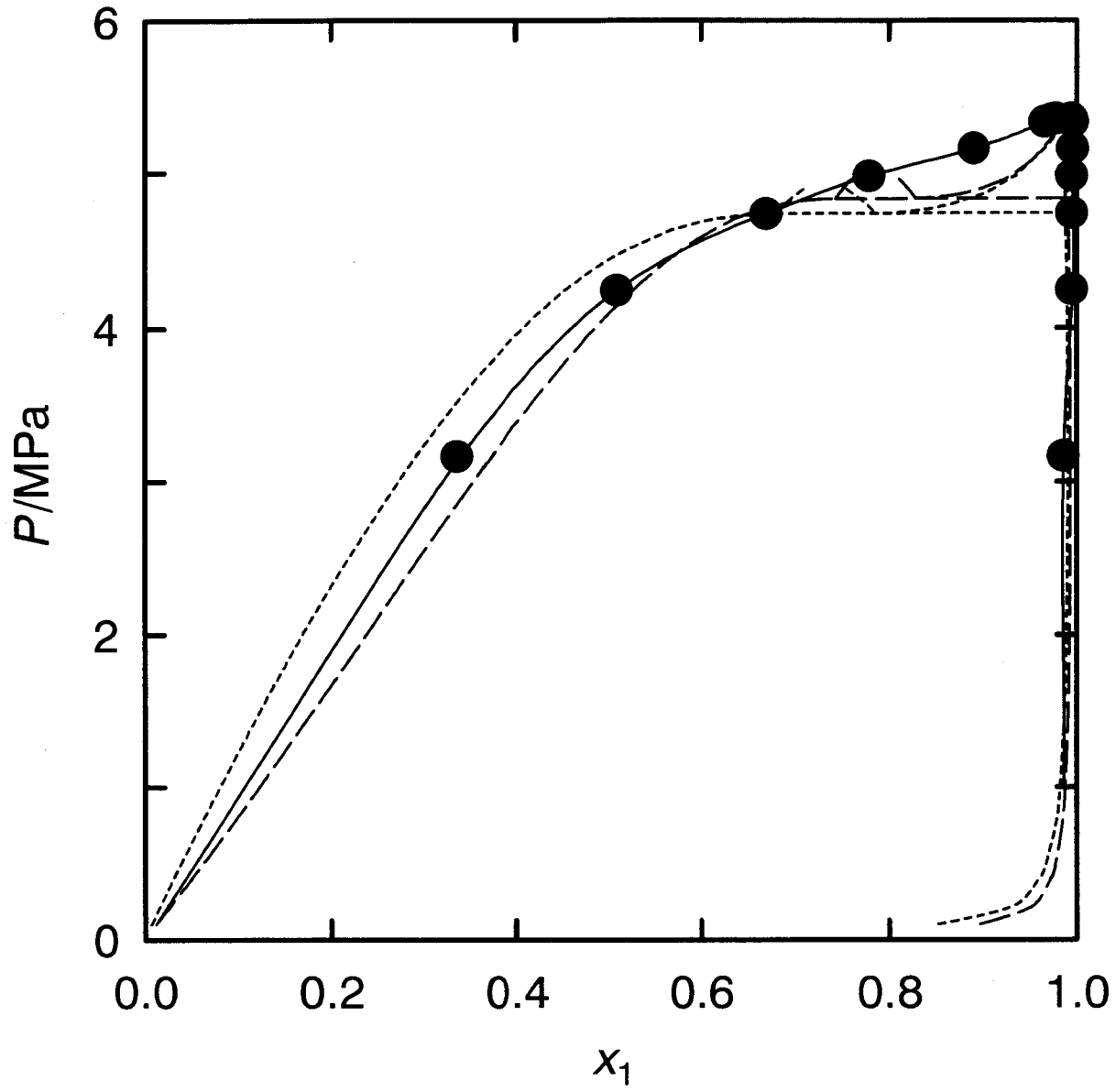

Fig. 5-3 Phase equilibria for the ethane (1) + 2-propanol (2) system at 313.15 K

—●—, this work; – – – – –, pseudocubic EOS (k_{12} =0.1097); ·····, SRK EOS (k_{12} =0.0736)

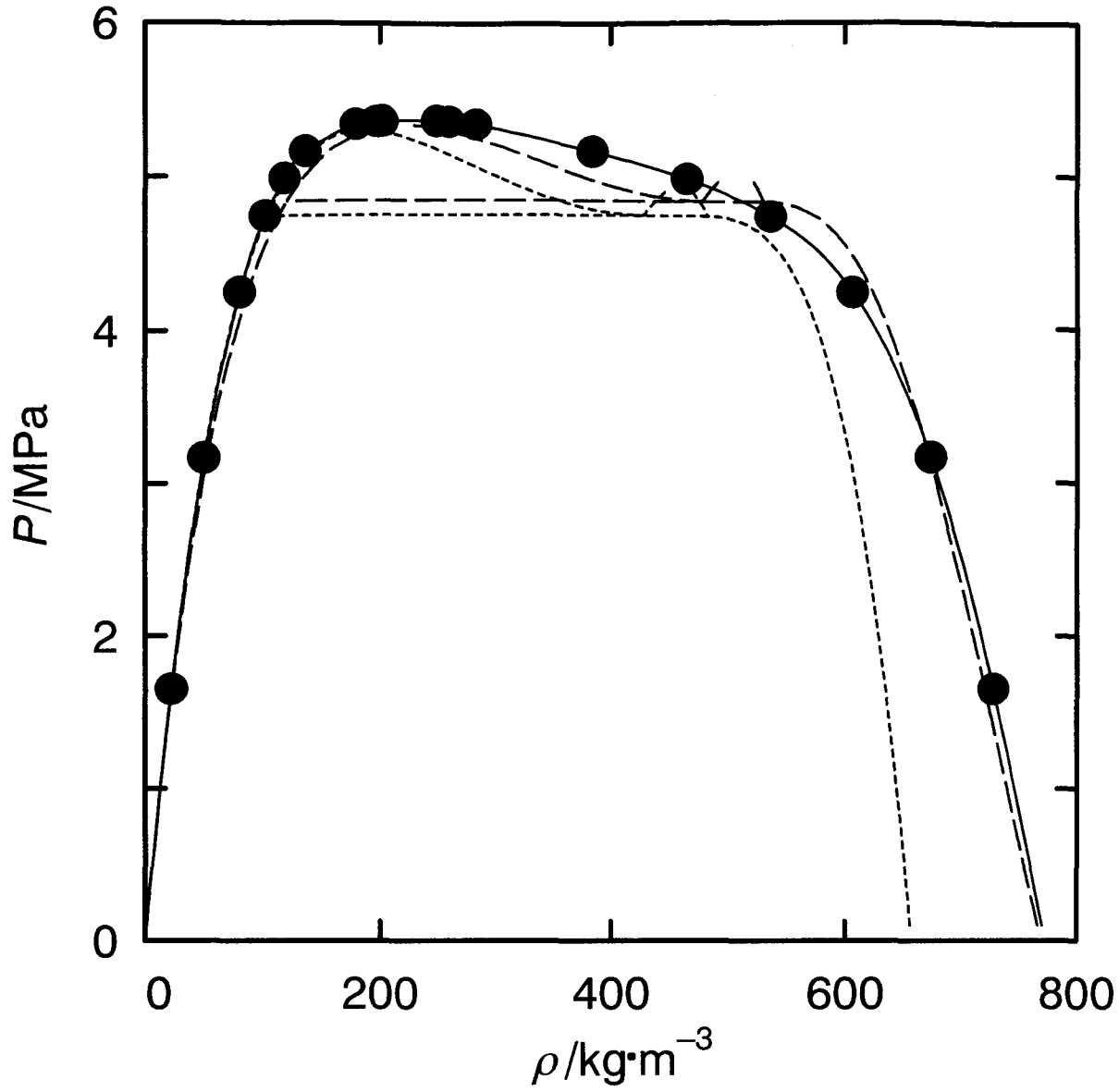

Fig. 5-4 Saturated densities for the ethane (1) + 2-propanol (2) system at 313.15 K —●—, this work; – – – – –, pseudocubic EOS (k_{12} =0.1097); ·····, SRK EOS (k_{12} =0.0736)

Chapter 6 Vapor-Liquid Equilibria in the Dilute Composition Range of Solutes

Introduction

It is well known that the small amount of heavy component such as carbonate is effective for eliminating an azeotrope. In the present study, the ferrocene is investigated as the inhibitor of azeotrope instead of carbonate. An unexpected result was occurred, that is, the useful partial pressure of ferrocene was observed in the alcoholic solution. Therefore, vapor-liquid equilibria in the dilute composition range of solutes were measured at atmospheric pressure.

Some metallic complexes are now attractive as new functional catalysts in chemical industries. For the development of chemical processes that involve complexes, vapor-liquid equilibrium behavior of solutions containing complexes is required. However, phase equilibrium data of complexes are not available. Ferrocene is a typical organometallic compound complex. In this chapter, vapor-liquid equilibrium behavior of ferrocene in methanol or ethanol was measured at atmospheric pressure in the dilute composition range of ferrocene. The vapor-liquid equilibrium behavior of 1,4-dihydroxybenzene in methanol or ethanol was further measured at atmospheric pressure in the dilute composition range of 1,4-dihydroxybenzene. 1,4-Dihydroxybenzene (hydroquinone) is practically used such as a polymerization inhibitor and assistant developer.

6.1 Experimental

6.1.1 Materials

Ferrocene was supplied by Wako Pure Chemical Industries, Ltd. with the guarantee 98% purity at least. 1,4-Dihydroxybenzene was supplied by Tokyo Chemical Industry Co., Ltd.

with a guaranteed 99% purity or better. Special grade reagents of methanol and ethanol were supplied by Wako Pure Chemical Industries, Ltd. and were used without further purification. The physical properties of methanol and ethanol used are listed in **Table 6-1**.

6.1.2 Experimental Apparatus and Procedures

The experimental apparatus and procedures are almost the same as those described previously by Tanaka *et al.* (1992). The schematic diagram of experimental apparatus is shown in **Fig. 6-1**. The recirculation still is entirely constructed from borosilicate glass. The amount of solution required is about 45 cm^3 per determination. The experimental atmospheric pressure was measured with a Fortin barometer with an accuracy of ±0.01 kPa. The equilibrium temperature was measured with a Hewlett-Packard 2804A quartz thermometer calibrated at the triple point of water in a reference cell with an accuracy of ±0.01 K. The equilibrium vapor and liquid compositions were determined with a Shimadzu UV265FS ultraviolet spectrophotometer at 440 nm with an accuracy of $\pm 1\times10^{-6}$ mole fraction of ferrocene, at 295 nm with an accuracy of liquid and vapor compositions seem to be $\pm 1\times10^{-6}$ and $\pm 1\times10^{-7}$ mole fraction of 1,4-dihydroxybenzene, respectively. Linear relations were experimentally observed between the absorbance and composition in the dilute range of ferrocene or 1,4-dihydroxybenzene.

6.2 Results and Discussion

Table 6-2 gives the experimental vapor-liquid equilibrium data obtained at atmospheric pressure in the dilute composition range of ferrocene in methanol or ethanol. The volatility K_1 of ferrocene is the ratio of the vapor composition and the liquid composition of ferrocene. **Fig. 6-2** shows the equilibrium vapor and liquid composition diagram at atmospheric pressure in the dilute composition range of ferrocene, giving linear relations for both systems. The linearity is only true within the range of the present experimental values. The extrapolation

of the linear relations cannot be recommended. The volatilities of ferrocene at infinite dilution were determined to be 0.032 and 0.036 in methanol and ethanol, respectively.

Table 6-3 gives the vapor-liquid equilibrium measurements obtained at atmospheric pressure in the dilute composition range of 1,4-dihydroxybenzene in methanol or ethanol. The volatility K_1 of 1,4-dihydroxybenzene is the ratio of vapor composition and liquid composition of 1,4-dihydroxybenzene. **Fig. 6-3** shows the equilibrium vapor and liquid composition diagram at atmospheric pressure in the dilute composition range of 1,4-dihydroxybenzene, giving linear relations for both systems. The linearity is only true within the range of the present experimental values. The extrapolation of the linear relations cannot be recommended. The volatilities of 1,4-dihydroxybenzene at infinite dilution were determined to be 0.0013 and 0.0007 in methanol and ethanol, respectively.

Summary

The vapor-liquid equilibrium behavior of ferrocene in methanol or ethanol was measured at atmospheric pressure in the dilute composition range of ferrocene with the recirculation still. Significantly, high volatilities of ferrocene were observed in methanol or ethanol.

The vapor-liquid equilibrium behavior of 1,4-dihydroxybenzene in methanol or ethanol was further measured at atmospheric pressure in the dilute composition range of 1,4-dihydroxybenzene with a recirculation still. The partial pressure of 1,4-dihydroxybenzene in methanol is higher than that in ethanol at the same temperature and infinite dilutions. The unexpected high volatility of 1,4-dihydroxybenzene in methanol would be explained by the high nonideality of the solution or activity coefficients at infinite dilution (see the appendix).

The author believes the present VLE data of solid components have a merit to evaluate the unknown parameters in the group contribution methods, such as UNIFAC and ASOG. The VLE of solid components seem powerful to evaluate the unknown parameters in the

group contribution methods.

Appendix

The author has calculated the abnormal vapor pressure of ferrocene or 1,4-dihydroxybenzene by use of Clausius-Clapeyron equation and Trouton's law. The activity coefficient at infinite dilution of ferrocene was estimated to be 10 in the ferrocene + methanol system and 6 in the ferrocene + ethanol system. The activity coefficient at infinite dilution of 1,4-dihydroxybenzene is 1.4 in the 1,4-dihydroxybenzene + methanol system and 0.4 in the 1,4-dihydroxybenzene + ethanol system.

Table 6-1 Normal boiling points T_b, densities ρ, and refractive indexes n_D of alcohols

material	T_b/K		ρ(298.15 K)/(kg·m^{-3})		n_D(298.15 K)	
	exptl	lit.[a]	exptl	lit.[b]	exptl	lit.[b]
methanol	337.67	337.651	786.6	786.64	1.3266	1.32652
ethanol	351.48	351.475	785.2	785.09	1.3596	1.35941

[a] Timmermans (1950). [b] TRC Thermodynamic Tables-Non-Hydrocarbons (1996).

Table 6-2 Experimental vapor-liquid equilibrium data, liquid-phase (x_1) and vapor-phase (y_1) mole fraction, volatility K_1, equilibrium temperature T, and atmospheric pressure P

x_1	y_1	$K_1(=y_1/x_1)$	T/K	P/kPa
		Ferrocene (1) + Methanol (2)		
0.001154	0.000037	0.032	337.00	98.91
0.001370	0.000044	0.032	336.98	98.82
0.001880	0.000060	0.032	336.99	98.78
0.002385	0.000079	0.033	336.98	98.70
0.002833	0.000088	0.031	336.98	98.68
		Ferrocene (1) + Ethanol (2)		
0.001121	0.000040	0.036	350.50	97.99
0.001539	0.000055	0.036	350.49	97.92
0.002333	0.000084	0.036	350.50	97.86
0.003363	0.000124	0.037	350.73	98.69
0.003917	0.000142	0.036	350.56	97.92

Table 6-3 Experimental vapor-liquid equilibrium data, liquid-phase (x_1) and vapor-phase (y_1) mole fraction, volatility K_1, equilibrium temperature T, and atmospheric pressure P

x_1	y_1	$K_1(=y_1/x_1)$	T/K	P/kPa
		1,4-Dihydroxybenzene (1) + Methanol (2)		
0.001379	0.0000018	0.0013	336.74	98.38
0.002039	0.0000028	0.0014	337.11	99.66
0.002345	0.0000031	0.0013	336.76	98.28
0.002901	0.0000039	0.0013	336.63	97.58
0.004349	0.0000060	0.0014	336.99	98.92
		1,4-Dihydroxybenzene (1) + Ethanol (2)		
0.001334	0.0000010	0.0007	350.53	98.85
0.001926	0.0000014	0.0007	350.53	98.86
0.002334	0.0000016	0.0007	350.54	98.85
0.002648	0.0000017	0.0007	350.56	98.90
0.004233	0.0000028	0.0007	350.59	98.78

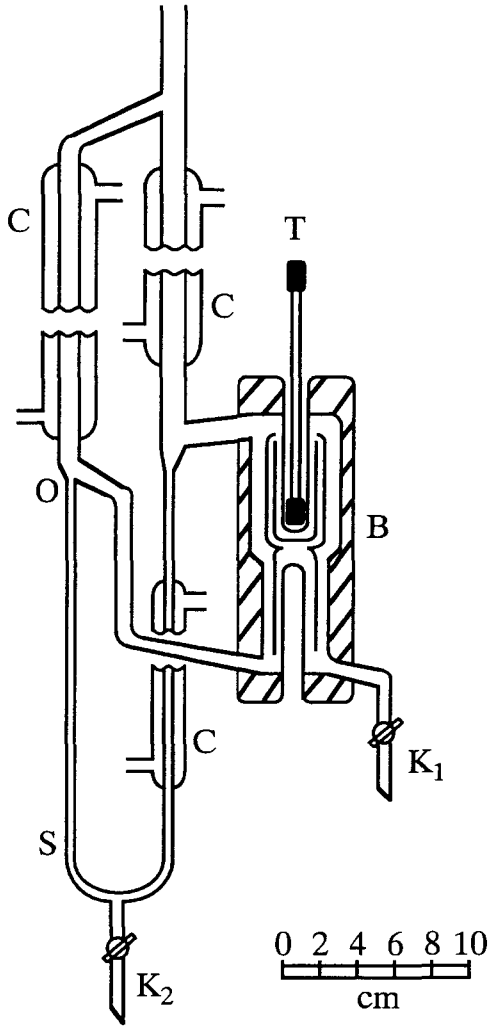

Fig. 6-1 Schematic diagram of experimental apparatus

B, boiling still; C, condenser; K, cock; O, overflow tube; S, condensate chamber, T, quartz thermometer

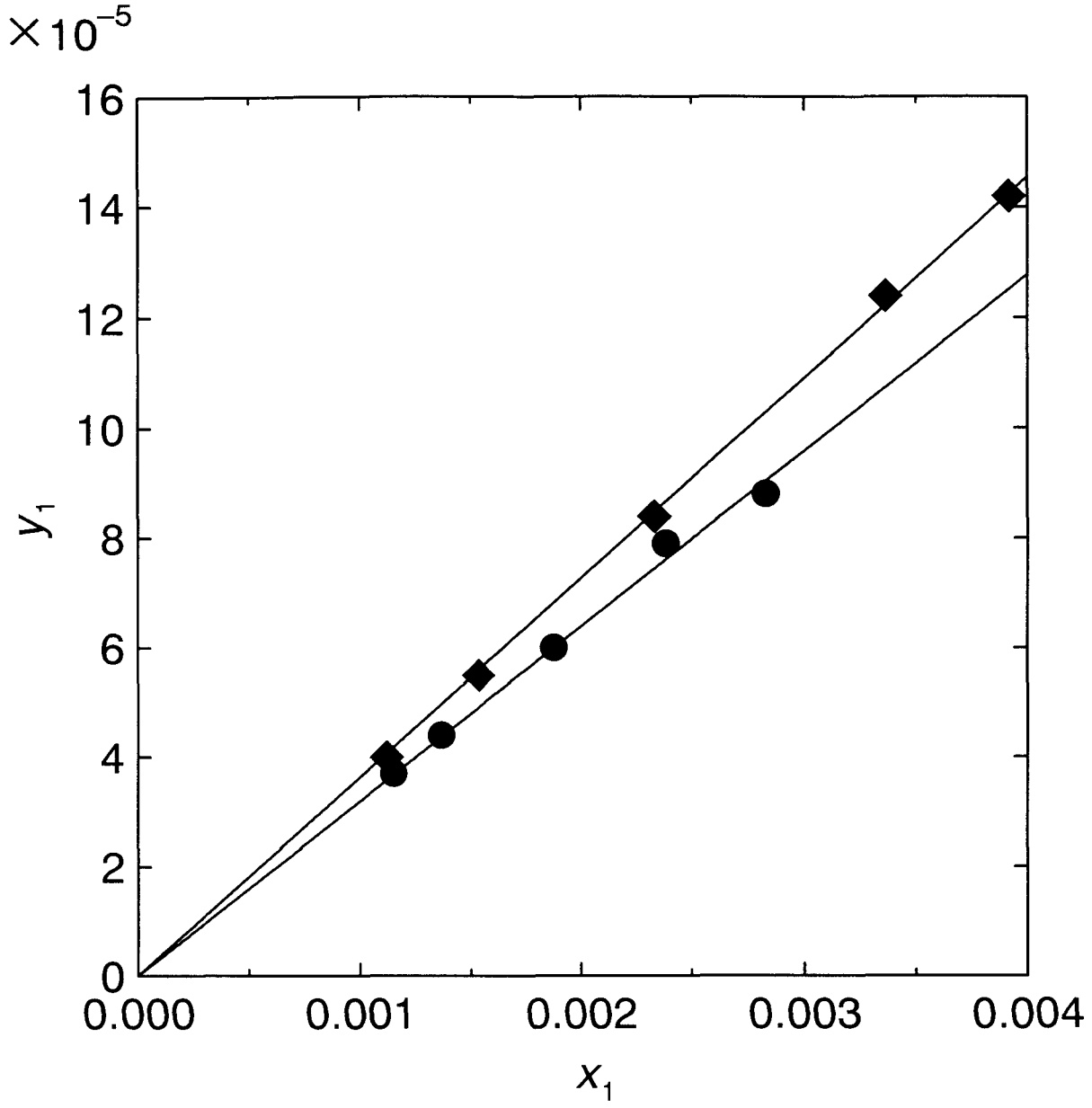

Fig. 6-2 Experimental vapor-liquid equilibrium composition diagram at atmospheric pressure

●, ferrocene (1) + methanol (2); ◆, ferrocene (1) + ethanol (2)

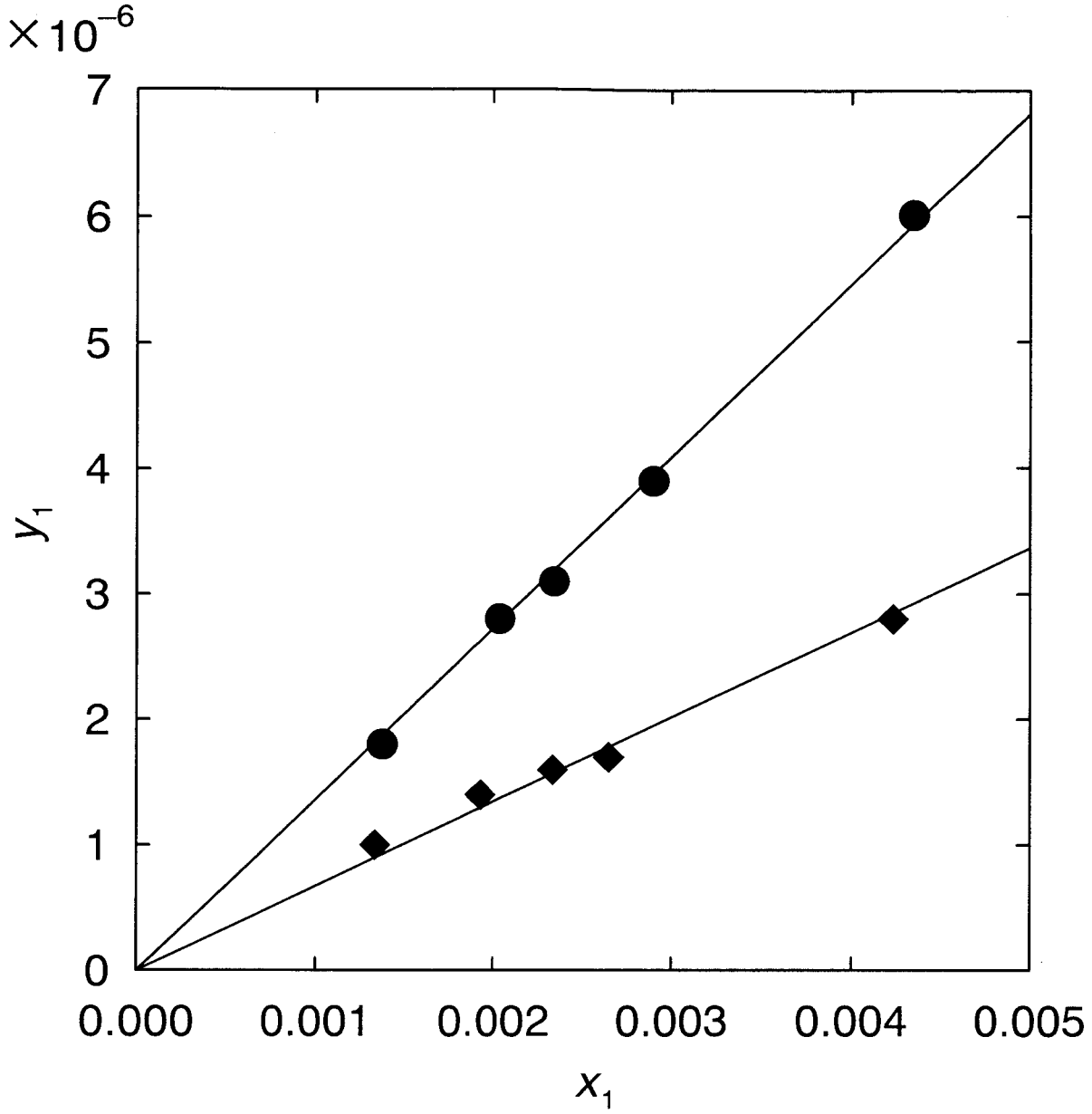

Fig. 6-3 Experimental vapor-liquid equilibrium composition diagram at atmospheric pressure

●, 1,4-dihydroxybenzene (1) + methanol (2); ◆, 1,4-dihydroxybenzene (1) + ethanol (2)

Chapter 7 Homogenizing Effect of Ethers Added to Immiscible Alcohol + Oil Binary Mixtures

Introduction

Ethers have a homogenization effect on immiscible binary-liquid mixtures. In the previous investigation on the boiling points and liquid densities of alcohol and diesel fuel mixtures, the internal of immiscible compositions was demonstrated, and then it was revealed that the addition of ethers is effective to homogenize the immiscible mixtures (Kato *et al.*, 1988, 1991). Homogenization is important for developing alternative automobile fuels based on mixtures of alcohols with diesel fuel or seed oils.

In this chapter, the homogenizing effect of six ethers: methyl *tert*-butyl ether (MTBE), ethyl *tert*-butyl ether (ETBE), *tert*-amyl methyl ether (TAME), tetrahydrofuran (THF), tetrahydropyran (THP), or 1,4-dioxane were investigated for immiscible binary fuels, in which methanol or ethanol was mixed with diesel fuel, with soybean oil, and with rapeseed oil, at 298.15 K. The ignition behaviors were observed for these ether + alcohol + diesel fuel mixtures.

7.1 Experimental

7.1.1 Materials

Special grade regents of MTBE and ETBE were supplied by Tokyo Kasei Co., Ltd. Special grade THF, THP, 1,4-dioxane, ethanol, and methanol were supplied by Wako Pure Chemical Industries, Ltd. The reagent of TAME with a guarantee of 97% purity was supplied by Aldrich Chemical Company, Inc. The popular commercial diesel fuel was supplied by Cosmo Oil Co. Soybean oil and rapeseed oil were supplied by Honen Corp., and Mashiko Oil Co., respectively. All reagents were used as received. The physical

properties of the materials used are listed in **Table 7-1**.

7.1.2 Experimental Apparatus and Procedures

An immiscible mixture of the desired composition of ethanol or methanol and oil was prepared in a glass flask with a stopper by precisely weighing each component using a syringe and an electronic balance. The flask was shaken and placed in a water bath controlled at 298.15±0.01 K. The temperature was measured by a Hewlett-Packard 2804A quartz thermometer. Two liquid phases were first observed. Ethers was added as a third component to the immiscible mixture while shaking the flask using a syringe until the interface of two liquid phases disappeared. The amount of ether added was calculated from its mass remained in the syringe. The uncertainty of solubility measurements was about ±0.001 mass fraction.

The ignition behaviors for ether + alcohol + diesel fuel mixtures were observed with the conventional ASTM equipment made from Yoshida Seisakusho Co., Ltd.

7.2 Results and Discussion

Experimental solubility data obtained in the present study at 298.15 K for ether + ethanol + oil mixtures are shown in **Tables 7-2** to **7-7** and **Figs. 7-1** to **7-3**. It was observed that the two-liquid phases of ethanol + diesel fuel, ethanol + soybean oil, or ethanol + rapeseed oil disappeared by adding a small amount of any of the ethers: MTBE, ETBE, TAME, THF, THP, or 1,4-dioxane. Liquid homogenization was observed always by adding 5% of ether, except 1,4-dioxane, to the ethanol + diesel fuel mixture.

Experimental solubility data obtained in the present study at 298.15 K for ether + methanol + oil mixtures are shown in **Tables 7-8** to **7-13** and **Figs. 7-4** to **7-6**. The boundary of the two-liquid phases methanol + diesel fuel, methanol + soybean oil, or methanol + rapeseed oil disappeared after adding any of the ethers: MTBE, ETBE, TAME,

THF, THP, or 1,4-dioxane. Liquid homogenization was observed always by adding 40% of ether, except 1,4-dioxane, to the methanol + diesel fuel mixture.

The dipole moments of the ethers are listed in **Table 7-1**. The largest value, 1.7 Debye, was assigned to THF and THP, and the smallest value, 0.4 Debye, to 1,4-dioxane, and 1.2 Debye to MTBE, ETBE, and TAME. Comparison of the dipole moments of the ethers and the experimental results shown in **Figs. 7-1** to **7-6**, the magnitude of dipole moments of the ethers corresponded to their homogenizing abilities observed in this study, similar to the previous chapter.

The ignition behaviors were observed for mixtures of ether + methanol + diesel fuel as shown in **Fig. 7-7**. MTBE, THF, and 1,4-dioxane were used as the ethers. The mass fractions of ether, methanol, and diesel fuel, respectively, were 0.375, 0.188, and 0.437. The experimental ignition temperatures for ether + ethanol + diesel fuel mixtures are shown in **Fig. 7-8**. The ethers are the same with the methanol system (Yaginuma *et al.*, 1999). The mass fractions of ether, ethanol, and diesel fuel, respectively, were 0.091, 0.273, and 0.636. In **Figs. 7-7** and **7-8**, the ignition behavior of diesel fuel is shown for reference. A high temperature was required for the ignition of MTBE mixtures, as shown in **Figs. 7-7** and **7-8**. Experimental ignition behaviors were similar to that of the diesel fuel for THF and 1,4-dioxane mixtures.

Summary

Homogenization was observed for immiscible mixtures prepared from ethanol or methanol with various oils: diesel fuel, soybean oil, or rapeseed oil, with a small addition of such ethers: MTBE, ETBE, TAME, THF, THP, or 1,4-dioxane. Ternary solubility curves were measured at 298.15 K for these ether + ethanol + oil, ether + methanol + oil mixtures. Immiscible mixtures of ethanol or methanol and oils were transformed into homogeneous solutions by addition of small amounts of ethers. However, the homogenization effect was

poor with 1,4-dioxane.

A higher temperature was required for ignition of MTBE mixtures, as shown in **Figs. 7-7** and **7-8**. Experimental ignition behaviors ware similar to those of diesel fuel for THF and 1,4-dioxane mixtures.

Based on the experimental homogenization effect and ignition behavior results, THF is recommended for homogenization of alcohol + oil fuels for the diesel engine.

Table 7-1 Physical properties of materials used at 298.15 K*

Materials	ρ, kg·m^{-3}		n_D		μ
	exptl	lit.	exptl	lit.	Debye
Methyl *tert*-Butyl Ether (MTBE)	735.3	735.3[a]	1.3664	1.3663[a]	1.2[c]
Ethyl *tert*-Butyl Ether (ETBE)	734.9	734.8[a]	1.3734	1.3729[a]	1.2[c]
tert-Amyl Methyl Ether (TAME)	766.2	765.6[a]	1.3860	1.3859[a]	1.2[c]
Tetrahydrofuran (THF)	881.9	882.5[a]	1.4046	1.4049[a]	1.7[c]
Tetrahydropyran (THP)	878.9		1.4186		1.7[c]
1,4-Dioxane	1027.9	1027.9[b]	1.4204	1.4201[b]	0.4[c]
Ethanol	785.4	785.1[a]	1.3596	1.3594[a]	
Methanol	786.6	786.6[a]	1.3266	1.3265	
Diesel fuel	827.8		1.4623		
Soybean oil	916.0		1.4729		
Rapeseed oil	911.7		1.4716		

[a] TRC Thermodynamic Tables-Non-Hydrocarbons (1996). [b] Kato *et al.* (1972). [c] Reid *et al.* (1987). * Yaginuma *et al.* (2001)

Table 7-2 Liquid solubility compositions mass fraction (x) at 298.15 K for mixtures of MTBE (1) + Ethanol (2) + Oil (3)

Diesel Fuel (3)			Soybean Oil (3)			Rapeseed Oil (3)		
x_1	x_2	x_3	x_1	x_2	x_3	x_1	x_2	x_3
0.000	0.122	0.878	0.000	0.132	0.868	0.000	0.125	0.875
0.014	0.197	0.789	0.053	0.199	0.748	0.023	0.139	0.838
0.026	0.292	0.682	0.098	0.270	0.632	0.076	0.185	0.739
0.036	0.386	0.578	0.125	0.350	0.525	0.133	0.267	0.600
0.040	0.480	0.480	0.139	0.431	0.430	0.163	0.334	0.503
0.039	0.529	0.432	0.151	0.510	0.339	0.178	0.401	0.421
0.035	0.603	0.362	0.153	0.593	0.254	0.191	0.486	0.323
0.022	0.685	0.293	0.139	0.689	0.172	0.194	0.557	0.249
0.000	0.771	0.229	0.088	0.817	0.095	0.188	0.649	0.163
			0.000	0.961	0.039	0.174	0.698	0.128
						0.140	0.773	0.087
						0.075	0.874	0.051
						0.000	0.960	0.040

Table 7-3 Liquid solubility compositions mass fraction (x) at 298.15 K for mixtures of ETBE (1) + Ethanol (2) + Oil (3)

Diesel Fuel (3)			Soybean Oil (3)			Rapeseed Oil (3)		
x_1	x_2	x_3	x_1	x_2	x_3	x_1	x_2	x_3
0.000	0.122	0.878	0.000	0.132	0.868	0.000	0.125	0.875
0.016	0.197	0.787	0.050	0.190	0.760	0.031	0.138	0.831
0.028	0.292	0.680	0.101	0.256	0.643	0.096	0.181	0.723
0.036	0.386	0.578	0.130	0.340	0.530	0.140	0.261	0.599
0.043	0.478	0.479	0.146	0.426	0.428	0.171	0.333	0.496
0.043	0.526	0.431	0.154	0.508	0.338	0.185	0.397	0.418
0.036	0.604	0.360	0.155	0.591	0.254	0.197	0.482	0.321
0.022	0.684	0.294	0.147	0.682	0.171	0.200	0.554	0.246
0.000	0.771	0.229	0.092	0.817	0.091	0.199	0.641	0.160
			0.000	0.961	0.039	0.188	0.687	0.125
						0.154	0.762	0.084
						0.089	0.861	0.050
						0.000	0.960	0.040

Table 7-4 Liquid solubility compositions mass fraction (x) at 298.15 K for mixtures of TAME (1) + Ethanol (2) + Oil (3)

Diesel Fuel (3)			Soybean Oil (3)			Rapeseed Oil (3)		
x_1	x_2	x_3	x_1	x_2	x_3	x_1	x_2	x_3
0.000	0.122	0.878	0.000	0.132	0.868	0.000	0.125	0.875
0.013	0.199	0.788	0.050	0.190	0.760	0.028	0.140	0.832
0.029	0.291	0.680	0.101	0.269	0.630	0.078	0.184	0.738
0.035	0.391	0.574	0.125	0.349	0.526	0.138	0.266	0.596
0.039	0.481	0.480	0.140	0.430	0.430	0.166	0.333	0.501
0.039	0.529	0.432	0.148	0.511	0.341	0.180	0.400	0.420
0.035	0.603	0.362	0.147	0.598	0.255	0.186	0.487	0.327
0.021	0.685	0.294	0.136	0.691	0.173	0.191	0.560	0.249
0.000	0.771	0.229	0.084	0.825	0.091	0.188	0.649	0.163
			0.000	0.961	0.039	0.171	0.700	0.129
						0.133	0.780	0.087
						0.054	0.895	0.051
						0.000	0.960	0.040

Table 7-5 Liquid solubility compositions mass fraction (x) at 298.15 K for mixtures of THF (1) + Ethanol (2) + Oil (3)

Diesel Fuel (3)			Soybean Oil (3)			Rapeseed Oil (3)		
x_1	x_2	x_3	x_1	x_2	x_3	x_1	x_2	x_3
0.000	0.122	0.878	0.000	0.132	0.868	0.000	0.125	0.875
0.014	0.197	0.789	0.048	0.190	0.762	0.028	0.140	0.832
0.023	0.293	0.684	0.099	0.270	0.631	0.070	0.186	0.744
0.033	0.387	0.580	0.118	0.354	0.528	0.114	0.273	0.613
0.040	0.480	0.480	0.127	0.437	0.436	0.136	0.346	0.518
0.037	0.530	0.433	0.129	0.523	0.348	0.152	0.415	0.433
0.033	0.604	0.363	0.129	0.610	0.261	0.165	0.501	0.334
0.021	0.685	0.294	0.118	0.706	0.176	0.168	0.577	0.255
0.000	0.771	0.229	0.075	0.832	0.093	0.165	0.667	0.168
			0.000	0.961	0.039	0.153	0.716	0.131
						0.127	0.784	0.089
						0.062	0.887	0.051
						0.000	0.960	0.040

Table 7-6 Liquid solubility compositions mass fraction (x) at 298.15 K for mixtures of THP (1) + Ethanol (2) + Oil (3)

Diesel Fuel (3)			Soybean Oil (3)			Rapeseed Oil (3)		
x_1	x_2	x_3	x_1	x_2	x_3	x_1	x_2	x_3
0.000	0.122	0.878	0.000	0.132	0.868	0.000	0.125	0.875
0.016	0.197	0.787	0.041	0.192	0.767	0.027	0.140	0.833
0.026	0.292	0.682	0.091	0.273	0.636	0.069	0.186	0.745
0.032	0.387	0.581	0.119	0.353	0.528	0.121	0.270	0.609
0.039	0.482	0.479	0.125	0.437	0.438	0.149	0.341	0.510
0.039	0.528	0.433	0.131	0.522	0.347	0.160	0.409	0.431
0.037	0.602	0.361	0.130	0.609	0.261	0.171	0.497	0.332
0.021	0.685	0.294	0.121	0.703	0.176	0.176	0.570	0.254
0.000	0.771	0.229	0.075	0.833	0.092	0.169	0.665	0.166
			0.000	0.961	0.039	0.160	0.711	0.129
						0.128	0.785	0.087
						0.072	0.877	0.051
						0.000	0.960	0.040

Table 7-7 Liquid solubility compositions mass fraction (x) at 298.15 K for mixtures of 1,4-Dioxane (1) + Ethanol (2) + Oil (3)

Diesel Fuel (3)			Soybean Oil (3)			Rapeseed Oil (3)		
x_1	x_2	x_3	x_1	x_2	x_3	x_1	x_2	x_3
0.000	0.122	0.878	0.000	0.132	0.868	0.000	0.125	0.875
0.026	0.200	0.774	0.051	0.190	0.759	0.031	0.138	0.831
0.043	0.287	0.670	0.110	0.267	0.623	0.093	0.182	0.725
0.057	0.377	0.566	0.137	0.345	0.518	0.149	0.262	0.589
0.069	0.466	0.465	0.150	0.425	0.425	0.178	0.328	0.494
0.073	0.510	0.417	0.161	0.503	0.336	0.199	0.391	0.410
0.069	0.582	0.349	0.164	0.585	0.251	0.221	0.468	0.311
0.042	0.671	0.287	0.152	0.676	0.172	0.223	0.538	0.239
0.000	0.771	0.229	0.096	0.814	0.090	0.218	0.626	0.156
			0.000	0.961	0.039	0.202	0.675	0.123
						0.163	0.753	0.084
						0.090	0.860	0.050
						0.000	0.960	0.040

Table 7-8 Liquid solubility compositions mass fraction (x) at 298.15 K for mixtures of MTBE (1) + Methanol (2) + Oil (3)

Diesel Fuel (3)			Soybean Oil (3)			Rapeseed Oil (3)		
x_1	x_2	x_3	x_1	x_2	x_3	x_1	x_2	x_3
0.000	0.971	0.029	0.000	0.987	0.013	0.000	0.970	0.030
0.104	0.848	0.048	0.276	0.682	0.042	0.320	0.641	0.039
0.207	0.713	0.080	0.333	0.600	0.067	0.378	0.560	0.062
0.280	0.576	0.144	0.368	0.506	0.126	0.398	0.480	0.122
0.300	0.485	0.215	0.365	0.438	0.197	0.399	0.413	0.188
0.294	0.426	0.280	0.357	0.386	0.257	0.387	0.378	0.235
0.281	0.351	0.368	0.333	0.326	0.341	0.362	0.310	0.328
0.266	0.294	0.440	0.316	0.273	0.411	0.333	0.263	0.404
0.254	0.229	0.517	0.285	0.220	0.495	0.308	0.213	0.479
0.224	0.155	0.621	0.223	0.155	0.622	0.241	0.154	0.605
0.167	0.082	0.751	0.132	0.086	0.782	0.152	0.086	0.762
0.000	0.013	0.987	0.000	0.073	0.927	0.000	0.055	0.945

Table 7-9 Liquid solubility compositions mass fraction (x) at 298.15 K for mixtures of ETBE (1) + Methanol (2) + Oil (3)

Diesel Fuel (3)			Soybean Oil (3)			Rapeseed Oil (3)		
x_1	x_2	x_3	x_1	x_2	x_3	x_1	x_2	x_3
0.000	0.971	0.029	0.000	0.987	0.013	0.000	0.970	0.030
0.130	0.823	0.047	0.277	0.681	0.042	0.300	0.657	0.043
0.207	0.713	0.080	0.335	0.596	0.069	0.373	0.560	0.067
0.274	0.580	0.146	0.367	0.508	0.125	0.396	0.479	0.125
0.298	0.487	0.215	0.368	0.437	0.195	0.401	0.415	0.184
0.306	0.416	0.278	0.364	0.382	0.254	0.395	0.362	0.243
0.295	0.344	0.361	0.358	0.312	0.330	0.369	0.307	0.324
0.284	0.286	0.430	0.335	0.263	0.402	0.349	0.259	0.392
0.276	0.224	0.500	0.299	0.216	0.485	0.314	0.208	0.478
0.246	0.151	0.603	0.238	0.152	0.610	0.257	0.150	0.593
0.190	0.079	0.731	0.143	0.083	0.774	0.145	0.084	0.771
0.000	0.013	0.987	0.000	0.073	0.927	0.000	0.055	0.945

Table 7-10 Liquid solubility compositions mass fraction (x) at 298.15 K for mixtures of TAME (1) + Methanol (2) + Oil (3)

Diesel Fuel (3)			Soybean Oil (3)			Rapeseed Oil (3)		
x_1	x_2	x_3	x_1	x_2	x_3	x_1	x_2	x_3
0.000	0.971	0.029	0.000	0.987	0.013	0.000	0.970	0.030
0.144	0.807	0.049	0.264	0.697	0.039	0.316	0.647	0.037
0.205	0.714	0.081	0.325	0.607	0.068	0.376	0.555	0.069
0.274	0.581	0.145	0.359	0.512	0.129	0.389	0.486	0.125
0.299	0.481	0.220	0.363	0.442	0.195	0.389	0.424	0.187
0.307	0.416	0.277	0.358	0.385	0.257	0.382	0.373	0.245
0.298	0.342	0.360	0.339	0.323	0.338	0.370	0.307	0.323
0.289	0.284	0.427	0.325	0.270	0.405	0.351	0.258	0.391
0.276	0.223	0.501	0.300	0.215	0.485	0.334	0.223	0.443
0.253	0.149	0.598	0.245	0.151	0.604	0.260	0.148	0.592
0.198	0.079	0.723	0.121	0.086	0.793	0.151	0.084	0.765
0.000	0.013	0.987	0.000	0.073	0.927	0.000	0.055	0.945

Table 7-11 Liquid solubility compositions mass fraction (x) at 298.15 K for mixtures of THF (1) + Methanol (2) + Oil (3)

Diesel Fuel (3)			Soybean Oil (3)			Rapeseed Oil (3)		
x_1	x_2	x_3	x_1	x_2	x_3	x_1	x_2	x_3
0.000	0.971	0.029	0.000	0.987	0.013	0.000	0.970	0.030
0.149	0.803	0.048	0.294	0.656	0.050	0.307	0.656	0.037
0.224	0.698	0.078	0.316	0.615	0.069	0.357	0.578	0.065
0.283	0.574	0.143	0.339	0.530	0.131	0.379	0.498	0.123
0.299	0.485	0.216	0.343	0.455	0.202	0.378	0.433	0.189
0.302	0.419	0.279	0.334	0.395	0.271	0.362	0.385	0.253
0.281	0.351	0.368	0.314	0.334	0.352	0.340	0.326	0.334
0.258	0.295	0.447	0.297	0.281	0.422	0.318	0.270	0.412
0.235	0.237	0.528	0.266	0.226	0.508	0.295	0.241	0.464
0.199	0.160	0.641	0.199	0.158	0.643	0.237	0.149	0.614
0.142	0.085	0.773	0.117	0.087	0.796	0.126	0.086	0.788
0.000	0.013	0.987	0.000	0.073	0.927	0.000	0.055	0.945

Table 7-12 Liquid solubility compositions mass fraction (x) at 298.15 K for mixtures of THP (1) + Methanol (2) + Oil (3)

Diesel Fuel (3)			Soybean Oil (3)			Rapeseed Oil (3)		
x_1	x_2	x_3	x_1	x_2	x_3	x_1	x_2	x_3
0.000	0.971	0.029	0.000	0.987	0.013	0.000	0.970	0.030
0.116	0.836	0.048	0.264	0.694	0.042	0.298	0.664	0.038
0.224	0.694	0.082	0.309	0.622	0.069	0.347	0.587	0.066
0.272	0.582	0.146	0.340	0.528	0.132	0.375	0.512	0.113
0.294	0.489	0.217	0.341	0.456	0.203	0.371	0.435	0.194
0.295	0.423	0.282	0.333	0.400	0.267	0.360	0.378	0.262
0.279	0.352	0.369	0.324	0.330	0.346	0.347	0.318	0.335
0.270	0.291	0.439	0.305	0.279	0.416	0.331	0.268	0.401
0.250	0.234	0.516	0.277	0.221	0.502	0.300	0.217	0.483
0.225	0.155	0.620	0.225	0.155	0.620	0.242	0.152	0.606
0.167	0.082	0.751	0.106	0.088	0.806	0.146	0.095	0.759
0.000	0.013	0.987	0.000	0.073	0.927	0.000	0.055	0.945

Table 7-13 Liquid solubility compositions mass fraction (x) at 298.15 K for mixtures of 1,4-Dioxane (1) + Methanol (2) + Oil (3)

Diesel Fuel (3)			Soybean Oil (3)			Rapeseed Oil (3)		
x_1	x_2	x_3	x_1	x_2	x_3	x_1	x_2	x_3
0.000	0.971	0.029	0.000	0.987	0.013	0.000	0.970	0.030
0.231	0.727	0.042	0.372	0.592	0.036	0.435	0.534	0.031
0.374	0.563	0.063	0.442	0.492	0.066	0.489	0.460	0.051
0.485	0.412	0.103	0.467	0.427	0.106	0.519	0.386	0.095
0.525	0.329	0.146	0.463	0.372	0.165	0.516	0.335	0.149
0.532	0.281	0.187	0.452	0.328	0.220	0.500	0.298	0.202
0.512	0.238	0.250	0.421	0.283	0.296	0.465	0.262	0.273
0.482	0.207	0.311	0.399	0.240	0.361	0.434	0.229	0.337
0.423	0.177	0.400	0.362	0.196	0.442	0.395	0.187	0.418
0.354	0.131	0.515	0.277	0.145	0.578	0.308	0.138	0.554
0.247	0.079	0.674	0.143	0.084	0.773	0.172	0.083	0.745
0.000	0.013	0.987	0.000	0.073	0.927	0.000	0.055	0.945

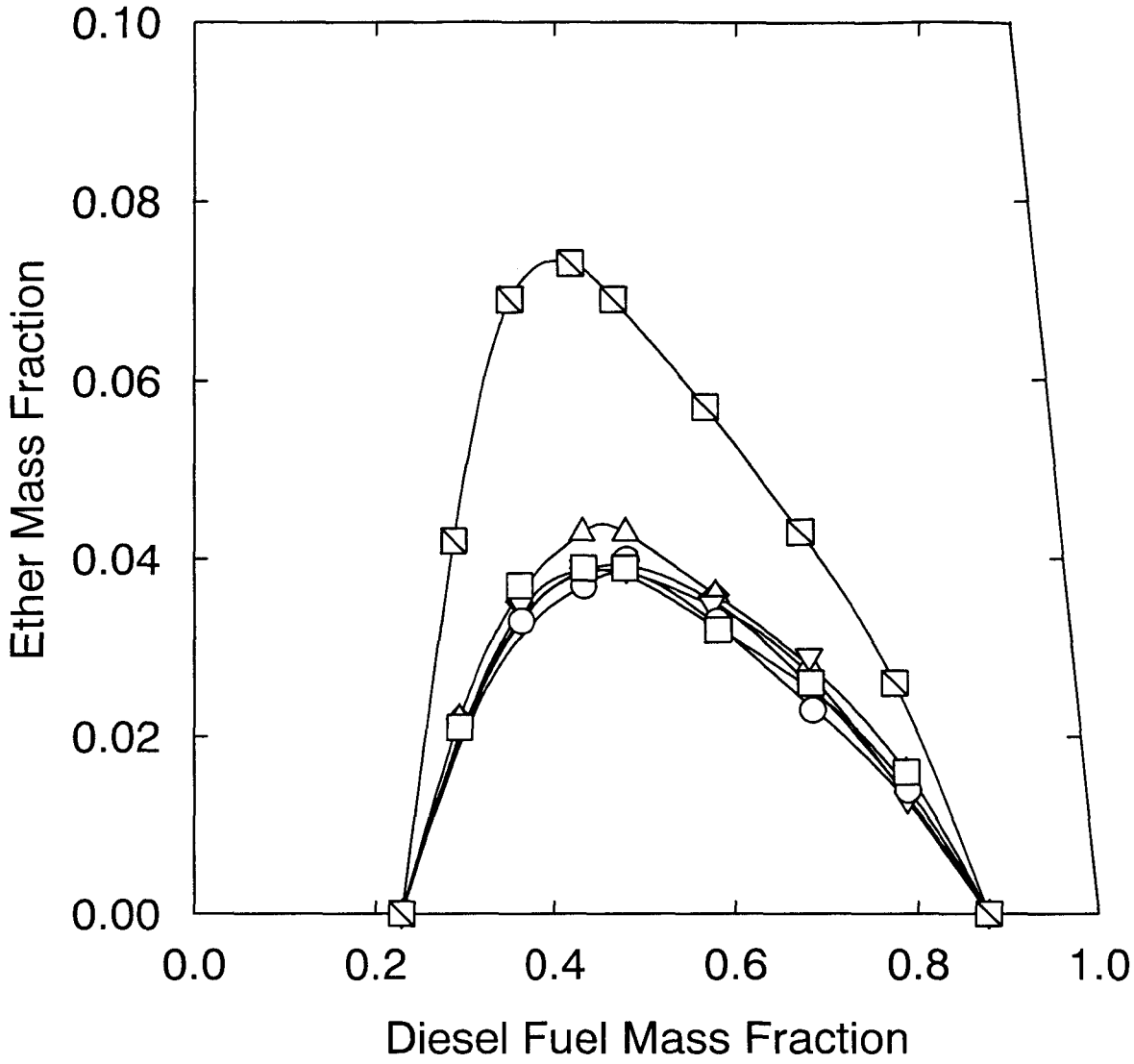

Fig. 7-1 Experimental solubility curves at 298.15 K for mixtures of diesel fuel, ethanol, and ether

◇, MTBE; △, ETBE; ▽, TAME; ○, THF; □, THP; ⊠ , 1,4-Dioxane

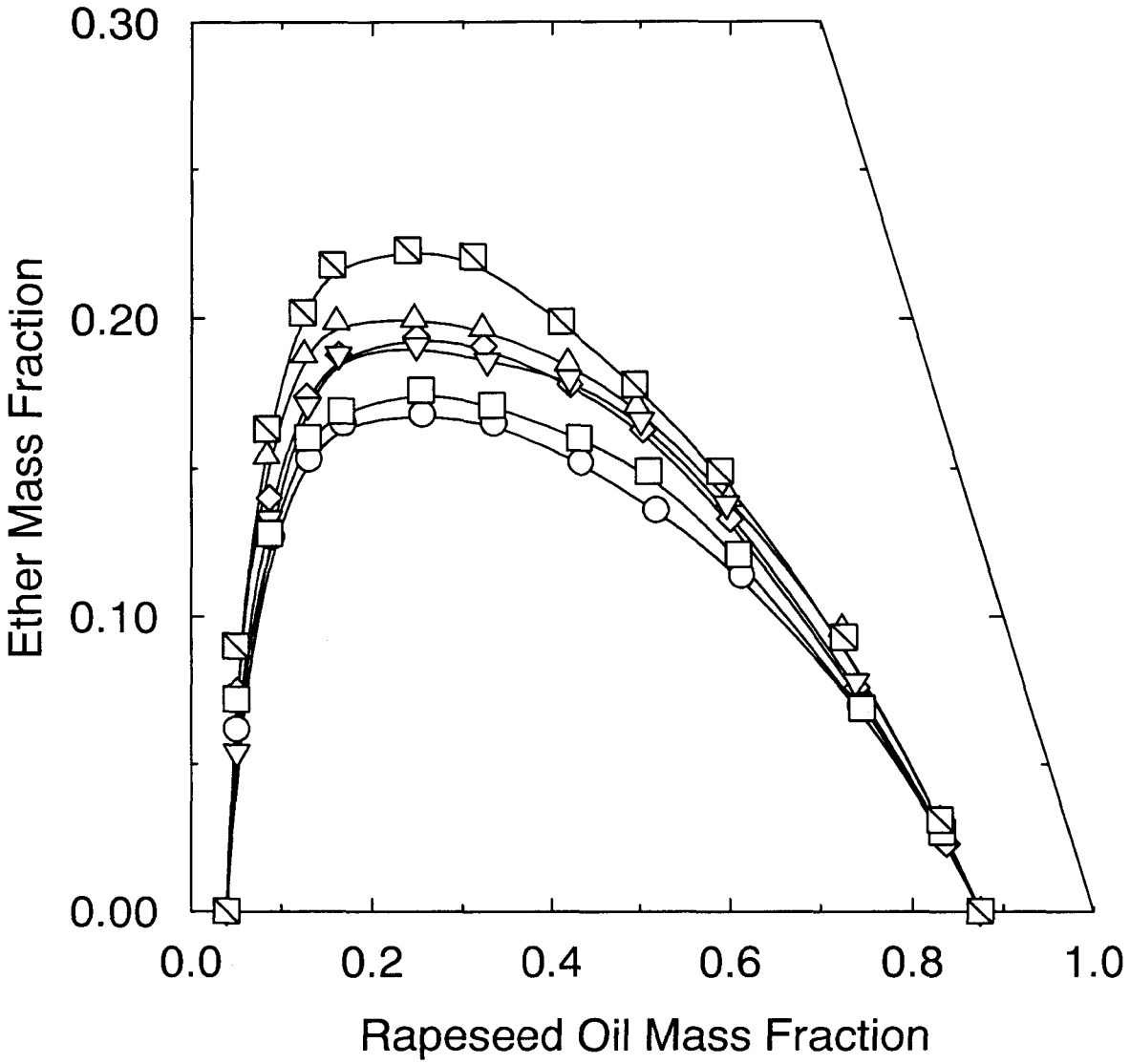

Fig. 7-2 Experimental solubility curves at 298.15 K for mixtures of soybean oil, ethanol, and ether

◇, MTBE; △, ETBE; ▽, TAME; ○, THF; □, THP; ⊠ , 1,4-Dioxane

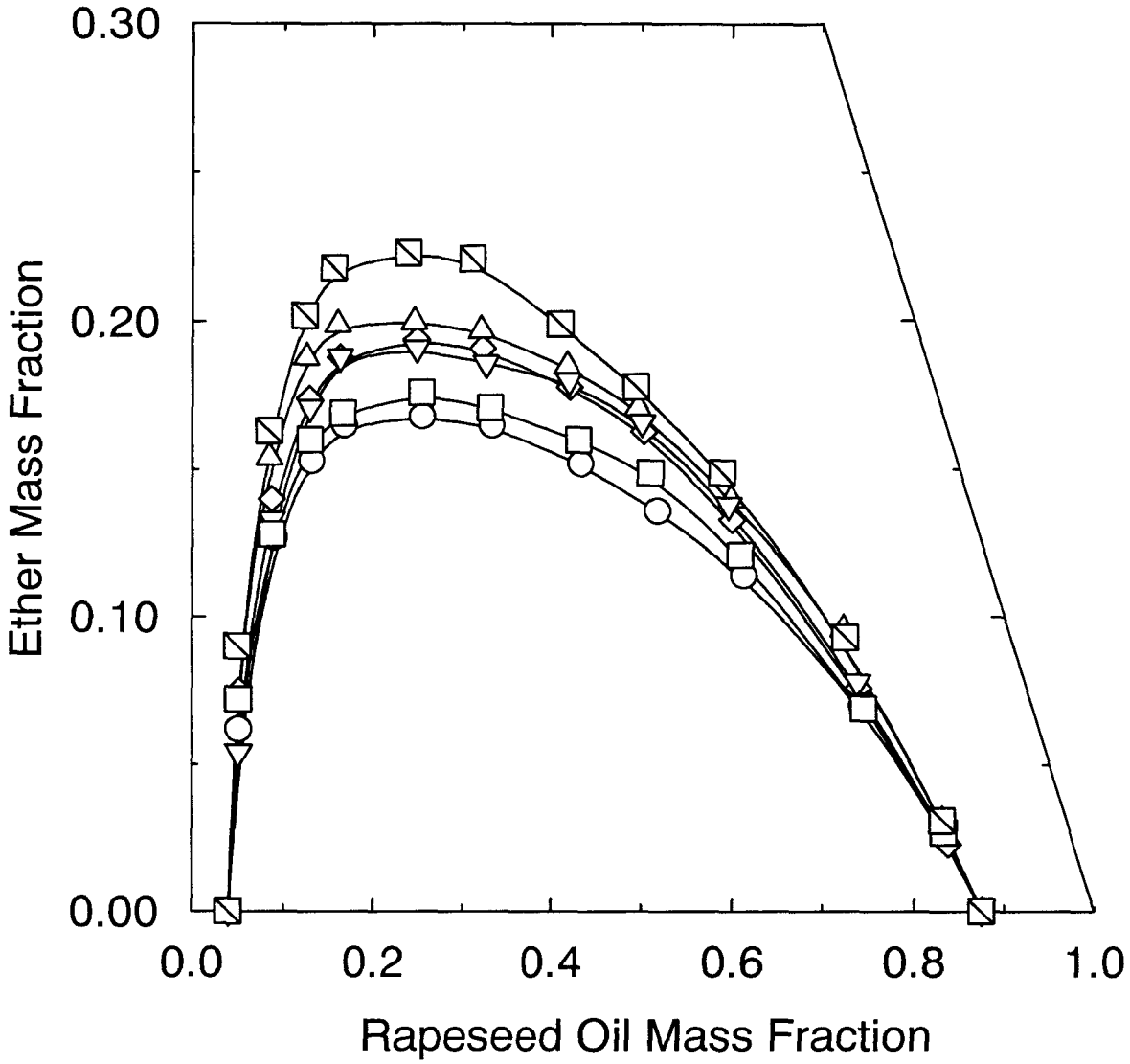

Fig. 7-3 Experimental solubility curves at 298.15 K for mixtures of rapeseed oil, ethanol, and ether

◇, MTBE; △, ETBE; ▽, TAME; ○, THF; □, THP; ⊠ , 1,4-Dioxane

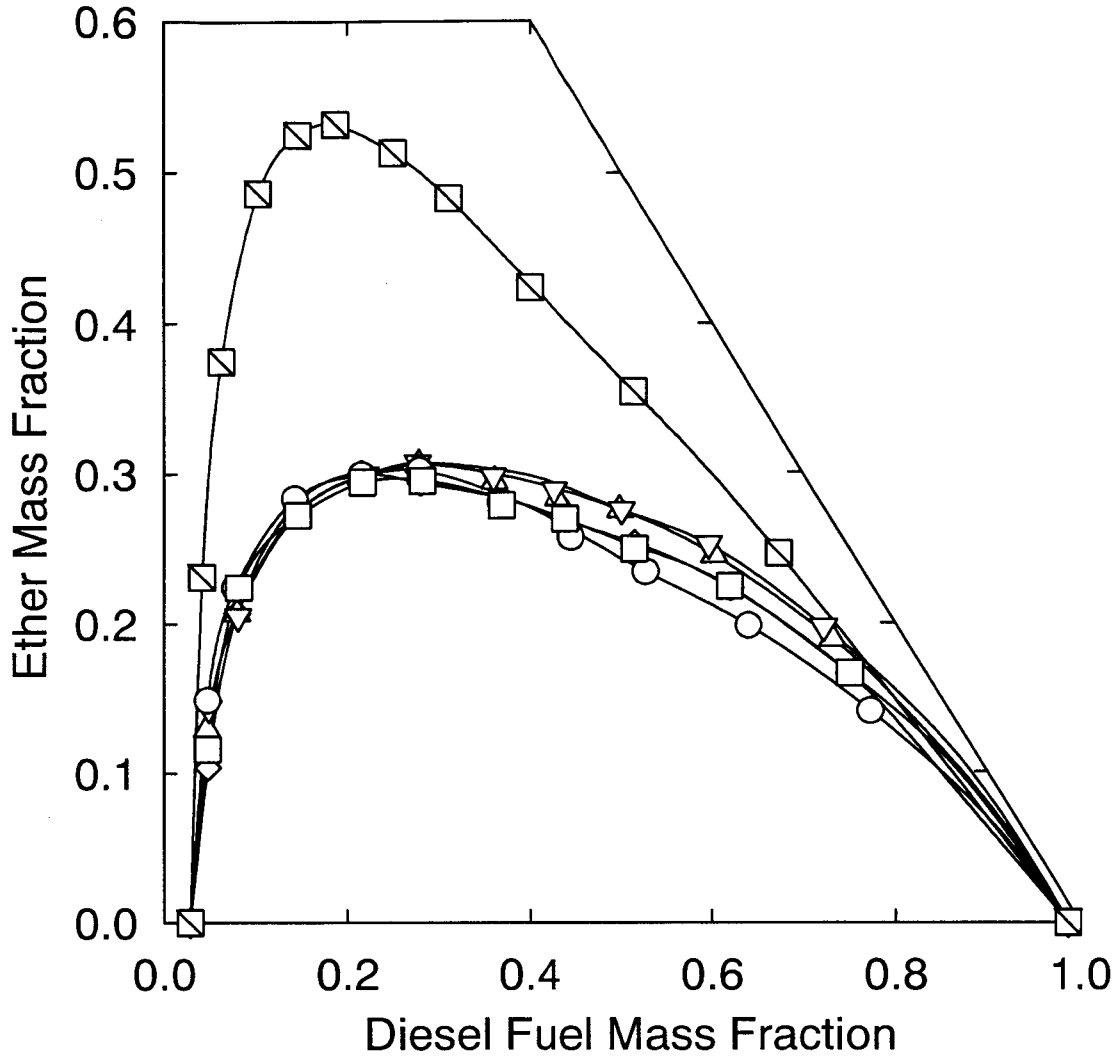

Fig. 7-4 Experimental solubility curves at 298.15 K for mixtures of diesel fuel, methanol, and ether

◇, MTBE; △, ETBE; ▽, TAME; ○, THF; □, THP; ⊠, 1,4-Dioxane

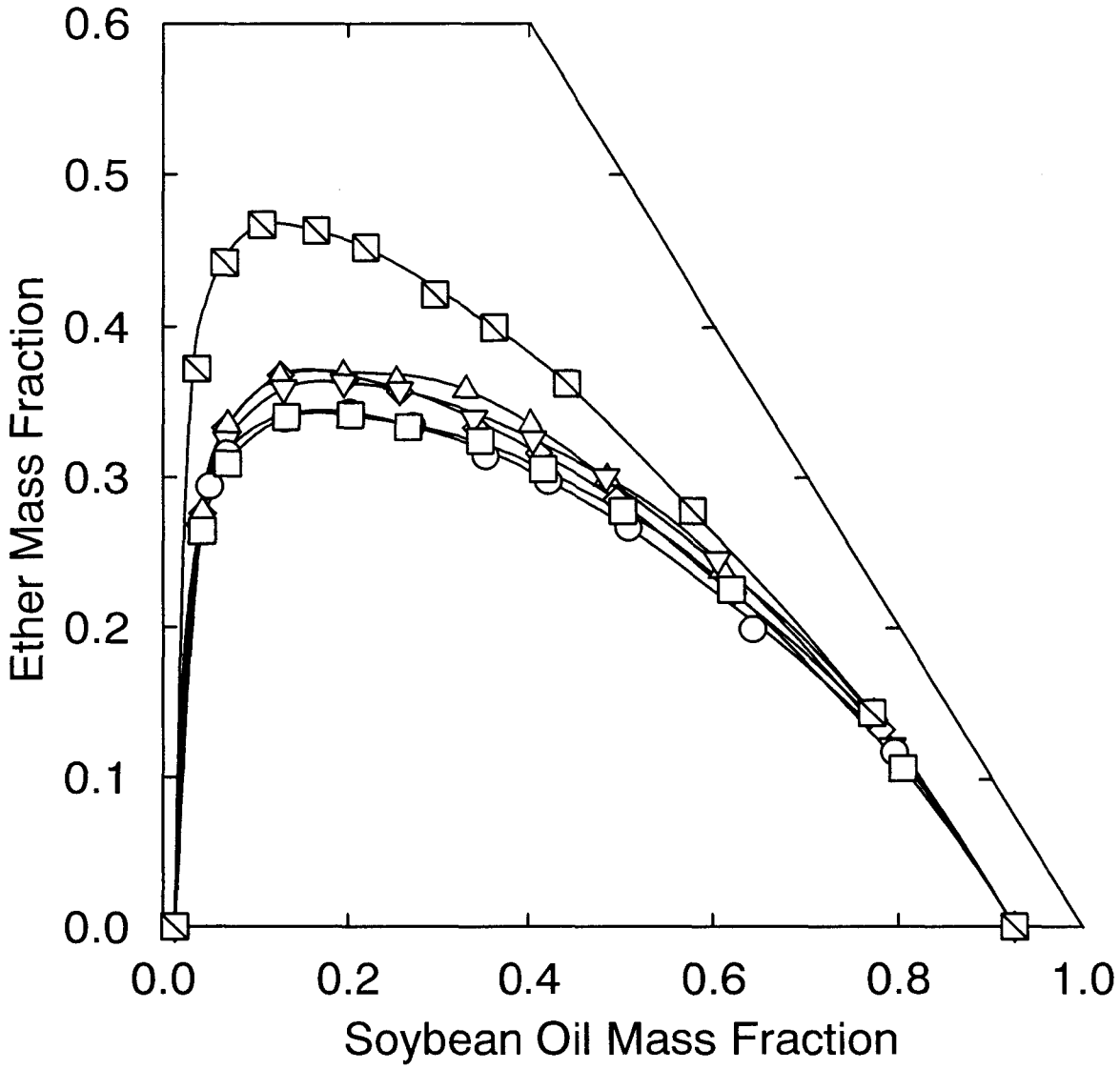

Fig. 7-5 Experimental solubility curves at 298.15 K for mixtures of soybean oil, methanol, and ether

◇, MTBE; △, ETBE; ▽, TAME; ○, THF; □, THP; ⧅, 1,4-Dioxane

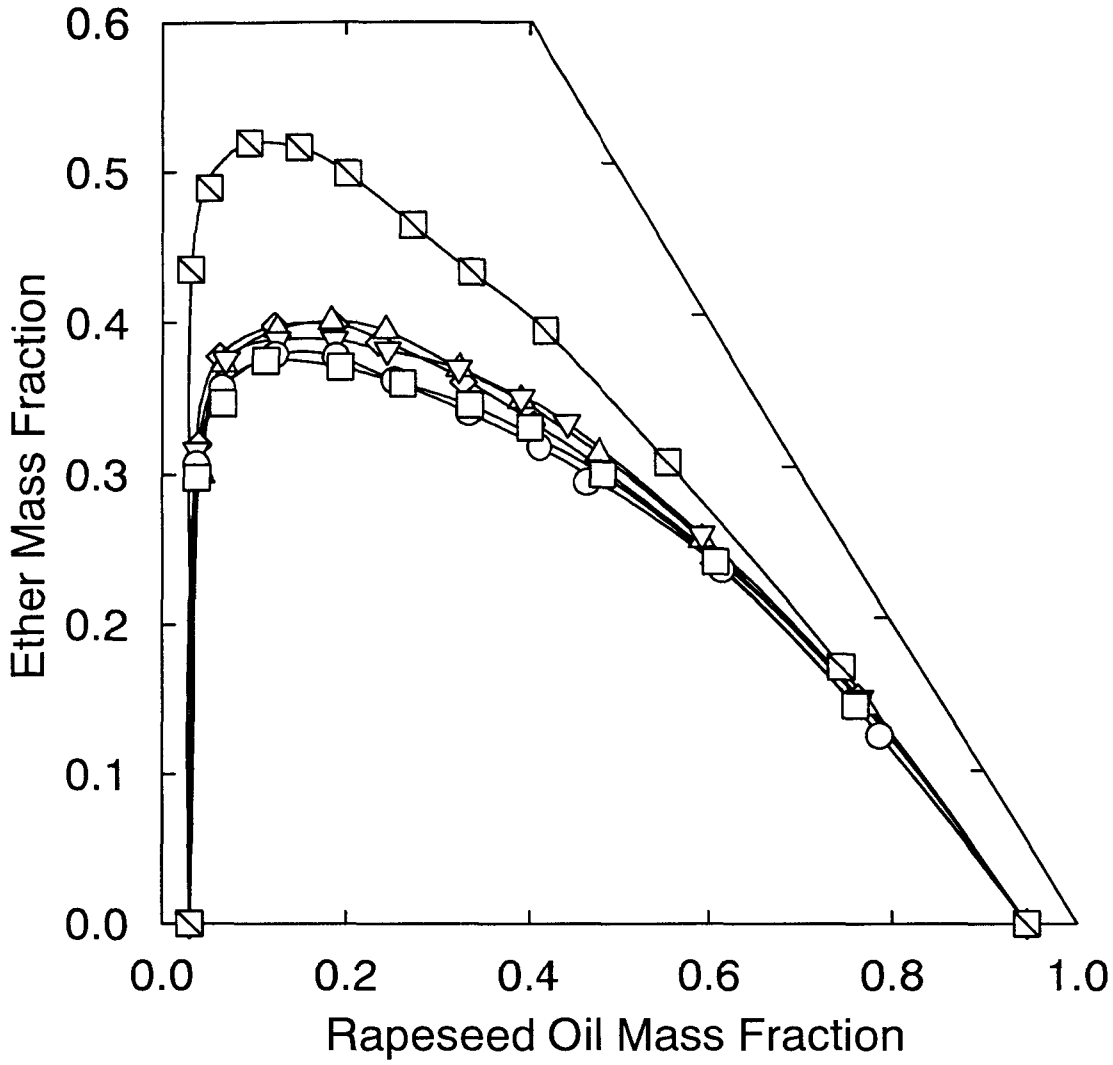

Fig. 7-6 Experimental solubility curves at 298.15 K for mixtures of rapeseed oil, methanol, and ether

◇, MTBE; △, ETBE; ▽, TAME; ○, THF; □, THP; ⧅, 1,4-Dioxane

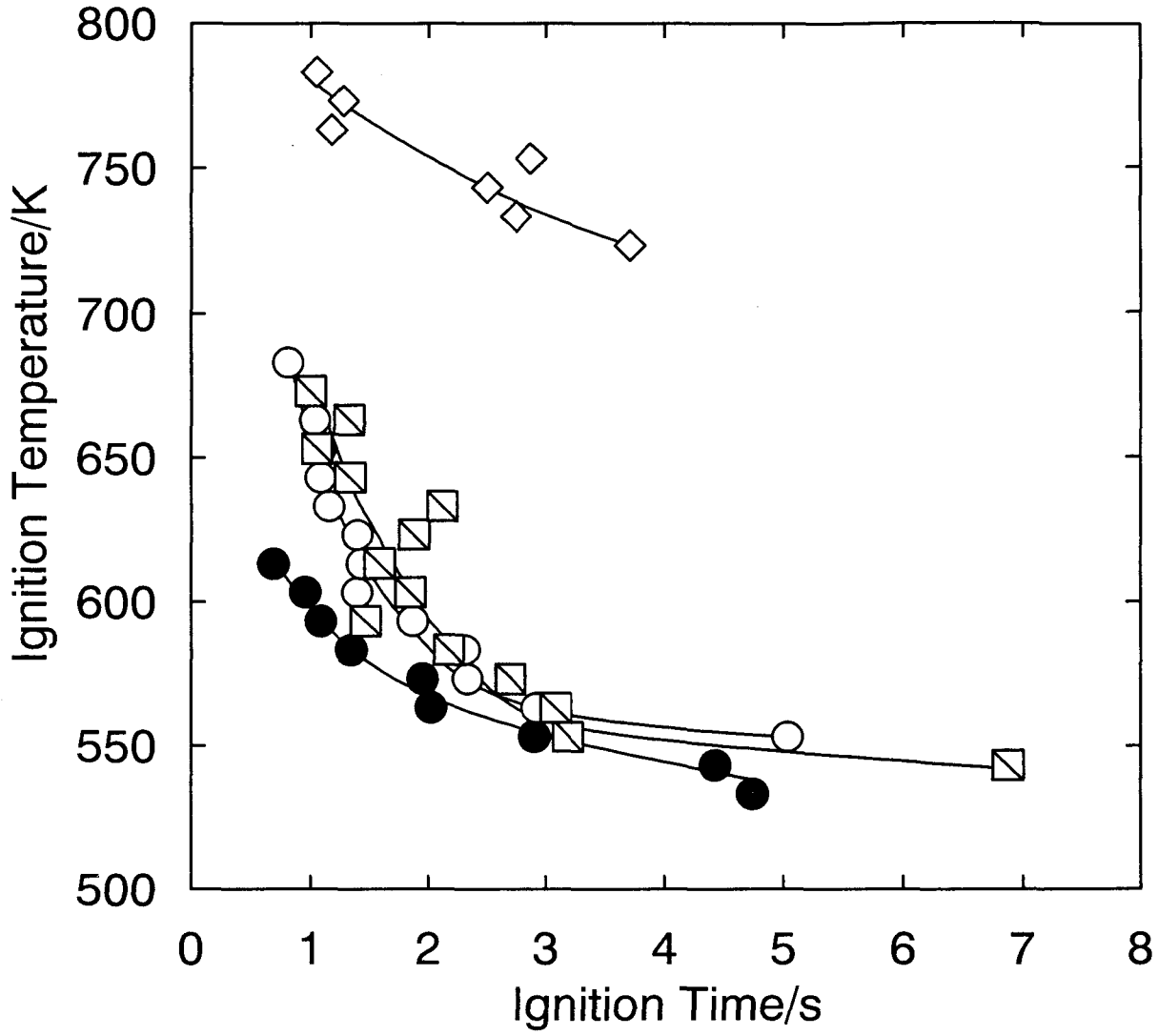

Fig. 7-7 Experimental ignition behaviors for mixtures of ether (1) + methanol (2) + diesel fuel (3)

x_1=0.375, x_2=0.188, x_3=0.437

ether ◇, MTBE; ○, THF; ▨, 1,4-Dioxane

standard ●, Diesel Fuel Only

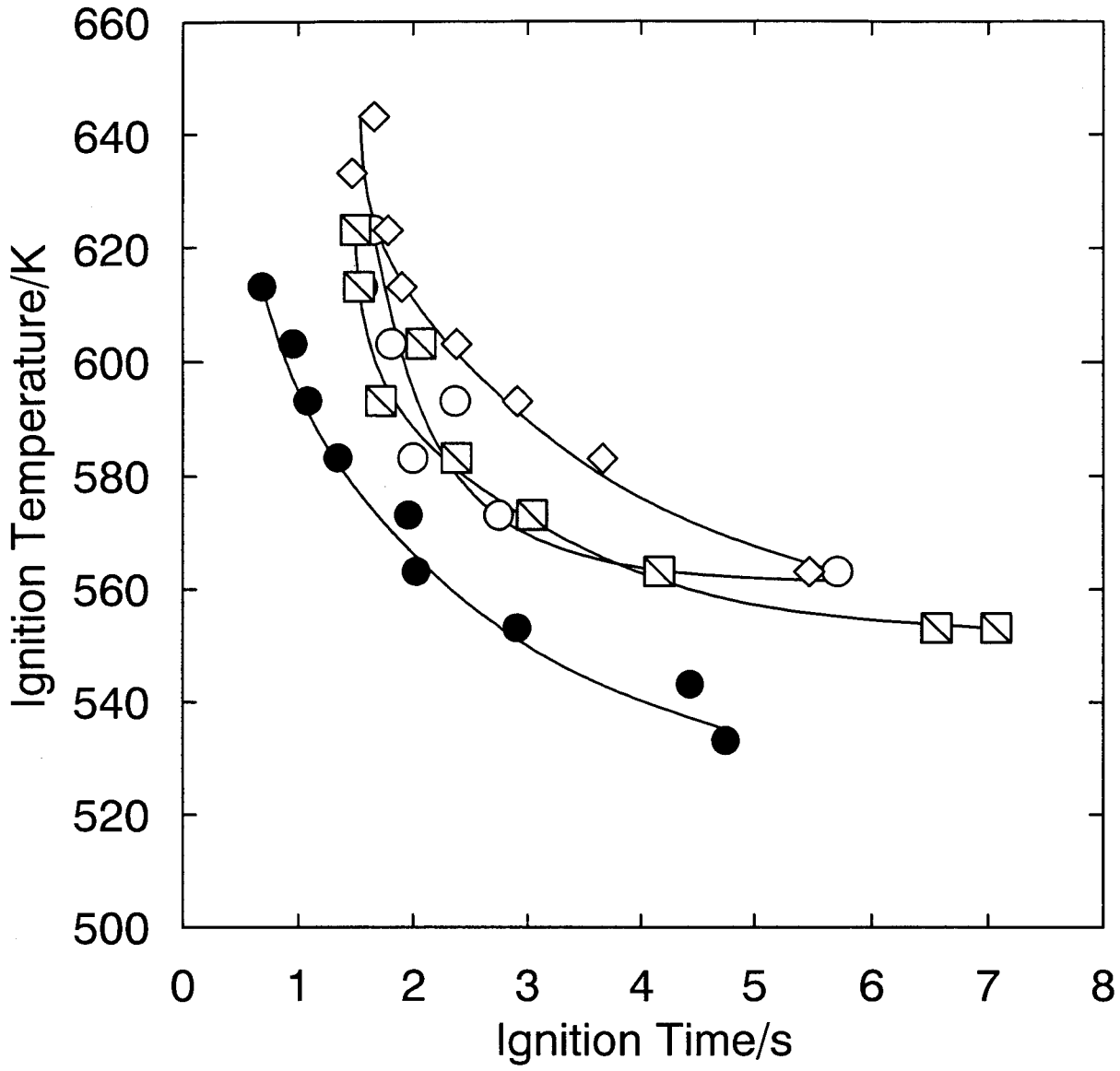

Fig. 7-8 Experimental ignition behaviors for mixtures of ether (1) + ethanol (2) + diesel fuel (3)

x_1=0.091, x_2=0.273, x_3=0.636

ether ◇, MTBE; ○, THF; ⊠, 1,4-Dioxane

standard ●, Diesel Fuel Only

General Conclusion

The studies collected in this thesis are concerned with the thermodynamic properties of phase equilibria for mixtures with supercritical fluids.

In Chapter 1, high-pressure vapor-liquid equilibria, saturated densities, and unsaturated densities were measured for the carbon dioxide + methanol system at 313.15 K. The equilibrium vapor and liquid compositions were evaluated from a couple of data at the same temperature and pressure, based on mass balance and the phase rule. At the critical region, the saturated points were measured by the conventional dew-bubble point pressure method. A technique was presented to determine the saturated vapor point. The experimental VLE data obtained were correlated with the PPHS (Kato *et al.*, 1989, Ozawa and Kato, 1991) and SRK (Soave, 1972) equations. By comparing the present VLE data obtained and the previous data by Ohgaki and Katayama (1976), the average differences in liquid and vapor compositions are shown to be 0.017 and 0.007 mole fractions, respectively. Comparisons on density behaviors are unfortunately impossible, as the data of Ohgaki and Katayama (1976) and Yoon *et al.* (1993) have no volumetric values. Volumetric data for the present system are not available in literature.

In Chapter 2, partial molar volumes of methanol at 313.15 K and ethanol at 308.15 K at infinite dilution in supercritical carbon dioxide were measured between 7 MPa and 10 MPa. Partial molar volumes of alcohol at infinite dilution were evaluated with the molar volume of pure carbon dioxide and the one of the homogeneous fluid made of carbon dioxide and a small amount of alcohol at the same temperature and pressure. The experimental data obtained were correlated with the SRK equation of state.

In the research field of vapor-liquid equilibria, the temperature-pressure-liquid composition-vapor composition relations were the main problem. The author however believes the volumetric properties will be required in the prediction and correlation of equilibrium properties in the near future. The author cannot satisfy the poor calculation

results on volumetric properties, even if the EOS gives satisfactory results on VLE prediction. The volumetric property data of mixtures are significant as well as the VLE data.

In Chapter 3, saturated densities of carbon dioxide + water mixture were measured at 304.1 K and pressures up to 10 MPa, using the apparatus equipped with vibrating tube density meters. The phase separations of vapor-liquid, liquid-liquid, and vapor-liquid-liquid were observed. The densities of pure water were also measured. The density of saturated liquid was greater than that of pure water at fixed pressure.

As the first step of the researches on storage of carbon dioxide in the sea to prevent the global warming, the experimental temperature was 304.1 K to keep the satisfactory accuracy on the temperature control. The average temperature of the seawater is about 280.15 K lower than the present temperature 304.1 K. At present, the author however cannot control the temperature at 280.15 K with the satisfactory accuracy. Some improvements are required for the experiments at 280.15 K. In the near future, the author will challenge for the experiments at the temperature of the seawater 280.15 K, after the improvement of the apparatus. The author believes the volumetric properties are essential in the design and development of the process to prevent the global warming.

In Chapter 4, phase equilibria and saturated densities for the ethane + 1-propanol system at high pressures were measured at 314.15 K with the static-circulation apparatus including the VLLE. The experimental data obtained were correlated by the equations of state with some little accuracy, due to the complex phase separation behaviors.

For the purification of ethanol from biomass alcohols, the supercritical carbon dioxide has a limitation, considering the similar shapes of the pressure-composition diagrams for different alcohols. Ethane seems to have the possibility as the effective supercritical fluids for the purification of ethanol from the biomass solution.

In Chapter 5, phase equilibria and saturated densities for the ethane + 2-propanol system at high pressures were measured at 308.15 K and 313.15 K with the static-circulation apparatus. The experimental data obtained were correlated by the equations of state.

The old literature of Kuenen *et al.* (1899) is however useful now because of their excellent experimental equilibrium data. The author believes the reliable equilibrium data have no death for worth in the present and future. The author sincerely hopes the unlimited life of the present equilibrium data reported here will be permanently alive.

The author has to say that the experimental temperature should be about 316.15 K, considering UCEP and LCEP given by Kuenen *et al.* (1899). It was not possible, however, the author thought about constraint of an experimental apparatus. The present experimental temperatures are not suitable to check the possibility of the three phase separations. The author would like to do it with future assignment.

In Chapter 6, the vapor-liquid equilibria in the dilute composition range of solutes were measured at atmospheric pressure. The equilibrium compositions were determined with an ultraviolet spectrometer. The vapor-liquid equilibrium behavior of ferrocene in methanol or ethanol was measured at atmospheric pressure in the dilute composition range of ferrocene with the recirculation still. Significantly, high volatilities of ferrocene were observed in methanol or ethanol.

The vapor-liquid equilibrium behavior of 1,4-dihydroxybenzene in methanol or ethanol was further measured at atmospheric pressure in the dilute composition range of 1,4-dihydroxybenzene with a recirculation still. The partial pressure of 1,4-dihydroxybenzene in methanol is higher than that in ethanol at the same temperature and infinite dilutions. The unexpected high volatility of 1,4-dihydroxybenzene in methanol would be explained by the high nonideality of the solution or activity coefficients at infinite dilution.

The author believes the present VLE data of solid components have a merit to evaluate the unknown parameters in the group contribution methods, such as UNIFAC and ASOG. The VLE of solid components seem powerful to evaluate the unknown parameters in the group contribution methods.

In Chapter 7, homogenization was observed in immiscible mixtures prepared from

ethanol or methanol with diesel fuel, soybean oil, or rapeseed oil, with the addition of the ethers: MTBE, ETBE, TAME, THF, THP, or 1,4-dioxane. Ternary solubility curves were obtained at 298.15 K for these ether + alcohol + oil mixtures. However, the homogenization effect was poor with 1,4-dioxane. A higher temperature was required for ignition of MTBE mixtures. Experimental ignition behaviors ware similar to those of diesel fuel for THF and 1,4-dioxane mixtures. Based on the experimental homogenization effect and ignition behavior results, THF is recommended for homogenization of alcohol + oil fuels for the diesel engine.

Suggestions for Future Work

Experimental Methods for Phase Equilibria

As described in Chapter 1, the synthetic method is especially useful for phase equilibria with fluid mixtures having some difficulty on composition analysis, such as the ones containing high boiling point substance. The dew-bubble point pressure method is useful in the vicinity of critical point as well as the aqueous solution and asymmetric mixtures; the composition analysis is sometimes accompanied with serious experimental troubles. In the future, the synthetic methods developed in this thesis would become essential for investigating phase equilibria which will be treated in chemical industries.

Complicated Behavior of Phase Separation

The complicated behavior of phase separation in the vicinity of a critical point is one of the most interesting subjects related to high-pressure phase equilibrium. In particular, it is useful to measure phase separation behaviors including the density data for the design and operation of distillation and supercritical fluid extraction, however, it is very difficult and needs efforts to measure phase separation behaviors in the vicinity of critical point, as described in Chapters 4 and 5. The behavior of saturated densities of carbon dioxide + water system shows three phase separation, as described in Chapter 3. In the future, the data of complicated behavior of phase separation measured in this thesis should contribute the development of new theory with highly precise equation of state or mixing rule.

For the theoretical works, we are impatient for the excellent equations of state and mixing rules. The prediction results should satisfy the complicated phase separation behaviors and further their volumetric properties. If possible, the author would like to challenge to find out the satisfactory equation of state and its theoretical mixing rule. In the future, the phase equilibria and physical properties should be predicted by the powerful and theoretical prediction method proposed with the satisfactory reliability.

Alternative Automobile Fuels

The fossil fuel is said to be dried up soon. The development of alternative fuel is, therefore, urgent technology. Biomass is promising as an alternative fuel from the viewpoint of utilization of resource. As described in Chapter 7, it is one of the most important purposes to clarify the suitable ether that homogenizes the immiscible binary mixtures for alternative automobile fuels. The ignition behaviors are also important for selecting artificial fuels consumed in the automobile diesel engine. Besides, viscosity characteristics, output characteristics, and exhaust characteristics will be required for the diesel engine.

Nomenclature

a, b, m, n	parameters in EOS	
k, l	binary interaction parameters	
K_a	correlation factor	
M	molar mass	[g·mol^{-1}]
N	cluster size	
P	pressure	[kPa]
R	gas constant	[kPa·m^3·mol^{-1}·K^{-1}]
S	parameters in EOS	
T	temperature	[K]
V	volume	[m^3]
v	molar volume	[m^3·mol^{-1}]
$\bar{v}$	partial molar volume	[m^3·mol^{-1}]
W	feed mass	[kg]
X	liquid mass fraction	
x	mole fraction	
Y	vapor mass fraction	
y	mole fraction	
Z	compressibility factor	
Δ	difference	
ρ	density	[kg·m^{-3}]
ω	acentric factor	
α	parameters in EOS	
μ	dipole moment	[Debye]
ψ	function given by Eq. (1-13)	

Subscripts

F	feed
L	liquid phase
T	total
V	vapor phase
c	critical property
i, j	components
r	reduced property
1, 2	components

Superscripts

G	given composition
nb	normal boiling point
0	pure substance
∞	infinite dilution
*	apparent value
'	second-run

Literature Cited

Akai, M.; "Carbon Dioxide Sequestration Technologies", *J. Jpn. Inst. Energy*, **12**, 1148-1155 (1997)

Cortesi, A., I. Kikic, B. Spicka, K. Magoulas and D. Tassios; "Determination of Partial Molar Volumes at Infinite Dilution of Alcohols and Terpenes in Supercritical Carbon Dioxide", *J. Supercrit. Fluids*, **9**, 141-145 (1996)

Eckert, C. A., D. H. Ziger, K. P. Johnston and S. Kim; "Solute Partial Molar Volumes in Supercritcal Fluids", *J. Phys. Chem.*, **90**, 2738-2746 (1986)

Hattori, K., Y. Arai, N. Yamana, H. Matsuura and C. Nishino; "Correlation for Vapor-Liquid Equilibria of Multicomponent Systems Containing Methanol by an Empirical Perturbed-Hard-Sphere Equation of State", *Sekiyu Gakkaishi*, **29**, 251-256 (1986)

Haugan, P. M. and H. Drange; "Sequestration of CO_2 in the Deep Ocean by Shallow Injection", *Nature*, **357**, 318-320 (1992)

Ishihara, K., A. Tsukajima, H. Tanaka, M. Kato, T. Sako, M. Sato and T. Hakuta; "Vapor-Liquid Equilibrium for Carbon Dioxide + 1-Butanol at High Pressure", *J. Chem. Eng. Data*, **41**, 324-325 (1996)

Ishihara, K., H. Tanaka and M. Kato; "Phase Equilibrium Properties of Ethane + Methanol System at 298.15 K", *Fluid Phase Equilib.*, **144**, 131-136 (1998)

Katayama, T., K. Ohgaki, G. Maekawa, M. Goto and T. Nagano; "Isothermal Vapor-Liquid Equilibria of Acetone-Carbon Dioxide and Methanol-Carbon Dioxide Systems at High Pressures", *J. Chem. Eng. Data*, **8**, 89-92 (1975)

Kato, M., H. Konishi, T. Sato, M. Hirata and T. Katayama; "Dew and Bubble Point Method for Ternary Systems —Methanol-Water-Dioxane System at 760 mm of Hg—", *J. Chem. Eng. Jpn.*, **5**, 1-4 (1972)

Kato, M. and H. Tanaka; "A New Three-Parameter Pseudo-Cubic Equation of State", *Adv. Cryog. Eng.*, **31**, 1169-1179 (1986)

Kato, M., Y. Yoshikawa, S. Moriya and B. C. -Y. Lu; "Boiling Point Behavior of

Alcohol-Diesel Fuel Mixtures", *Sekiyu Gakkaishi*, **31**, 258-261 (1988)

Kato, M., M. Yamaguchi and T. Kiuchi; "A New Pseudocubic Perturbed Hard-Sphere Equation of State", *Fluid Phase Equilib.*, **47**, 171-187 (1989)

Kato, M., K. Aizawa, T. Kanahira and T. Ozawa; "A New Experimental Method of Vapor-Liquid Equilibria at High Pressures", *J. Chem. Eng. Jpn.*, **24**, 767-771 (1991)

Kato, M., T. Muramatsu, H. Tanaka, S. Moriya, F. Yaginuma and N. Isshiki; "Density Behavior of Alcohol-Diesel Fuel Mixtures", *Sekiyu Gakkaishi*, **34**, 186-190 (1991)

Kato, M., K. Aizawa, T. Kanahira, H. Tanaka, T. Muramatsu, T. Ozawa and B. C. -Y. Lu; "A New Experimental Method for Measuring Gas Solubilities in Nonvolatile Liquid Mixtures", *Sekiyu Gakkaishi*, **35**, 318-323 (1992)

Kato, M., H. Tanaka and H. Yoshikawa; "High-Pressure Phase Equilibrium for Ethane + Ethanol at 311.15 K", *J. Chem. Eng. Data*, **44**, 116-117 (1999)

King, M. B., A. Mubarak, J. D. Kim and T. R. Bott; "The Mutual Solubilities of Water with Supercritical and Liquid Carbon Dioxide", *J. Supercrit. Fluids*, **5**, 296-302 (1992)

Kodama, D., N. Kubota, Y. Yamaki, H. Tanaka and M. Kato; "High Pressure Vapor-Liquid Equilibria and Saturated Density Behaviors for Carbon Dioxide + Methanol System at 313.15 K", *Netsu Bussei*, **10**, 16-20 (1996)

Kodama, D., H. Tanaka and M. Kato; "Vapor-Liquid Equilibrium of Ferrocene in Methanol or Ethanol", *J. Chem. Eng. Data*, **44**, 1252-1253 (1999)

Kodama, D., H. Tanaka and M. Kato; "High Pressure Phase Equilibrium for Ethane + 1-Propanol at 314.15 K", *J. Chem. Eng. Data*, **46**, 1280-1282 (2001)

Kojima, T.; "Evaluation of Various Measures for Global Warming and CO_2 Problems", *J. Jpn. Inst. Energy*, **12**, 1112-1118 (1997)

Kuenen, J. P. and W. G. Robson; "On the Mutual Solubility of Liquids—Vapour-pressure and Critical Points", *Philos. Mag.*, **48**, 180-203 (1899)

Lam, D. H., A. Jangkamolkulchai and K. D. Luks; "Liquid-Liquid-Vapor Phase Equilibrium Behavior of Certain Binary Ethane + n-Alkanol Mixtures", *Fluid Phase Equilib.*, **59**,

263-277 (1990)

Liong, K. K., N. R. Foster and S. L. J. Yun; "Partial Molar Volume of DHA and EPA Esters in Supercritical Fluids", *Ind. Eng. Chem. Res.*, **30**, 569-574 (1991)

Liu, H. and E. A. Macedo; "A Study on the Models for Infinite Dilution Partial Molar Volumes of Solutes in Supercritical Fluids", *Ind. Eng. Chem. Res.*, **34**, 2029-2037 (1995)

Meyer, C. A., R. B. McClintock, G. J. Silvestri and R. C. Spencer Jr.; "ASME Steam Tables, 6th edn.", ASME, New York (1967)

Ohgaki, K. and T. Katayama; "Isothermal Vapor-Liquid Equilibrium Data for Binary Systems Containing Carbon Dioxide at High Pressures: Methanol-Carbon Dioxide, n-Hexane-Carbon Dioxide, and Benzene-Carbon Dioxide Systems", *J. Chem. Eng. Data*, **21**, 53-55 (1976)

Ohgaki, K. and Y. Inoue; "A Proposal for Gas Storage on the Ocean Floor Using Gas Hydrates", *Kagaku Kogaku Ronbunshu*, **17**, 1053-1055 (1991)

Ozawa, T. and M. Kato; "Correlation of High Pressure Vapor-Liquid Equilibria with Pseudocubic Perturbed Hard Sphere Equation of State", *Sekiyu Gakkaishi*, **34**, 562-566 (1991)

Reid, R. C., J. M. Prausnitz and T. K. Sherwood; "The Properties of Gases and Liquids, 3rd edn.", McGraw-Hill, New York, (1977).

Reid, R. C., J. M. Prausnitz and B. E. Poling; "The Properties of Gases and Liquids, 4th edn.", McGraw-Hill, New York (1987)

Soave, G.; "Equilibrium Constants from a Modified Redlich-Kwong Equation of State", *Chem. Eng. Sci.*, **27**, 1197-1203 (1972)

Spicka, B., A. Cortesi, M. Fermeglia and I. Kikic; "Determination of Partial Molar Volumes at Infinite Dilution Using SFC Technique", *J. Supercrit. Fluids*, **7**, 171-176 (1994)

Srinivasan, M. P. and B. J. McCoy; "Partial Molar Volumes of Ethyl Acetate from Supercritical CO_2 Desorption Data", *J. Supercrit. Fluids*, **4**, 69-71 (1991)

Suzuki, K., H. Sue, M. Itou, R. L. Smith, H. Inomata, K. Arai and S. Saito; "Isothermal

Vapor-Liquid Equilibrium Data for Binary Systems at High Pressures: Carbon Dioxide-Methanol, Carbon Dioxide-Ethanol, Carbon Dioxide-1-Propanol, Methane-Ethanol, Methane-1-Propanol, Ethane-Ethanol, and Ethane-1-Propanol Systems", *J. Chem. Eng. Data*, **35**, 63-66 (1990)

Takishima, S., K. Sakai, K. Arai and S. Saito; "Phase Equilibria for CO_2-C_2H_5OH-H_2O System", *J. Chem. Eng. Jpn.*, **19**, 48-56 (1986)

Tanaka, H., T. Muramatsu and M. Kato; "Isobaric Vapor-Liquid Equilibria for Three Binary Systems of 2-Butanone with 3-Methyl-1-Butanol, 1-Butanol, or 2-Butanol", *J. Chem. Eng. Data*, **37**, 164-166 (1992)

Tanaka, H., Y. Yamaki and M. Kato; "Solubility of Carbon Dioxide in Pentadecane, Hexadecane, and Pentadecane + Hexadecane", *J. Chem. Eng. Data*, **38**, 386-388 (1993)

Tanaka, H. and M. Kato; "Solubilities of Carbon Dioxide in Heavy Hydrocarbons", *Netsu Bussei*, **8**, 74-78 (1994)

Tanaka, H. and M. Kato; "Vapor-Liquid Equilibrium Properties of Carbon Dioxide + Ethanol Mixtures at High Pressures", *J. Chem. Eng. Jpn.*, **28**, 263-266 (1995)

Thermodynamics Research Center; "TRC-Thermodynamics Tables-Non-Hydrocarbons", The Texas A&M University System, College Station, TX (1996)

Timmermans, J.; *Physico-Chemical Constants of Pure Organic Compounds*, Vol. 1; Elsevier: New York, **1950**

Wiebe, R. and V. L. Gaddy; "The Solubility in Water of Carbon Dioxide at 50, 75 and 100°, at Pressures to 700 Atmospheres", *J. Am. Chem. Soc.*, **61**, 315-318 (1939)

Wiebe, R. and V. L. Gaddy; "Vapor Phase Composition of Carbon Dioxide-Water Mixtures at Various Temperatures and Pressure to 700 Atmospheres", *J. Am. Chem. Soc.*, **63**, 475-477 (1941)

Yaginuma, R., S. Moriya, Y. Sato, T. Sako, D. Kodama, H. Tanaka and M. Kato; "Homogenizing Efeect of Addition of Ethers to Immiscible Binary Fuels of Ethanol and Oil", *Sekiyu Gakkaishi*, **42**, 173-177 (1999)

Yoshikawa, H., T. Kanahira and M. Kato; "Solubility and Liquid Density Behavior for Two Binary Systems of 2,2,4-Trimethylpentane with Methanol or Nitroethane", *Fluid Phase Equilib.*, **94**, 255-265 (1994)

Yoon, J. -H., H. -S. Lee and H. Lee; "High-Pressure Vapor-Liquid Equilibria for Carbon Dioxide + Methanol, Carbon Dioxide + Ethanol, and Carbon Dioxide + Methanol + Ethanol", *J. Chem. Eng. Data*, **38**, 53-55 (1993)

Yun, S. L. J., K. K. Liong, G. S. Gurdial and N. R. Foster; "Solubility of Cholesterol in Supercritical Carbon Dioxide", *Ind. Eng. Chem. Res.*, **30**, 2476-2482 (1991)

List of Publications

1) Kodama, D., N. Kubota, Y. Yamaki, H. Tanaka and M. Kato; "High Pressure Vapor-Liquid Equilibria and Density Behaviors for Carbon Dioxide + Methanol System at 313.15 K", *Netsu Bussei*, **10**, 16-20 (1996)

2) Kodama, D., T. Nakajima, H. Tanaka and M. Kato; "Partial Molar Volumes of Methanol and Ethanol at Infinite Dilution in Supercritical Carbon Dioxide", *Netsu Bussei*, **12**, 186-190 (1998)

3) Yaginuma, R., S. Moriya, Y. Sato, T. Sako, D. Kodama, H. Tanaka and M. Kato; "Homogenizing Effect of Ethers Addition to Immiscible Binary Fuels of Ethanol + Oil", *Sekiyu Gakkaishi*, **42**, 173-177 (1999)

4) Kodama, D., H. Tanaka and M. Kato; "Vapor-Liquid Equilibrium of Ferrocene in Methanol or Ethanol", *J. Chem. Eng. Data*, **44**, 1252-1253 (1999)

5) Yaginuma, R., Y. Sato, D. Kodama, H. Tanaka and M. Kato; "Saturated Densities of Carbon Dioxide + Water Mixture at 304.1 K and Pressure to 10 MPa", *J. Jpn. Inst. Energy*, **79**, 144-146 (2000)

6) Kodama, D., H. Tanaka and M. Kato; "High Pressure Phase Equilibrium for Ethane + 1-Propanol at 314.15 K", *J. Chem. Eng. Data*, **46**, 1280-1282 (2001)

7) Yaginuma, R., S. Moriya, Y. Sato, D. Kodama, H. Tanaka and M. Kato; "Homogenizing Effect of Ethers Added to Immiscible Methanol / Oil Binary Mixtures", *Sekiyu Gakkaishi*, **44**, 401-406 (2001)

8) Kodama, D., H. Tanaka and M. Kato; "Vapor-Liquid Equilibrium of 1,4-Dihydrobenzene in Methanol or Ethanol", *J. Chem. Eng. Data*, **47**, 91-92 (2002)

9) Kodama, D., M. Ogawa, T. Kimura, H. Tanaka and M. Kato; "High-Pressure Phase Equilibrium for Ethane + 2-Propanol at 308.15 K and 313.15 K", *J. Chem. Eng. Data*, in press (2002)

Others

1) Kato, M., H. Tanaka, Y. Yamaki, D. Kodama, N. Kubota and B. C. -Y. Lu; "An Apparatus for Measuring Vapor-Liquid Equilibria at High Pressures", Proc. The Third Korea-Japan Symp. on Sep. Tech., Seoul, Korea, 237-240, 10/25-27 (1993)

2) Kato, M., H. Tanaka, Y. Yamaki, D. Kodama and N. Kubota; "Vapor-Liquid Equilibrium Properties of Carbon Dioxide + Methanol System at High Pressures", Proc. Third Inter. Symp. on Supercritical Fluids, Strasbourg, France, 10/18 (1994)

3) Kodama, D., N. Kubota, T. Nakajima, H. Tanaka and M. Kato; "Partial Molar Volumes at Infinite Dilution of Methanol or Ethanol in Supercritical Carbon Dioxide", Proc. The 4th Inter. Symp. on Supercritical Fluids, Sendai, Japan, 5/11-14 (1997)

4) Moriya, S., F. Yaginuma, H. Watanabe, D. Kodama, M. Kato and N. Isshiki; "Utilization of Ethanol and Gas Oil Blended Fuels for Diesel Engine (Addition of Decanol and Isoamyl Ether)", Proc. 34th Intersociety Energy Conversion Engineering Conference, Vancouver, Canada, 8/2-5 (1999)

5) Tanaka, H., D. Kodama, R. Yaginuma and M. Kato; "Vapor-Liquid Equilibria of Aqueous Solutions Containing 2-Aminoethanol or Cyclohexylamine", *Netsu Bussei*, **15**, 182-184 (2001)

6) Tanaka, H., D. Kodama and M. Kato; "Measurement and Correlation of High-Pressure Phase Equilibrium for Ethane +1-Propanol System which Showing a Complicated Phase Separation", *JASCO Report*, **5**, 71-74 (2001)

7) Kodama, D., T. Kimura, H. Tanaka and M. Kato; "High Pressure Phase Equilibrium Properties for Ethane + 1-Butanol System at 313.15 K", *Fluid Phase Equilib.*, in press (2002)

Acknowledgement

The author is greatly indebted to Professor Masahiro Kato (Department of Materials Chemistry and Engineering, College of Engineering, Nihon University) for his valuable guidance and helpful suggestions throughout the work.

The author is also grateful to Professor Kazunari Ohgaki (Division of Chemical Engineering, Graduate School of Engineering Science, Osaka University), Professor Tomoshige Nitta (Division of Chemical Engineering, Graduate School of Engineering Science, Osaka University), Professor Korekazu Ueyama (Division of Chemical Engineering, Graduate School of Engineering Science, Osaka University), and Professor Emeritus Isao Komasawa (Division of Chemical Engineering, Graduate School of Engineering Science, Osaka University) for their helpful comments and suggestion to this work.

Grateful acknowledgements are also made to Dr. Hiroyuki Tanaka (Department of Materials Chemistry and Engineering, College of Engineering, Nihon University), Professor Shinji Moriya (Department of Mechanical Engineering, College of Engineering, Nihon University), Professor Takeshi Sako (Department of Material Science, Faculty of Engineering, Shizuoka University), and Dr. Dmitry S. Bulgarevich (National Institute of Advanced Industrial Science and Technology).

The author also wishes to acknowledge his grateful thanks to Messrs. Rikio Yaginuma, Yoshikazu Sato, Takashi Kanahira, Yoshikazu Yamaki, Shin-ichi Abo, Nobuo Kubota, Hidefumi Takato, Akira Tsukajima, Katsuo Ishihara, and Takashi Nakajima who carried out much of the experimental and constructional work.

It is also his pleasure to acknowledge a pleasant and stimulative atmosphere, which many other members of the Kato Laboratory have produced.

Finally, the author's grateful thanks are also due to his parents, Hironori Kodama and Yukie Kodama.